December 2020

Solvent as a Tool to Tune the Association of Structured Ionic Block Co-Polymers: Neutron Scattering and Computational Study

Manjula Senanayake
Clemson University, manjulasmmp@gmail.com

SOLVENT AS A TOOL TO TUNE THE ASSOCIATION OF STRUCTURED IONIC BLOCK CO-POLYMERS: NEUTRON SCATTERING AND COMPUTATIONAL STUDY

A Dissertation
Presented to
the Graduate School of
Clemson University

In Partial Fulfillment
of the Requirements for the Degree
Doctor of Philosophy
Chemistry

---

by
Manjula Senanayake
December 2020

Accepted by:
Dr. Dvora Perahia, Committee Chair
Dr. Gary S. Grest
Dr. Rhett C. Smith
Dr. Steve Stuart

ABSTRACT

The work probes the behavior of associating polymers including their assembly in different environments, using neutron scattering techniques coupled with molecular dynamics (MD) simulations. Polymers interact with their surroundings through van der Waals forces and through stronger association groups such as ionizable groups and π-π stacking, as well as specific chemical binding, where assembly depends on the strength of the interactions of the associating groups as well as the interactions of the polymers with their solvent environment. The current effort centers on understanding the assembly of structured polymers that consists of multiple blocks or components, each with their distinct interactions with solvents. The main body of the work focuses on the assembly of a multi-functional ionic polymers of the form ABCBA in which the center block is a sulfonated polystyrene (C) that enables transport tethered to, B, a polyethylene propylene (PEP) block, terminated by A, a t-butyl polystyrene (t-BPS) block. These polymers find broad uses in transport-controlled applications such as clean energy, separation membranes, and biotechnology. The aggregation of this polymer is driven by segregation of the ionizable block from the rest of the polymer as well as the interactions of each bock with solvents. The first part introduces experimental studies of assembly of this polymer as the solvent polarity is changed, followed by atomistic MD simulations insight into the assembly process. A more general insight into the assembly process is obtained by coarse grained MD studies. Finally, synthetic routes to obtain polymers with specific binding for sensing applications is discussed.

The structural SANS studies have shown that the polymer forms core-shell aggregates with the ionic blocks in the core of the micelles in non-polar solvents such as cyclohexane. These micelles become gradually elongated with the addition of propanol to a propanol fraction of about 0.4. This change in shape of the micelles is driven by increasing of core-corona interfacial energy while collapsing the non-polar segments. Further increase in propanol results in reentrance to spherical micelles but with a smaller number of polymer molecules and significantly higher portion of solvent in the core.

Solvent tuning of assembly to pentablock copolymer was further probed by fully atomistic MD simulation in cyclohexane, THF and propanol, solvents with different polarity. We find that the structure of the assemblies is driven by the different binding affinities of the solvents with polar and non-polar segments as well as the ionic fraction. Cyclohexane predominantly resides in the non-polar segments that are swollen, while the ionic blocks remain segregated in the micellar core. In contrast to cyclohexane, propanol and THF, which have an affinity towards both the ionic and non-ionic segments, swell the ionic blocks. With increasing sulfonation, the ionic blocks form a more stable spherical ionic core with cyclohexane associating around the core while THF and propanol penetrate into the core.

To further understand the interactions of this structured block co polymer interactions with solvents, a thin polymer film in contact with solvent films were prepared, and the solvents were followed as they propagated across the interfaces, using MD simulations. We observed that exposure of water to pentablock copolymer membrane

decreases the interfacial width, exposing more ionizable groups whereas the interfacial width for the film in contact propanol and THF increases and is dominated by hydrophobic blocks. Water molecules associate predominantly with the ionic blocks while propanol and THF reside in both the ionic and non-ionic segments.

In order to understand the effects of associating groups in a more general way, coarse grained MD simulations of association were carried out. The polymer chains are modeled by a bead-spring model and the associating groups are incorporated in the form of associating beads with a stronger interaction strength between them than between the non-associating beads. The structure and dynamics of linear and star polymer melts was followed as a function of the interaction strength of the associating beads. The results show that addition of even a small number of associating groups has dramatic effects on the mobility and viscoelastic response of polymer melts. The associating group aggregate forming a polymer network. With increasing interaction strength between the associating beads, the mobility of the chains decreases. Blends of chains with and without associating groups macroscopically phase separation even for relatively weak interaction between the associating beads.

To the last part of the work was focused on understanding the effects of associating groups in soft nanoparticles. For this purpose, we synthesized polyparaphenylene ethylene (PPE) with biotin groups attached to the side chains with the ultimate goal of understanding the effect of associating groups on structure and dynamics of biocompatible soft nanoparticles. The last chapter describes the synthesis of biotin substituted PPEs, where the effect of biotin groups on assembly of PPE will be carried out in the future.

DEDICATION

This work is dedicated to my family whose boundless love and encouragement made this work possible; to my loving mother, Arachchilalage Kusumawathi, who has always cared and protected me, my father Senanayake Mudiyanselage Gunadasa who was always been an example and source of strength to me; to my sisters Ramani Malkanthi and Nilanthi Senanayake who shared every step of my life; thank you for making me who I am. Finally, I am grateful to my wife Arachchige Duleeka and to my two sons Anuja Tharinda and Anuka Nethun who make every day of my life a celebration. Duleeka, without your love and support, this work would have not been impossible.

ACKNOWLEDGMENTS

I would like to thank my research advisors Dr. Dvora Perahia and Dr. Gary S. Grest. Their guidance and encouragement have been invaluable. Without their careful guidance, this work would have not been impossible. I would also like to thank my committee members, Dr. Rhett C. Smith who guided my polymer synthesis efforts and believed I could do it; and to Dr. Steve Stuart, who is one of the best teachers I have ever I met.

I would like to thank my current and former group members whose science input and friendship has been instrumental to my success. Dr. Thusthita Etampawala, Dr. Naresh C. Osti, Dr. Umesh M. Shrestha, Dr. Sabina Maskey, Dr. Dipak Aryal, Dr. Anupriya Agrawal, Dr. Sidath Wijesinghe, Anuradhi Wickramasinghe, Supun Samindra, Chathurika Kosgallana, Shalika Meedin and Rosita Sivaraj, thank you for your support, valuable scientific discussions and most important your friendship. Thank you for walking with me along the way.

Finally, no work can be done without a financial and resource funding. I am thankful for the National Science Foundation, DOE and Chemistry Department, Clemson University for their financial support, Department of Energy for neutron facility, Palmetto Cluster, Clemson University and NERSC, National Energy Research Scientific Computing Center, for computational resources and the Center for Integrated Nanotechnologies (CINT)-Sandia National Laboratories for the opportunity of training.

TABLE OF CONTENTS

LIST OF TABLES

LIST OF FIGURES

List of Figures (Continued)

List of Figures (Continued)

CHAPTER ONE

INTRODUCTION

The research work investigates the effects of solvent polarity on association of structured ionic block copolymer in solutions using small angle neutron scattering (SANS) and classical atomistic molecular dynamics (MD) simulations. Ion containing polymers have a large number of current and potential applications such as drug delivery,[1-3] clean energy[4-6] and separation membranes.[7-9] Ion transport capability of ionic polymers is the key which opens the door for their use in those applications. Polymers in this class have a relatively higher glass transition temperature Tg, therefore, polymer solutions are often used for processing. These polymers aggregate at low concentrations and solution structure serves as building blocks for membranes. However, under the conditions where transport property is optimized, structure of the polymer become unstable. Therefore, these polymers are often tethered to additional blocks to enhance the mechanical stability.

Diblock co-polymers in selective solvents, often self-assemble into aggregates.[10-24] The simplest polymer micelles are formed by van der Waals diblock co-polymers in solutions with different structural morphologies, lamellae,[10, 16] vesicles,[15, 22] cylinders[10, 18, 23] and spheres,[11-16] depending on the chemistry of the polymer as well as the nature of the solvent and the temperature. Introducing an ionizable block into diblock co-polymers increases the incompatibility of the different blocks, which drives aggregation in solutions.[25-31] Because of the strong interactions between different groups, the ionizable groups often associate faster than the other segments driving out of equilibrium aggregates. Increasing

complexity by increasing the number of different blocks present in the polymer chain dramatically expand the spectrum of the morphologies of aggregates observed in solutions.[32] The solvent polarity is the optimal tool to control the association of the ionic groups. Therefore, understanding association of highly structured ionic block copolymers in different solvent environment is critical.

Here, we will be using solvent polarity as a tool to tune the morphology of the aggregates formed by highly structured ionic block co-polymer in solutions. We will probe the effects of solvent polarity on a symmetric ABCBA type pentablock copolymer which contains randomly sulfonated polystyrene (PSS) in the center, tethered to poly (ethylene/propylene) block and terminated by poly (t-butyl styrene) using SANS and classical atomistic MD simulations. SANS is an optimal tool to probe aggregation in polymer solutions. It takes the advantage of isotopic labeling where the solution or polymer are deuterated.[33, 34] Classical atomistic MD simulation will be used to probe the response of each segments in atomic scale to changing of solvent polarity of the medium.

This dissertation is organized as follows; First, will address the background of polymer solutions, ionic polymers, block co-polymers, ionic block co-polymers and structured ionic block co-polymers in solutions. Following that our experimental tools, SANS and classical MD simulations will be explained. Finally, results will be introduced including solvent polarity effects on micellar structure in solution, solvent polarity effects of structure and

dynamics of membrane, effects of associating groups on dynamics of linear and star polymer melts and the synthesis of biotin substituted polpara phenylene ethylene.

Polymer solutions

Dissolution of polymer molecules is more challenging than small molecules. A polymer dissolves in a solvent when solvation lowers the free energy. The free energy change of mixing (ΔG_{mix}) for mixtures is given in equation 1, where ΔH_{mix} is the enthalpy change of mixing and ΔS_{mix} is entropy change of mixing and T is temperature,[35, 36]

$$\Delta G_{mix} = \Delta H_{mix} - T\Delta S_{mix} \qquad (1.1)$$

For polymer-solvent systems, ΔS_{mix} is not dominant, especially for lower concentrations.[35] Therefore, miscibility of polymer-solvent system is governed by the changed in interactions upon mixing ($=\Delta H_{mix}$). The possible interaction terms in polymer-solvent systems are illustrated in Figure 1.

The energy change upon polymer-solvent mixing is given by the Flory-Huggins χ parameter,[35-38] which is given in equation 2. In this model polymer solvent systems are defined as a particle on a lattice. Each lattice point is occupied by either monomer or solvent molecule,

$$\chi_{AB} = \left(\frac{z}{k_{bB}T}\right)\left[\epsilon_{ms} - \frac{1}{2}(\varepsilon_{mm} + \varepsilon_{ss})\right] \qquad (1.2)$$

Here, z is the number of nearest neighbors per monomer unit, k_B is the Boltzmann constant, T is the temperature and ϵ_{ms}, ϵ_{mm}, ϵ_{ss} are the interaction energies between the monomer-solvent, monomer-monomer and solvent-solvent. Positive χ_{AB} denotes that the monomer–solvent contacts are less favored compared with the monomer–monomer and solvent–solvent contacts. A negative χ_{AB} means that polymer–solvent contacts are preferred, promoting solvation of the polymer.

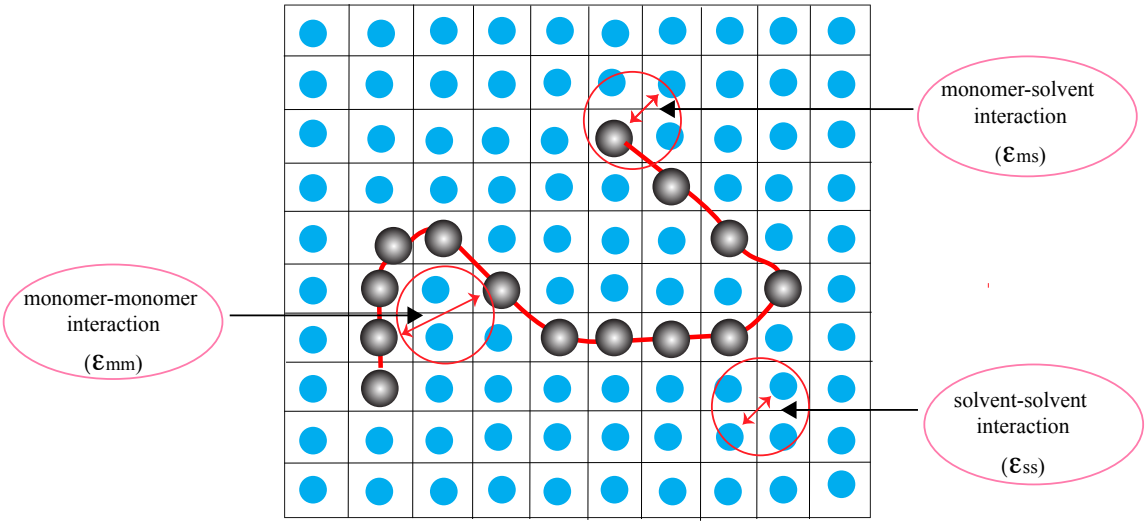

Figure 1.1 Flory-Huggins lattice model which illustrates the possible interactions present in polymer–solvent system. Blue: solvent molecules on lattice. Black: monomers on lattice.

Depending on the strength of the monomer-solvent interactions, solvents are classified as "good", "theta" or "poor". In a theta solvent, monomer-solvent interactions are balanced which facilitate the ideal behavior of the chains. In a good solvent, monomer-solvent interactions are stronger than the monomer-monomer interactions ($\epsilon_{ms} > \epsilon_{mm}$) and in poor solvents monomer-solvent interactions are weaker than the monomer-monomer

interactions ($\epsilon_{ms} < \epsilon_{mm}$). Polymer dimensions are governed by solvent quality. Radius of gyration $R_g \propto N^{\nu}$, where N is the degree of polymerization[35]. The exponent ν =3/5 for good solvent, 1/2 for theta solvent and 1/3 for poor solvent. A good solvent for a given polymer could be a poor solvent for a different polymer. As an example, water is a good solvent for the polyethylene glycol but is a poor solvent for the polystyrene[39] The behavior of polymer under good, poor and theta solvents is summarized in Figure 1.2.

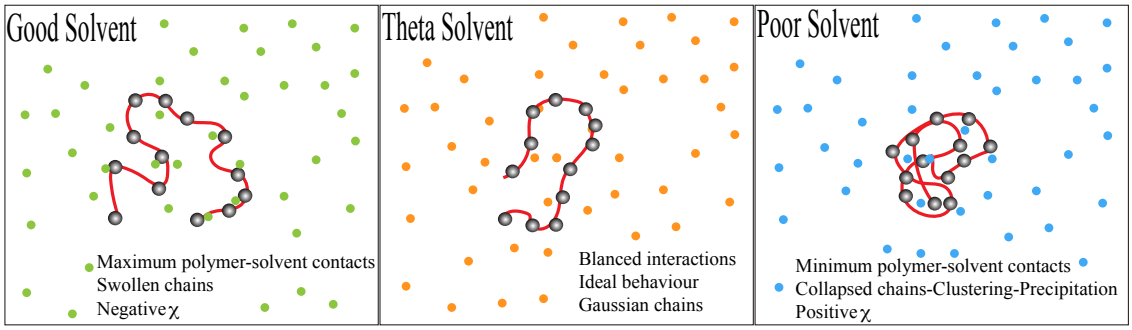

Figure 1.2 Single polymer chain in good, theta and poor solvents. green: good solvent molecules, orange: theta solvent molecules, blue: poor solvent molecules, black: monomers in polymer chain

In a good solvent, polymer-solvent contacts are maximized, and the chains are extended (swollen). In theta solvent all interactions are balanced, and chains are Gaussian. In poor solvent, polymer-solvent contacts are minimum, hence the polymer chain collapses which often results in clustering and precipitation.

1.2 Ionic polymers

Ionic polymers are macromolecules which have ionic or ionizable groups bounded to their structure.[40] They have current and potential applications in current energy related applications where transport of ions, electrons and solvent is required while maintaining

the chemical and mechanical stability. Ionic polymers which have only few ionic groups (<15%), bonded to polymer backbone, are called ionomers.[40-42] Those containing many ionic groups are water-soluble and called polyelectrolytes.[40-42] The morphology of ionomers is governed by properties of the ionizable groups as well as the backbone structure such as ionic fraction, type of ionic group, type of counter ion, solvation fraction, which finally affects the transport properties.

Nafion® (DuPont™),[43-46] a copolymer of perfluoro-3, 6-dioxa-4-methyl-7octene-sulfonic acid and tetrafluoroethylene, is one of the most extensively studied ionomer in last few decades. The chemical structure of Nafion is given in figure 3.

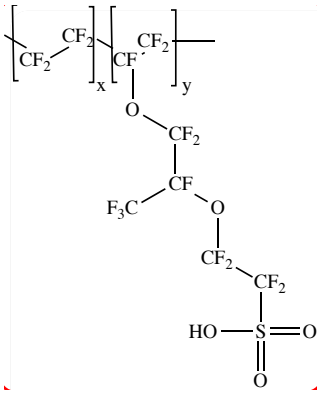

Figure 1.3 Chemical structure of Nafion®

With the exception of the sulfonic acid group, Nafion® is a fluorocarbon polymer which is extremely resistant to chemical attack. Membrane and solution studies[47-52] show sulfonic acid group adds capability of Nafion® to act as acid catalyst,[48, 49] ion exchange membranes[50, 51] and water absorption membranes.[52] Sulfonated polystyrene (PSS) has attracted attention in current energy applications due to its transport capability. Solution

and membrane studies have shown PSS can also be used as ion exchange membrane in fuel cells,[53, 54] acid catalysts in synthesis[55, 56] and in water softening.[34, 57]

The formation of ionic clusters in solutions and membranes controls the overall structure and dynamics as well as the transport properties of the ionomers. Cluster formation in ionomers is driven by the balance between the electrostatic interactions of the ionic groups and the segregation of hydrophilic and hydrophobic domains.[58-60] One of the first theoretical approaches to explain the cluster formation was done by Eisernberg.[34] According to his theory, the factors involved in cluster formation include the elastic forces of the hydrophobic chains and the electrostatic interactions between the ionizable groups. Ionizable groups form multiplets which finally ended up in clusters. The constraints affecting this ionic collapse to yield an ionic multiplet are the dimensions of polymer chains and the ion pairs, the tension on the chains resulting from ionic aggregation and the electrostatic energy released upon multiplet formation. Finally, a cluster will form when electrostatic interactions between ionizable groups are stronger than the elastic forces between hydrophobic domains.

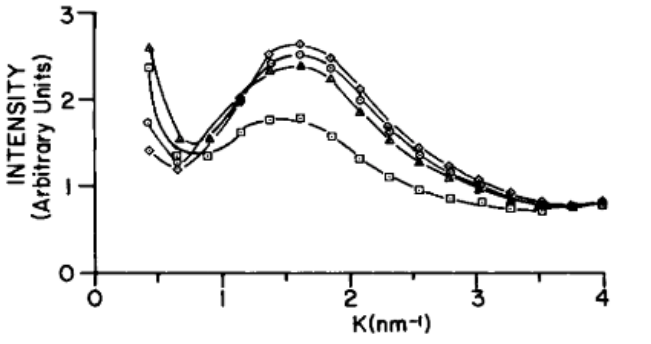

Figure 1.4 Small Angle X-ray Scattering (SAXS) intensity as a function of scattering vector for 3.85% sulfonated PS melt containing (◊) 0%, (O) 1%, (Δ) 2.3% and (□) 6.3% (wt) methanol.[64] The peak in scattering curve corresponds to ~40 Å in length scale which corresponds to ionic cluster.

The cluster formation of PSS and their morphology have observed by many groups by using X-rays and electron spin resonance (ESR) techiques[61-66]. Some experiments have shown that, the solvent quality also significantly affects the morphology of ionic clusters. Weiss and co-workers have observed the loading of methanol destroys the ionic domains formed in PSS membranes.[64]

Agrawal and co-workers have recently captured effect of dielectric constant on cluster morphology of PSS melts in their atomistic MD simulation studies.[67, 68] They have studied atactic polystyrene melt which has 80 PSS chains. Each chain was randomly sulfonated and to 0% sulfonation. The length of each chains was N=80, where N is the degree of polymerization. This system has followed with time under different dielectric constant (ϵ). There results show at ϵ =1 ionic groups associate into string like large aggregates. However, these large aggregates break into smaller domains with time with increasing dielectric constant of the medium. Cluster morphology as a function of dielectric constant is illustrated in Figure 1.5. These results reflect that the quality of the environment effects the morphology of ionic domains.

Even if ionomers have a better ion transport capability, under the conditions where ion transportation is optimized, ionic polymers becomes unstable. For many applications the ionic block is imbedded in nonionic segments for enhance the mechanical stability of the ionic co-polymer.

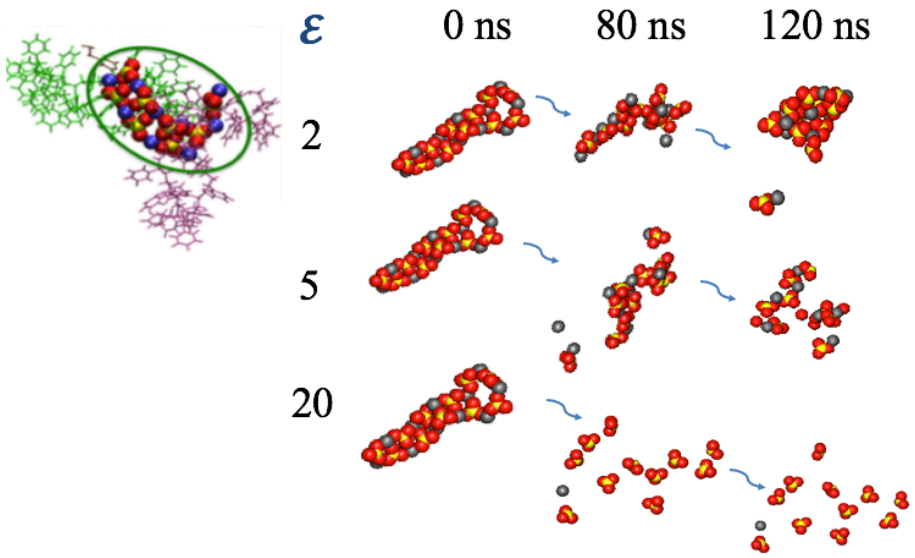

Figure 1.5 Effects of dielectric constant on cluster morphology of PSS melts studied by classical MD simulation. Image in the upper left corner shows a one ionic cluster and associated PS chains. Red color beads represent the O, yellow represent the S atoms and gray represents the Na+ ions. With increasing dielectric constant of the medium big ionic clusters break into smaller domains [67].

Block co-polymers

To understand the effects of polymer architectures coupled with charges, it is important to understand the assembly of neutral block co-polymers. Block co-polymers are hybrid macromolecules constructed by linking chemically distinct homo polymer blocks.[69] The precise synthesis of these self-assembling macro molecules gives extraordinary control over their morphology in solutions and melts. Tailoring different homo-polymer blocks to make a single block co-polymer molecule results extremely diverse topology. Some of the possible molecular architectures of dilblock and triblock copolymers are illustrated in Figure 1.6[32].

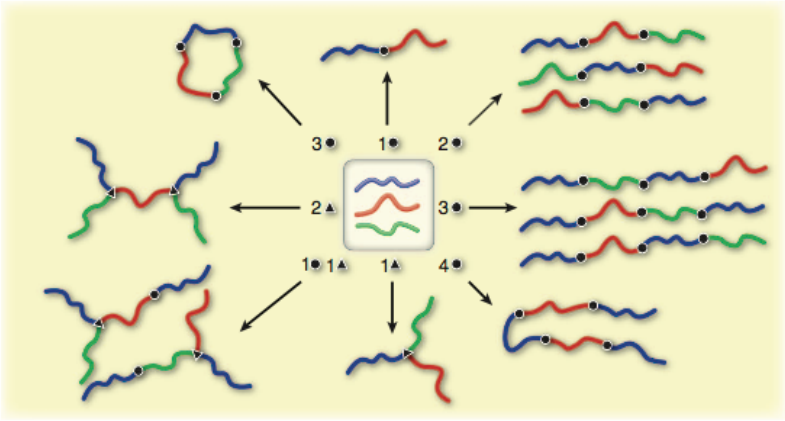

Figure 1.6 Schematic illustration of different architectures of diblock and triblocks by varying the number of blocks. Different color corresponds to different homo polymer segments. Black "dots" and "starts" corresponds to the different functional groups which are used to combined different segments.[32]

Association of linear AB type diblock co-polymers have been extensively studied in solutions[10-24]. AB type diblock copolymer segregate into lamellae, double- gyroid,

cylinders, and spheres in solutions depending on the relative fraction of the A and B blocks. Some of the neutral diblock morphologies formed by polystyrene-polyisoprene (PS-PI) in solutions are shown in Figure 1.7.[15]

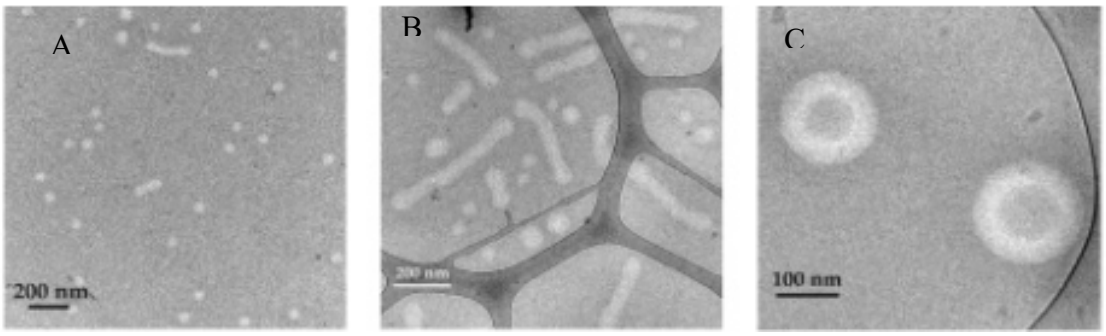

Figure 1.7 cryo-Transmission electron microscopy (cryo-TEM) images of different morphologies A) sphere B) cylinder C) vesicles formed by PS-PI diblock polymer in dialkyl phthalates solutions[15].

Extension of linear block co-polymers to ABA or ABAB, etc. affect only the physical properties of the polymer but not their phase behavior.[32, 70] However, addition of a third C block can dramatically expand the spectrum of the nano structures observed in solutions for ABC type triblock co-polymer.[70] Other than the sequence of the different blocks, different molecular variables such as polymer topology, number of blocks, number of block types, degree of polymerization and interaction parameter (χ)govern the phase behavior of multiblock co-polymers in solutions.[70]

Ionic block co-polymers

Ionic block co-polymers are type of block co-polymers which has an ioniziable group

attached to the chain. Addition of ionizable block converts block co-polymer to amphiphilic molecules. This results the dramatic change of chemical, structural and mechanical properties. The biggest advantage of tailoring ionic block to non-polar block is getting the capability to optimize transport property of the ionic block while maintain the structural stability of the polymer. Sulfonated polystyrene-*b*-polyisooprene (PSS-*b*-PI),[25] polystyrene-*b*-methyl methacrylate (PS-*b*-PMMA),[26] polystyrene-*b*-poly(acrylic acid) (PS-*b*-PAA),[27] are few examples for well-studied ionic block co-polymers. The structure of polystyrene based diblock co-polymer is shown in figure 1.8.

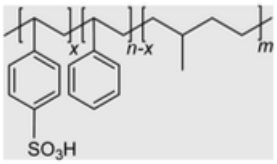

Figure 1.8 Chemical structure of di-block poly(styrene-b-methylbuthylene).

Introducing an ionizable block into block co-polymer increases the incompatibility of the different blocks, which causes to form thermodynamically stable micellar structures in solutions[25-27, 29-31]. Morphology of these micellar structures are governed by the degree of polymerization, volume fraction of each block and the χ. As an example, Eisenberg and co-workers have observed spherical, rod, bicontinous rod, lamellae, vesicles shape micelles for PS-*b*-PAA diblock copolymer in dimethylforamide (DMF)[31]. Some of these morphologies are illustrated in Figure 1.9.

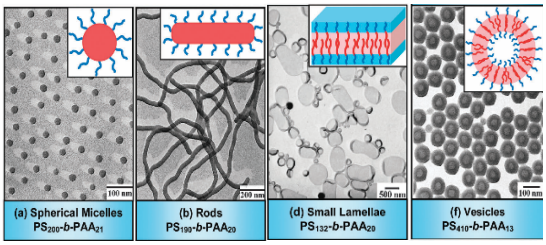

Figure 1.9 Transmission electron microscopy (TEM) images of different micellar morphologies formed by PS-b-PAA block copolymer in DMF for different volume fractions of PS and PAA[71].

1.5 Structured ionic block co-polymers

As discussed in previous section, phase behavior of ionic block co-polymers in solutions becomes more complicated with increasing the complexity of the polymer structure. However, increasing the number of block types allows one to tailor the different chemical identity to the polymer. This makes ionic block co-polymer highly structured. In the current research we are focusing on structured ABCBA type symmetric ionic pentablock co-polymer. This well-structured ionic block copolymer consists of randomly sulfonated PS block at center and polyethylene-polypropylene (PEP) block attaching to both side of the PSS block and tertiary butyl polystyrene (t-BPS) block at the end. The exact chemical composition is given is Figure 1.10.

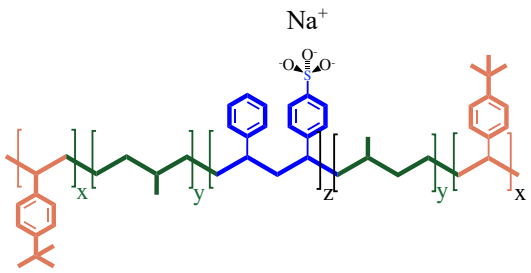

Figure 1.10 Chemical structure of pentablock (poly(t-butyl-styrene)-*b*-ethylene-r-propylene-*b*-styrene-r-styrenesulfonate-*b*-ethylene-r-propylene-*b*-poly(t-butyl-styrene) molecule. Volume fractions of t-BPS: 20%, PEP:40% and PSS:40%. Polymer synthesized by Kraton polymer LLSC.

The different blocks in this complex block co-polymer have different chemical identity, thus they can perform different tasks. The center PSS blocks governs the transport properties of the polymer. It can attract counter ions such as H^+, Na^+ or K^+. Transportability can be optimized by changing the sulfonation level. The tethered PEP block modifies the elasticity which gives a flexibility to the polymer. The end t-BPS block is a chemically inert bulky group which gives a mechanical stability to the polymer.

Different research groups are working to understand the behavior of pentablock copolymer in solutions and in films experimentally[72-79] as well as computaionally.[80-84] Geise et al. have observed that water uptake, water permeability and salt permeability of the membrane increases with increasing the sulfonation level.[72-74] Winey and coworkers have observed formation of spherical micelle by X-ray scattering experiments in a nonploar mixed solvent (cyclohexane:heptane (1:1)) at higher polymer concentrations >10wt%.[76] Etempawala et al. have studied the association of pentablock in a cyclohexane:heptane (1:1) mixture in lower concentrations (<6wt%) by neurons scattering experiments.[85] They have concluded that polymer assembles into micellar structures where ionic block form an inner ellipsoidal core and end block and PEP blocks retain in the corona.

Aryal and coworkers have studied to aggregation of polymer in a 1:1 cyhclohexane:heptane mixture and in water by atomistic MD simulations.[80, 81] Their study shows that in a non-polar solvent, the t-BPS and PI blocks stay at interface to form outer corona while PSS block collapsed to form an inner dense core. However, in water where dielectric constant is higher, the PSS block migrates to the water polymer interface. Their aggregation study results are illustrated in Figure 1.11.

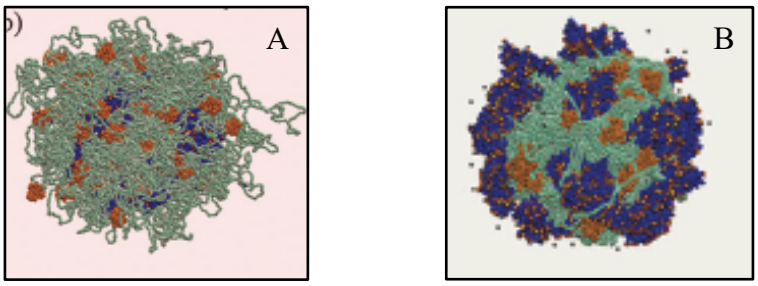

Figure 1.11 Aggregates (30 chains, molecular weight of each chains ~50000 g/mol) of polymer shown in Figure 10, studied by atomistic MD simulations in A) cyclohexane:heptane (1:1) and B) in water. Green represents the PI blocks, orange represents the t-BPS blocks and blue represents the ionic PSS blocks.[73] The solvent is not shown for clarity.

The above studies reflect the fact that this pentablock co-polymer forms aggregates in both polar and non-polar solvents. However, the solution behavior of this complex molecule is not well understood. The effects of solvent quality on aggregation, response of different blocks to different solvent environments, possible morphological changes of the aggregates as a response to different solvent stimuli, are questions that remain to be addressed.

Outline and Contribution

This dissertation includes several approaches to understand the fundamentals of structure and dynamics of highly structured ionic block co-polymer in solutions and. membrane. This also address the effects of associating groups on structure and dynamics of linear and star polymer melts. Finally, the dissertation also includes the synthesis of bio compatible luminous polymer and their characterization. The dissertation is organized as follows..

Chapter 2 will review the principals of experimental and computational techniques. Our investigation required to probe the solution and membrane structure of polymers in multiple length scale, which includes atomistic to nanoscale. We used the small angle neutron scattering (SANS) as our tool to investigate solution structure of polymer and we used the atomistic molecular dynamics simulation (MD) to probe the structure of polymer in solution and membrane in atomistic scale.

Chapter 3 discusses discuss the effects of solvent polarity on aggregation of ionic block copolymer in solution for 26% and 52% sulfonation levels. We changed the solvent polarity by addition of propanol to cyclohexane and observed a phase transition of polymer upon addition of propanol to cyclohexane.

Chapter 4 discusses effects of solvent polarity on assembly of pentablock ionic co-polymer by MD simulations. We observed that pentablock aggregate into micelle structure at very low concentrations in both polar and non-polar medium. We further observed that polar and non-polar blocks response to solvent polarity of the medium due selective binding of solvents to the different blocks.

Chapter 5 probe a symmetric block co-polymer with a sulfonated polystyrene center tethered to polyethylene-r-propylene and terminated by poly(t-butyl styrene) at the interface with water, propanol and THF using molecular dynamics simulations. We find that the interfacial width at the water interface decreases, exposing more ionizable groups whereas the interfacial width for the propanol and THF systems increases and is dominated by hydrophobic blocks. Water molecules associate predominantly with the ionic blocks while propanol and THF reside in both the ionic and non-ionic segments.

Chapter 6 explore the effect of associating groups on structure and dynamics of linear and star polymer melts using molecular dynamics simulations. We found with increasing associating strength, the polymers associate into clusters of increasing size, independent of the polymer topography. Blends of chains with and without associating groups globally phase segregate even for relatively weak interaction between the associating groups.

Chapter 7 discusses synthesis of biotin substituted PPE and their characterization. We synthesized biotin substituted PPE with 50% of monomers having the biotin groups. We observed that biotin substituted PPE has lower CMC than the PPE with no biotin groups.

Reference:

1. Kataoka, K.; Harada, A.; Nagasaki, Y., Block copolymer micelles for drug delivery: design, characterization and biological significance. *Advanced drug delivery reviews* **2012,** *64*, 37-48.
2. Jeong, B.; Bae, Y. H.; Lee, D. S.; Kim, S. W., Biodegradable block copolymers as injectable drug-delivery systems. *Nature* **1997,** *388* (6645), 860-862.

3. Gaucher, G.; Dufresne, M.-H.; Sant, V. P.; Kang, N.; Maysinger, D.; Leroux, J.-C., Block copolymer micelles: preparation, characterization and application in drug delivery. *Journal of controlled release* **2005,** *109* (1-3), 169-188.

4. Orilall, M. C.; Wiesner, U., Block copolymer based composition and morphology control in nanostructured hybrid materials for energy conversion and storage: solar cells, batteries, and fuel cells. *Chemical Society Reviews* **2011,** *40* (2), 520-535.

5. Darling, S. B., Block copolymers for photovoltaics. *Energy & Environmental Science* **2009,** *2* (12), 1266-1273.

6. Liu, J.; Sheina, E.; Kowalewski, T.; McCullough, R. D., Tuning the electrical conductivity and self-assembly of regioregular polythiophene by block copolymerization: nanowire morphologies in new di-and triblock copolymers. *Angewandte Chemie International Edition* **2002,** *41* (2), 329-332.

7. Jackson, E. A.; Hillmyer, M. A., Nanoporous membranes derived from block copolymers: from drug delivery to water filtration. *ACS nano* **2010,** *4* (7), 3548-3553.

8. Bondar, V.; Freeman, B.; Pinnau, I., Gas sorption and characterization of poly (ether-b-amide) segmented block copolymers. *Journal of Polymer Science Part B: Polymer Physics* **1999,** *37* (17), 2463-2475.

9. Bondar, V.; Freeman, B.; Pinnau, I., Gas transport properties of poly (ether-b-amide) segmented block copolymers. *Journal of Polymer Science Part B: Polymer Physics* **2000,** *38* (15), 2051-2062.

10. LaRue, I.; Adam, M.; Da Silva, M.; Sheiko, S. S.; Rubinstein, M., Wormlike micelles of block copolymers: Measuring the linear density by AFM and light scattering. *Macromolecules* **2004,** *37* (13), 5002-5005.

11. Cheng, G.; Hammouda, B.; Perahia, D., Effects of Intermicellar Interactions on the Dissociation of Block Copolymer Micelles: SANS and NMR Studies. *Macromolecular Chemistry and Physics* **2014,** *215* (4), 341-350.

12. Balsara, N.; Perahia, D.; Safinya, C.; Tirrell, M.; Lodge, T., Birefringence detection of the order-to-disorder transition in block copolymer liquids. *Macromolecules* **1992,** *25* (15), 3896-3901.

13. Balsara, N.; Hammouda, B.; Kesani, P.; Jonnalagadda, S.; Straty, G., In-situ small-angle neutron scattering from a block copolymer solution under shear. *Macromolecules* **1994,** *27* (9), 2566-2573.

14. Pedersen, J. S.; Gerstenberg, M. C., The structure of P85 Pluronic block copolymer micelles determined by small-angle neutron scattering. *Colloids and Surfaces A: Physicochemical and Engineering Aspects* **2003,** *213* (2-3), 175-187.

15. Bang, J.; Jain, S.; Li, Z.; Lodge, T. P.; Pedersen, J. S.; Kesselman, E.; Talmon, Y., Sphere, cylinder, and vesicle nanoaggregates in poly (styrene-b-isoprene) diblock copolymer solutions. *Macromolecules* **2006,** *39* (3), 1199-1208.

16. Bang, J.; Viswanathan, K.; Lodge, T. P.; Park, M. J.; Char, K., Temperature-dependent micellar structures in poly (styrene-b-isoprene) diblock copolymer solutions near the critical micelle temperature. *The Journal of chemical physics* **2004,** *121* (22), 11489-11500.

17. LaRue, I.; Adam, M.; Zhulina, E. B.; Rubinstein, M.; Pitsikalis, M.; Hadjichristidis, N.; Ivanov, D. A.; Gearba, R. I.; Anokhin, D. V.; Sheiko, S. S., Effect of the soluble block size on spherical diblock copolymer micelles. *macromolecules* **2008,** *41* (17), 6555-6563.

18. Lund, R.; Pipich, V.; Willner, L.; Radulescu, A.; Colmenero, J.; Richter, D., Structural and thermodynamic aspects of the cylinder-to-sphere transition in amphiphilic diblock copolymer micelles. *Soft Matter* **2011,** *7* (4), 1491-1500.

19. Jensen, G. V.; Shi, Q.; Deen, G. R.; Almdal, K.; Pedersen, J. S., Structures of PEP–PEO Block Copolymer Micelles: Effects of Changing Solvent and PEO Length and Comparison to a Thermodynamic Model. *Macromolecules* **2012,** *45* (1), 430-440.

20. Zhulina, E. B.; Adam, M.; LaRue, I.; Sheiko, S. S.; Rubinstein, M., Diblock copolymer micelles in a dilute solution. *Macromolecules* **2005,** *38* (12), 5330-5351.

21. Yu, K.; Eisenberg, A., Bilayer morphologies of self-assembled crew-cut aggregates of amphiphilic PS-b-PEO diblock copolymers in solution. *Macromolecules* **1998,** *31* (11), 3509-3518.

22. Schillen, K.; Bryskhe, K.; Mel'Nikova, Y. S., Vesicles formed from a poly (ethylene oxide)− poly (propylene oxide)− poly (ethylene oxide) triblock copolymer in dilute aqueous solution. *Macromolecules* **1999,** *32* (20), 6885-6888.

23. Wang, X.; Guerin, G.; Wang, H.; Wang, Y.; Manners, I.; Winnik, M. A., Cylindrical block copolymer micelles and co-micelles of controlled length and architecture. *Science* **2007,** *317* (5838), 644-647.

24. Dean, J. M.; Verghese, N. E.; Pham, H. Q.; Bates, F. S., Nanostructure Toughened Epoxy Resins. *Macromolecules* **2004,** *37* (5), 1998-1998.

25. Mani, S.; Weiss, R.; Williams, C.; Hahn, S., Microstructure of ionomers based on sulfonated block copolymers of polystyrene and poly (ethylene-alt-propylene). *Macromolecules* **1999,** *32* (11), 3663-3670.

26. Rubatat, L.; Li, C.; Dietsch, H.; Nykänen, A.; Ruokolainen, J.; Mezzenga, R., Structure− properties relationship in proton conductive sulfonated polystyrene− polymethyl methacrylate block copolymers (PSS− PMMA). *Macromolecules* **2008,** *41* (21), 8130-8137.

27. Lim Soo, P.; Eisenberg, A., Preparation of block copolymer vesicles in solution. *Journal of Polymer Science Part B: Polymer Physics* **2004,** *42* (6), 923-938.

28. Zhang, L.; Eisenberg, A., Multiple morphologies and characteristics of "crew-cut" micelle-like aggregates of polystyrene-b-poly (acrylic acid) diblock copolymers in aqueous solutions. *Journal of the American Chemical Society* **1996,** *118* (13), 3168-3181.

29. Zhang, L.; Barlow, R. J.; Eisenberg, A., Scaling relations and coronal dimensions in aqueous block polyelectrolyte micelles. *Macromolecules* **1995,** *28* (18), 6055-6066.

30. Khougaz, K.; Astafieva, I.; Eisenberg, A., Micellization in block polyelectrolyte solutions. 3. Static light scattering characterization. *Macromolecules* **1995,** *28* (21), 7135-7147.

31. Cameron, N. S.; Corbierre, M. K.; Eisenberg, A., 1998 EWR Steacie Award Lecture Asymmetric amphiphilic block copolymers in solution: a morphological wonderland. *Canadian journal of chemistry* **1999,** *77* (8), 1311-1326.

32. Bates, F. S.; Hillmyer, M. A.; Lodge, T. P.; Bates, C. M.; Delaney, K. T.; Fredrickson, G. H., Multiblock polymers: panacea or Pandora's box? *Science* **2012,** *336* (6080), 434-440.

33. AJ., J., Introduction to small-angle neutron scattering and neutron reflectometry. NIST Center for Neutron Research: Gaitherburg, MD, 2008.

34. Eisenberg, A., Clustering of ions in organic polymers. A theoretical approach. *Macromolecules* **1970,** *3* (2), 147-154.

35. I., T., *Frontmatter and Index*. John Wiley & Sons, Inc.: 2002.

36. PJ., F., *Principles of polymer chemistry*. Cornell University Press: 1953.

37. De Gennes, P.-G.; Gennes, P.-G., *Scaling concepts in polymer physics*. Cornell university press: 1979.

38. Rubinstein M, C. R., Polymer physics. Oxford university press: New York, 2003.

39. Brandrup, J.; Immergut, E., Polymer Handbook, Solubility Parameter Values. Wiley: New York: 1989.

40. Hendy, B., Ionic polymers. In *Specialty Polymers*, Springer: 1987; pp 110-149.

41. Weiss, R.; Turner, S.; Lundberg, R., Sulfonated polystyrene ionomers prepared by emulsion copolymerization of styrene and sodium styrene sulfonate. *Journal of Polymer Science: Polymer Chemistry Edition* **1985,** *23* (2), 525-533.

42. Weiss, R.; Sen, A.; Willis, C.; Pottick, L., Block copolymer ionomers: 1. Synthesis and physical properties of sulphonated poly (styrene-ethylene/butylene-styrene). *Polymer* **1991,** *32* (10), 1867-1874.

43. Mauritz, K. A.; Moore, R. B., State of understanding of Nafion. *Chemical reviews* **2004,** *104* (10), 4535-4586.

44. Gebel, G.; Lambard, J., Small-angle scattering study of water-swollen perfluorinated ionomer membranes. *Macromolecules* **1997,** *30* (25), 7914-7920.

45. Gebel, G., Structural evolution of water swollen perfluorosulfonated ionomers from dry membrane to solution. *Polymer* **2000,** *41* (15), 5829-5838.

46. Rubatat, L.; Gebel, G.; Diat, O., Fibrillar structure of Nafion: Matching Fourier and real space studies of corresponding films and solutions. *macromolecules* **2004,** *37* (20), 7772-7783.

47. Harmer, M. A.; Farneth, W. E.; Sun, Q., High surface area nafion resin/silica nanocomposites: a new class of solid acid catalyst. *Journal of the American Chemical Society* **1996,** *118* (33), 7708-7715.

48. Olah, G. A., Synthetic methods and reactions. li: a convenient and improved method for esterification over nafion h2, a superacidic perfluorinated resinsulfonic acid catalysts. **1978**.

49. Yeager, H.; Steck, A., Cation and water diffusion in Nafion ion exchange membranes: influence of polymer structure. *Journal of the Electrochemical Society* **1981,** *128* (9), 1880.

50. Szentirmay, M. N.; Martin, C. R., Ion-exchange selectivity of Nafion films on electrode surfaces. *Analytical chemistry* **1984,** *56* (11), 1898-1902.

51. Morris, D. R.; Sun, X., Water-sorption and transport properties of Nafion 117 H. *Journal of applied polymer science* **1993,** *50* (8), 1445-1452.

52. Duplessix, R.; Escoubes, M.; Rodmacq, B.; Volino, F.; Roche, E.; Eisenberg, A.; Pineri, M., Water absorption in acid Nafion membranes. ACS Publications: 1980.

53. LeBlanc Jr, O. H.; Ward, W. J.; Matson, S. L.; Kimura, S. G., Facilitated transport in ion-exchange membranes. *Journal of Membrane science* **1980,** *6*, 339-343.

54. Siril, P.; Cross, H. E.; Brown, D., New polystyrene sulfonic acid resin catalysts with enhanced acidic and catalytic properties. *Journal of Molecular Catalysis A: Chemical* **2008,** *279* (1), 63-68.

55. Zuo, Y.; Zhang, Y.; Fu, Y., Catalytic conversion of cellulose into levulinic acid by a sulfonated chloromethyl polystyrene solid acid catalyst. *ChemCatChem* **2014,** *6* (3), 753-757.

56. Bekri-Abbes, I.; Bayoudh, S.; Baklouti, M., The removal of hardness of water using sulfonated waste plastic. *Desalination* **2008,** *222* (1-3), 81-86.

57. Baum, R. N.; Rebis, E. N.; Reilly, P. B., Sulfonated polystyrene compositions and methods of treating boiler water. Google Patents: 1971.

58. Eisenberg, A.; Hird, B.; Moore, R., A new multiplet-cluster model for the morphology of random ionomers. *Macromolecules* **1990,** *23* (18), 4098-4107.

59. Yarusso, D. J.; Cooper, S. L., Microstructure of ionomers: interpretation of small-angle x-ray scattering data. *Macromolecules* **1983,** *16* (12), 1871-1880.

60. Kruczala, K.; Schlick, S., Interaction of ionomers and polyelectrolytes with divalent transition metal cations (Cu2+ and VO2+): A study by electron spin resonance (ESR) spectroscopy and viscosimetry. *The Journal of Physical Chemistry B* **1999,** *103* (11), 1934-1943.

61. Weiss, R.; Fitzgerald, J.; Kim, D., Viscoelastic behavior of lightly sulfonated polystyrene ionomers. *Macromolecules* **1991,** *24* (5), 1071-1076.

62. Register, R. A.; Cooper, S. L., Anomalous small-angle x-ray scattering from nickel-neutralized ionomers. 1. Amorphous polymer matrixes. *Macromolecules* **1990,** *23* (1), 310-317.

63. Lu, X.; Weiss, R., Specific interactions and ionic aggregation in miscible blends of nylon-6 and zinc sulfonated polystyrene ionomer. *Macromolecules* **1992,** *25* (23), 6185-6189.

64. Fitzgerald, J.; Kim, D.; Weiss, R., The effect of diluents on the ionic interactions in sulfonated polystyrene ionomers. *Journal of Polymer Science Part C: Polymer Letters* **1986,** *24* (6), 263-268.

65. Kim, J.-S.; Kim, H.-S.; Nah, Y. H.; Eisenberg, A., Morphology and mechanical properties of styrene homoblends of methacrylate and sulfonate ionomers. *Polymer Bulletin* **1998,** *41* (5), 609-614.

66. Castagna, A. M.; Wang, W.; Winey, K. I.; Runt, J., Influence of cation type on structure and dynamics in sulfonated polystyrene ionomers. *Macromolecules* **2011,** *44* (13), 5420-5426.

67. Agrawal, A.; Perahia, D.; Grest, G. S., Clustering effects in ionic polymers: Molecular dynamics simulations. *Physical Review E* **2015,** *92* (2), 022601.

68. Agrawal, A.; Perahia, D.; Grest, G. S., Cluster morphology-polymer dynamics correlations in sulfonated polystyrene melts: computational study. *Physical review letters* **2016,** *116* (15), 158001.

69. Bates, F. S.; Fredrickson, G., Block copolymers-designer soft materials. *Physics today* **2000,** *52*.

70. Hermel, T.; Hahn, S.; Chaffin, K.; Gerberich, W.; Bates, F., Role of molecular architecture in mechanical failure of glassy/semicrystalline block copolymers: CEC vs CECEC lamellae. *Macromolecules* **2003,** *36* (7), 2190-2193.

71. Palanisamy, A. *Synthesis and self-assembly of block copolymer/conjugated polymer complexes*; Deakin University: 2015.

72. Geise, G. M.; Willis, C. L.; Doherty, C. M.; Hill, A. J.; Bastow, T. J.; Ford, J.; Winey, K. I.; Freeman, B. D.; Paul, D. R., Characterization of aluminum-neutralized sulfonated styrenic pentablock copolymer films. *Industrial & Engineering Chemistry Research* **2013,** *52* (3), 1056-1068.

73. Geise, G.; Freeman, B.; Paul, D., Characterization of a sulfonated pentablock copolymer for desalination applications. *Polymer* **2010,** *51* (24), 5815-5822.

74. Geise, G. M.; Doherty, C. M.; Hill, A. J.; Freeman, B. D.; Paul, D. R., Free volume characterization of sulfonated styrenic pentablock copolymers using positron annihilation lifetime spectroscopy. *Journal of membrane science* **2014,** *453*, 425-434.

75. Choi, J.-H.; Willis, C. L.; Winey, K. I., Effects of neutralization with Et3Al on structure and properties in sulfonated styrenic pentablock copolymers. *Journal of membrane science* **2013,** *428*, 516-522.

76. Choi, J.-H.; Kota, A.; Winey, K. I., Micellar morphology in sulfonated pentablock copolymer solutions. *Industrial & engineering chemistry research* **2010,** *49* (23), 12093-12097.

77. Fan, Y.; Cornelius, C. J., Raman spectroscopic and gas transport study of a pentablock ionomer complexed with metal ions and its relationship to physical properties. *Journal of Materials Science* **2013,** *48* (3), 1153-1161.

78. Lee, J.-W.; Hong, S. M.; Kim, J.; Koo, C. M., Novel sulfonated styrenic pentablock copolymer/silicate nanocomposite membranes with controlled ion channels and their IPMC transducers. *Sensors and Actuators B: Chemical* **2012,** *162* (1), 369-376.

79. Choi, J.-H.; Willis, C. L.; Winey, K. I., Structure–property relationship in sulfonated pentablock copolymers. *Journal of membrane science* **2012,** *394*, 169-174.

80. Aryal, D.; Etampawala, T.; Perahia, D.; Grest, G. S., Phase Behavior of a Single Structured Ionomer Chain in Solution. *Macromolecular Theory and Simulations* **2014,** *23* (9), 543-549.

81. Aryal, D.; Grest, G. S.; Perahia, D., Soft nanoparticles: nano ionic networks of associated ionic polymers. *Nanoscale* **2017,** *9* (6), 2117-2122.

82. Aryal, D.; Perahia, D.; Grest, G. S., Solvent controlled ion association in structured copolymers: Molecular dynamics simulations in dilute solutions. *The Journal of chemical physics* **2015,** *143* (12), 124905.

83. Aryal, D.; Agrawal, A.; Perahia, D.; Grest, G. S., Structure and Dynamics of Ionic Block Copolymer Melts: Computational Study. *Macromolecules* **2017,** *50* (18), 7388-7398.

84. Aryal, D.; Agrawal, A.; Perahia, D.; Grest, G. S., Structured Ionomer Thin Films at Water Interface: Molecular Dynamics Simulation Insight. *Langmuir* **2017,** *33* (41), 11070-11076.

85. Etampawala, T. N.; Aryal, D.; Osti, N. C.; He, L.; Heller, W. T.; Willis, C. L.; Grest, G. S.; Perahia, D., Association of a multifunctional ionic block copolymer in a selective solvent. *The Journal of chemical physics* **2016,** *145* (18), 184903.

CHAPTER TWO

METHODOLOGY

Small angle neutron scattering (SANS)

Scattering is a result of the interactions occurs between waves and the objects which have same dimension of wavelength. It depends on the type of the interaction occurs between waves and objects. In X-ray scattering, incident waves interact with the electrons while neutrons interact with the nucleus. Possible interactions between different electromagnetic radiations and different types of particles are illustrated in Figure 2.1.[1]

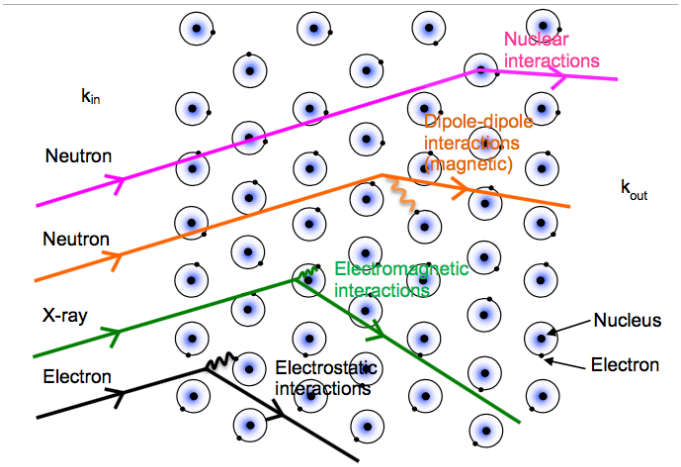

Figure 2.1 Schematic illustration of scattering occurs between different electromagnetic radiations and the matter.[1]

Scattering changes direction of the incident beam while energy may or may not be affected. In an elastic scattering where no energy exchange is occurred, magnitude of the incident wave vector (k_i) is equal to the magnitude of scattered wave vector (k_f). However, changing the direction of the incident wave vector results a momentum change and it is called momentum transfer vector (q). k*i*, k_f and q is illustrated in Figure 2.2.[2-5]

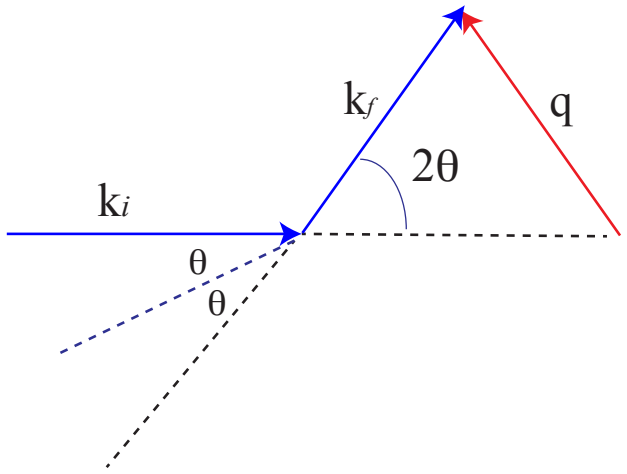

Figure 2.2 Vector diagram of elastic scattering which illustrates the relationship between incident and scattered wave vector (k_i, k_f), scattering angle (θ) and momentum transfer vector (q).

For elastic scattering, where no energy change occurs, absolute value of the wave vector is given in equation 2.1. Here, λ is the wavelength.

$$|k_i| = |k_f| = {}^{2\pi}/_{\lambda} \qquad (2.1)$$

$$q = k_i - k_f \qquad (2.2)$$

$$q = \frac{4\pi * sin\theta}{\lambda} \quad (2.3)$$

The momentum transfer vector, which given in equation 2.2, is the difference between incident and final wave vector. The dependency of q on scattering angle (θ) and the corresponding wavelength (λ) is given in equation 2.3.

Scattered neutrons should follow the Bragg's equation, which is given in equation 2.4, to occur a constructive interference. Here d is the spacing between the two scattering points[2, 3].

$$2d * sin\theta = n\lambda \quad (2.4)$$

By equation 2.3 and 2.4, relationship between the q and the length scale (d) of the object can be written as in equation 2.5.

$$q = \frac{2\pi n}{d} \quad (2.5)$$

In Equation 2.5, d is the distance between two scattering planes and n is a positive integer. It shows that q is inversely proportional to the d. This suggests that in a scattering

experiment large dimensions are captured at lower q while small dimensions are captured at higher q.

The physical quantity which is measured in scattering experiment is the scattering intensity (I). it is often recorded as a function of q or function of 2θ. The fraction of neutrons scattered into solid angle (dΩ) (Figure 2.3) with a scattering angle θ is known as the microscopic scattering cross-section (dσ)[2, 3].

.

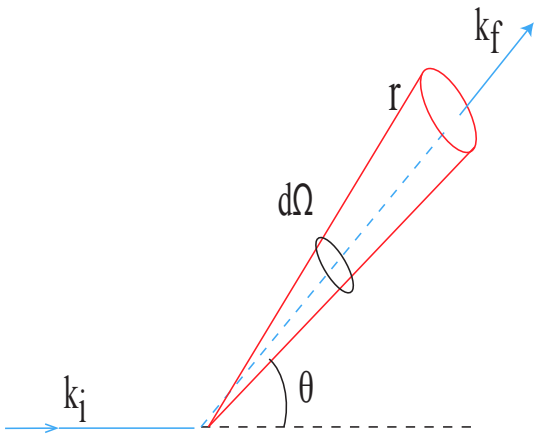

Figure 2.3 Schematic for the defining of solid angle

The differential cross-section, which gives the macroscopic scattering cross section is equal to the measured absolute intensity (I(q)), is given in equation 2.6,[1, 2, 4-6]

$$\frac{d\sigma}{d\Omega}(q) = I(q) = \frac{1}{N}\left|\sum_{j=1}^{N} b_i\, e^{iq_{rj}}\right|^2 \qquad (2.6)$$

Here, r is the position of nuclei, b is the scattering length of nuclei i, and N is the total number of atoms. Above equation can be rewrite as equation 2.7, by integrating over the volume of the sample. Here, $\rho(r)$ is called local scattering length density.

$$\frac{d\sigma}{d\Omega}(q) = I(q) = \frac{1}{N}\left|\int dr\rho(r)\, e^{iq_r}\right|^2 \tag{2.7}$$

Scattering length (b_i) is a characteristic of the nucleus which measures strength of the interactions between nucleus and the electromagnetic radiations. The scattering length density (b) which is the normalized sum of scattering length of all the elements in the scattering object is as given in equation 2.8.[2]

$$b = \frac{\rho N_A}{M_W}\sum_0^i b_i \tag{2.8}$$

In this equation, ρ is the density of scattering object, N_A is the Avogadro's number, M_W is the molecular weight of the scattering objects and b_i is the scattering length of each element in the scattering object.

SANS experiments measure the absolute intensity as a function of q. The factors affect the total absolute intensity is given in equation 2.9.[2, 3]

$$I(q) = \left[\frac{N}{V}\right] * V_p^2 * \Delta\rho * P(q) * S(q) \tag{2.9}$$

Here, N/V is the number density, V_p is particle volume, Δρ is contrast factor, P(q) is form factor of the object and S(q) is the structure factor.

Contrast factor: The contrast factor for a two-component system is defined in equation 2.10 which is the scattering length density difference of the two objects. In SANS experiments, isotopic labeling of one object will results a higher contras factor which gives a better special resolution.

$$\Delta\rho^2 = (\rho_A - \rho_B)^2 \qquad (2.10)$$

Form factor: The scattering experiments are performed in Fourier space not in real space. Therefore, like in microscopic technique, scattering pattern does not give the information of the scattered object directly. In order to get the information in the real space, we have to do the inverse furrier transform or a fitting of data to a model. Model fitting is more popular in the scattering community. The reciprocal spaces of most of real space shapes are mathematically modeled and available with different open source programs to use in. Some of the well-established form factors are summarized in following table 2.1 [2, 3, 7-9].

With increasing the complexity of the shape of the aggregate, more variables are needed to describe the complete form factor. As an example, form factor for a core-shell structure which has homogeneous spherical center (core) and Gaussian decaying corona (brush) is given in equation 2.11. This form factor is first derived by Pederson[10, 11] and being using to model the micelles.

Form factor geometry	Form factor
Spherical[3]	$P(q) = \frac{[\sin(qR) - qRcos(qR)}{qR^3}$ R=Radios of sphere
Cylindrical[3]	$P(q) = \frac{scale}{V_{cyl}} \int_o^{\pi/2} f^2\,(q,\alpha) sin\alpha d\alpha$ $f(q,\alpha) = 2(\rho_{cyl} - \rho_{solv}) V_{cyl} j_0(qHcos\alpha) \frac{J_1(qrsin\alpha)}{(qrsin\alpha)}$ H=Length of the cylinder r = Radios of the cylinder α = Orientation of the cylinder J1 = first order Bessel function
Lamella[9]	$P(q) = \frac{2\Delta\rho^2}{\rho^2}\left[1 - \cos\,(q\delta) e^{-q^2\sigma^2/2}\right]$ δ = Bilayer thickness σ = Polydispersity σ
Gaussian chain[8]	$P(q) = scale \frac{2\left[(1+Ux)^{-1/U} + x - 1\right]}{(1+U)x^2} + bkg$ U = Polydispersity

Table 2.1 Different form factors used in SANS data

Four different interaction terms are encapsulated in this complex form factor. Two of them are self-correlation terms, P_{core} and P_{brush}, for core and corona and other two, $S_{brush-core}$, $S_{brush-brush}$, are cross terms between core-corona and the corona-corona.

$$P_{micell} = N_{agg}^2 \beta_{core}^2 P_{core}(q) + N_{agg} \beta_{brush}^2 P_{brush}(q) + 2N_{agg}^2 \beta_{core} \beta_{brush} S_{brush-core}(q) + N_{agg}(N_{agg} - 1) \beta_{brush}^2 S_{brush-brush}(q) \quad (2.11)$$

P_{core} describe the interactions of chains in the homogeneous core in the center and decaying core segments density at core-corona interface. P_{brush} describe Gaussian chains in corona and it follows the Debye function. $S_{brush-core}$ address the roughness of the interface between core and corona and $S_{brush-brush}$ consists of the interaction between chains in the corona. Here, β_{core} and β_{brush} are the total excess scattering length densities of the core and the corona. P_{core}, P_{brush}, $S_{brush-core}$, $S_{brush-brush}$ terms are mathematically defined in separate set of functions where aggregate dimensions are accounted. The schematic representation of this form factor is shown in Figure 2.4.

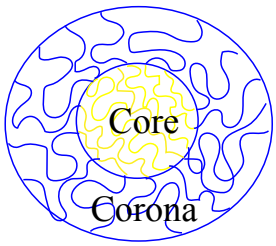

Figure 2.4 Schematic representation of core-shell model which has spherical core and Gaussian decaying corona.

Structure factor: Structure factor represent the effect of inter particle scattering on the absolute intensity. As form factor this is also mathematically formulated for different object and available to use. However, for the very dilute solutions, the effect of structure factor is not intense enough to visible in scattering profiles.

Molecular dynamics simulations

Even though experimental techniques like SAXS or SANS are capable of giving details about microphase structure and the dynamic of a given system, they are not capable enough to give atomic level information that govern the macroscopic properties. To study the behavior of a system in atomic scale, classical molecular dynamics simulations would be a grate tool.

In classical molecular dynamics simulations Newton's second law of motions is solved numerically for set of particles to generate the trajectory, velocity and the positions. Newton's law of motions is given in equation 2.12[12].

$$F_i = m_i a_i \tag{2.12}$$

Where F_i is the force acting on the desired particle i, m_i is the mass of the particle i an a_i is the acceleration of the particle i. Force (F_i) is the first time derivate of v where v is the potential energy.

$$F_i = \frac{\partial U_i}{\partial t} \tag{2.13}$$

With knowing the acceleration of the particles velocity (v) and the new positions (r) of the particles can be calculated after a given period of time Δt. Velocity-Verlet[13, 14] algorithms will be used to generate the new positions and velocities.

$$r(t + \Delta t) = r(t) + v(t)\Delta t + \frac{1}{2}\, a(t)\Delta t^2 \qquad (2.14)$$

$$v(t + \Delta t) = v(t) + \frac{1}{2}\Delta t[a(t) + a(t + \Delta t)] \qquad (2.15)$$

A flow chart of classical MD simulation is illustrated in Figure 2.5. First, system is built by assigning correct bond, angles, position and velocities. Second, force on each atom is calculated. Third, equation of motion is solved for a given Δt time step by an integrator to generate the new positions and velocities. This second and third steps are loop in MD algorithm and carried out until system become equilibrated.

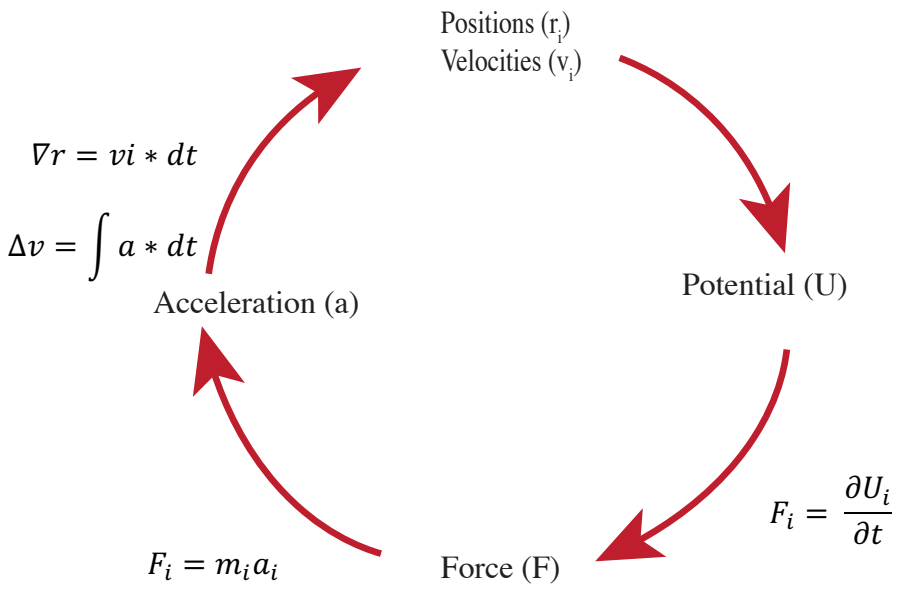

Figure 2.5 Flow chart of classical MD simulations. m_i is the mass of the object

Force fields

Set of mathematical equations and associated constants, which is known as force field, is essential in molecular dynamics simulations in order to reproduce the molecular geometry

and selected properties of tested structures. In current research optimized potential for liquid simulation–all atom (OPLS-AA) force field, developed by Jorgensen[14, 15] and coworkers, will be used. Different potential terms in OPLS-AA force field is given in equations[4].

$$U_{OPLS} = U_{bonded} + U_{nonbonded} \tag{2.16}$$

$$U_{non-bonded} = U_{Lennard-jones\,(Lj)} + U_{Coulombic} \tag{2.17}$$

$$U_{non-bonded} = U_{Lj} = U_{coulombic} = 4\varepsilon_{ij}\left|\left[\frac{\sigma_{ij}}{r_{ij}}\right]^{12} - \left[\frac{\sigma_{ij}}{r_{ij}}\right]^{6}\right| + \frac{q_i q_j}{4\pi\varepsilon_0 r_{ij}} \tag{2.18}$$

In equation 2.18, r_{ij} is the distance between atoms i and j, ε_{ij} is the Lennard-jones energy, σ_{ij} is the distance where inter particle potential is zero for atom i an j, q is partial charges

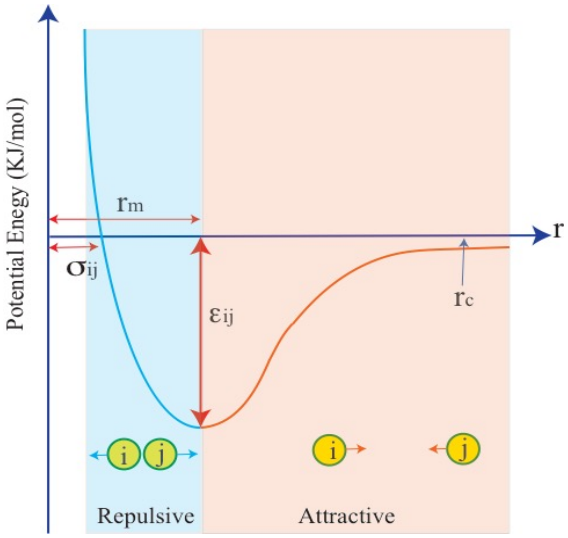

Figure 2.6 illustration of Lennard-jones potential. σ_{ij} is the distance where inter particle potential is zero for atom i an j, q is partial charges for atoms i and ε_0 is the permeability of free space. r_m is the equilibrium distance and r_c is the cut off radius.

for atoms i and ε_0 is the permeability of free space. r, ϵ and σ are illustrated in Figure 2.6

Figure 2.6 illustrate the interaction potential between two objects as a function of distance (r). at infinite r, there are no forces between the objects. When two objects come closer attractive forces starts to form which minimizes the potential energy. The distance, where potential energy is minimum, called equilibrium distance (r_m). When r becomes smaller than r_m, repulsive forces generated between the particles. Calculating calculation of force between atoms which are far a part is a challenge. Therefore, non-bonded potential is truncated at r_c which is called cut off radius. For current study, cut-off radius was set to 12 Å for all the LJ interactions. All electrostatic interactions are calculated between atoms in 12 Å radii. Geometric mixing rules are used for atoms of different species: $\varepsilon_{ij} = (\varepsilon_i \varepsilon_j)^{1/2}$ and $\sigma_{ij} = (\sigma_i \sigma_j)^{1/2}$. Interactions between atoms outside to 12 Å radii are calculated in reciprocal space by using particle-particle-particle-mesh (PPPM)[16] algorithm in Large-Scale Atomic/Molecular Massively Parallel simulator (LAMMPS)[17] software.

The bonded interactions are in different types. Bonding potential, angle potential and dihedral potentials are three of the bonding interactions terms used in force fields. These interaction terms are illustrated in Figure 2.7.

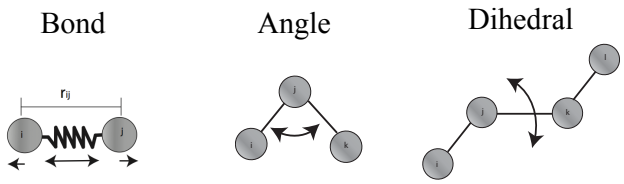

Figure 2.7 Different types of bonding interaction

These interactions are mathematically defined in following equations.

$$U_{bonded} = U_{bond} + U_{angle} + U_{torsion} \tag{2.19}$$

$$U_{bond}(r_{ij}) = k_r(r_{ij} - r_0)^2 \tag{2.20}$$

$$U_{angle}(\theta_{ijk}) = k_\theta(\theta_{ijk} - \theta_0)^2 \tag{2.21}$$

$$U_{torsion}(\phi_{ijkl}) = \sum_{n=i}^{n=l} \frac{k_n}{2} [1 - (1-1)^n \cos(n\phi)] \tag{2.22}$$

In above equations 16-18, r_{ij} is the equilibrium bond length between atoms i and j, θ_{ijk} is the equilibrium bond angle between atom i, j and k, ϕ_{ijkl} is the dihedral angle between atoms i, j, k and l, k_r is the force constant of the bond spring and k_θ is the force constant of the angle spring.

References

1. Osti, N., Neutron study of structure and dynamics of rigid polymers. **2014**.
2. Hammouda, B., Probing Nanoscale Structures: The SANS Toolbox (2009). *NIST Center for Neutron Research* **2008**.
3. Roe, R.-J.; Roe, R., *Methods of X-ray and neutron scattering in polymer science*. Oxford University Press New York: 2000; Vol. 739.
4. Primer N.S., *The Mathematical Foundations of Neutron Scattering*. Los Alamos Science: 1990; Vol. 29.
5. Jackson A.J., *Introduction to small-angle neutron scattering and neutron reflectometry*. NIST Center for Neutron Research: 2008.
6. Pynn, R., Editon edn: 2009.
7. Kline, S. R., Reduction and analysis of SANS and USANS data using IGOR Pro. *Journal of applied crystallography* **2006,** *39* (6), 895-900.
8. Nallet, F.; Laversanne, R.; Roux, D., Modelling X-ray or neutron scattering spectra of lyotropic lamellar phases: interplay between form and structure factors. *Journal de Physique II* **1993,** *3* (4), 487-502.
9. Higgins, J. S.; Benoit, H. C., Polymers and neutron scattering. **1994**.
10. Svaneborg, C.; Pedersen, J. S., Form factors of block copolymer micelles with excluded-volume interactions of the corona chains determined by Monte Carlo simulations. *Macromolecules* **2002,** *35* (3), 1028-1037.

11. Allen MP, Tildesley. D., *J.Molecular Simulation of Liquids*. Clarendon, Oxford: 1987.

12. Swope, W. C.; Andersen, H. C.; Berens, P. H.; Wilson, K. R., A computer simulation method for the calculation of equilibrium constants for the formation of physical clusters of molecules: Application to small water clusters. *The Journal of chemical physics* **1982,** *76* (1), 637-649.

13. Frenkel, D.; Smit, B., *Understanding molecular simulation: from algorithms to applications*. Elsevier: 2001; Vol. 1.

14. Jorgensen, W. L.; Madura, J. D.; Swenson, C. J., Optimized intermolecular potential functions for liquid hydrocarbons. *Journal of the American Chemical Society* **1984,** *106* (22), 6638-6646.

15. Aryal, D., Computational Insight into Structured Ionic Co-polymers from Molecule to Membrane. **2017**.

16. http://lammps.sandia.gov.

17. Breßler, I.; Kohlbrecher, J.; Thünemann, A. F., SASfit: a tool for small-angle scattering data analysis using a library of analytical expressions. *Journal of applied crystallography* **2015,** *48* (5), 1587-1598.

CHAPTER THREE

SOLVENT TUNING OF STRUCTURED IONIC BLOCK CO POLYMERS: SANS INSIGHT

ABSTRACT

Tuning the association of ionizable co-polymers in solution is fundamental to their integration in numerous current and potential applications, as the assemblies propagate through processing and determine the structure and therefore the function of membranes. The current study probes the effects of solvents on assemblies of an ABCBA co-polymer with polystyrene sulfonate as the center block, tethered symmetrically to polyethylene propylene and terminated by poly(t-butyl styrene), as the solvent is tuned through addition of a polar solvent, propanol, to cyclohexane using small angle neutron scattering. Similar to van der Waals block co-polymers in selective solvents, core- shell aggregates are formed with the ionic blocks in the core of the micelles in both cyclohexane and propanol. In contrast however, the highly incompatible nature of the blocks and the multiple sites available for the solvents drive transformations from spherical to elongated micelles and to a transitional region were large swarms dominate with increasing propanol fractions. At high propanol fractions, spherical micelles with a smaller number of polymer molecules and significantly higher portion of solvent in the core are found

INTRODUCTION

Solvent tuning and adaptation underline processing of multifunctional ionizable block co-polymers. These polymers exhibit an immense potential as components of light-weight clean energy generation and storage devices,[1, 2] water purification,[3-5] sensors,[6, 7] and

actuators.[8, 9] They are predominantly solvent cast because of their high glass transition temperature that stem from ionic clustering.[10, 11] The ionizable groups form physical crosslinks, facilitate transport, and often respond to triggers such as electric fields. The distribution, morphology and dynamics of these ionic groups control the polymer ability to function.[12, 13] Tuning the shape, size and distribution of ionic clusters through solvent interactions opens the way for tailoring polymeric materials with new functionalities. While solvent effects on van der Waals block co-polymers have been long realized,[14, 15] introducing an ionizable segments drives the polymers into the high segregation regime, where the assembly of the polymers are strongly affected by long range electrostatic interactions. [16, 17] Increasing the number of blocks and varying their degree of segregation, results in assemblies whose overall symmetries are similar to those of van der Waals co-polymers, however their internal structure often reflects their complexity And expand their range of applications.[18] Here we probe solvent adaptation of ionic block co-polymers that consist of multiple blocks through systematic tuning of the solvent, providing a fundamental insight into controlling soft polymeric assemblies.[19-21] Understanding and controlling structured ionic co-polymers presents a path forward in understanding the fundamental interactions that control these complex systems and impact their applications.[1, 2, 4-8, 18]

Using small angle neutron scattering (SANS) we probe solvent adaptation of assemblies of a pentablock co-polymer, whose center block consists of polystyrene sulfonate (PSS), tethered symmetrically to a poly-ethylene-propylene block (PEP) and terminated by poly (t-butyl styrene) (t-BPS). This polymer consists of three blocks whose interactions with

solvents is distinctive providing an excellent model system for investigating solvent adaptation. This co-polymer was designed with the rational of tethering a transport enabling block to additional polymers that will provide mechanical stability and tactility.[22] With advances in polymer synthesis, the pentablock topology have gained recent interest, particularly since it offers a means to tailor blocks with multiple functions together to drive specific applications.[23-28] Here the ionic block, PSS has been well studied[29] as a homopolymer and in diblock copolymers providing insight into its solvent response.[30] The nature of the solvent is altered by addition of propanol, a polar solvent, to cyclohexane. These two solvents are fully miscible though presenting different environments for the polymer blocks. Using the inherent contrast for neutrons between the blocks, SANS studies were able to resolve the evolution of the structure as the polar solvent is added to a non-polar one. We find that the overall shape of the aggregate changes, however the ionic block remains segregated and are caged by the hydrophobic segments. In contrast to assemblies of van der Waals polymers, solvents occupy multiple sites, where solvent polarity affects its distribution between these locations.

Extensive studies of membranes made from this pentablock have probed the correlations of its unique chemical structure with membrane structure and transport characteristics.[25-27, 31, 32] In contrast to van der Waals block co-polymers with similar molecular weights, this polymer does not exhibit long-range correlations,[27] however transport pathways with defined selectivity were identified. These studies have also demonstrated the immense effects counterions have on transport. With the realization that solvents alter transport pathways,[25, 26] several groups have studied the effects of different solvent environments on

the structure of membranes and transport.[24, 31, 33] The assembly of these polymers in hydrophobic solutions has been driven by segregation of the ionic block to the center of a core-shell micelle. Winey and coworkers[28] were first to observe formation of core-shell spherical micelles in concentrated solutions (10wt%) 1:1 cyclohexane:heptane, using small angle x-ray scattering (SAXS) and scanning tunneling microscopic. This solvent is used industrially to cast this polymer. Further insight into the assemblies of this pentablock was obtained by Etempawala et al.[34] using small angle neutron scattering (SANS). They showed that even at low concentrations, below 0.1 Wt% the ionic blocks segregate and form unimolecular micelles. With increasing concentration, core-shell assemblies with elliptical cores that consist predominantly of the PSS, are formed. However, the core also entraps segments of the PEP blocks and some of the solvent. The core is surrounded by a swollen corona that consists of both the PEP and the t-BPS blocks. Molecular insight was attained by Aryal et al. using atomistic molecular dynamics (MD) simulation.[35, 36] They revealed that in contrast to well defined polymeric micelles the core of the PB assembly consists of a nano-network the ionic blocks intertwined with the PEP block. In hydrophobic solvents such as cyclohexane heptane, the corona consists of a hydrophobic Gaussian-like shell. In water, however, the ionic corona remains almost unchanged, but the hydrophobic segments retract into the network, exposing the PSS to the surface.

These studies demonstrated that this pentablock forms a solvent responsive micelle that is driven by formation of ionic clusters and distinct solvation characteristics for all blocks. Studies by Mineart et. al. probed the effects of polar solvent, iso-propanol on the structure of the pentablock in toluene. Approximating the core of the micelle to a hard sphere, they

found a preferential segregation of the polar solvent to the core.[37] The current study is set to resolve the mechanism of solvent response of the ABCBA co=polymer, through tuning the nature of the solvent. This requires accounting of a delicate balance of interactions between the blocks and each of the blocks with solvents and the kinetics of the assembly, a process that leads to interpenetrating blocks, forming structures beyond hard-sphere micelles. To follow the response, micelles of the pentablock were studied in a 1Wt% of the polymer with two sulfonation fractions f = 0.26 and f = 0.52, focusing on the polymer in cyclohexane/propanol solutions. All three blocks exhibit distinctive affinity to both solvents where the polymer concentration chosen is in the micellar regime at room temperature. The results provide the foundation to controlling assemblies of highly incompatible block-copolymers that consist of ionizable blocks transcending fundamental knowledge and processing condition of structured ionic polymers.

EXPERIMENTAL

Materials

The block co-polymer obtained from Kraton Polymers™ was synthesized by anionic polymerization with a weight distribution of 15-10-28-10-15 kg/mol of the five blocks. The middle PS block was is randomly sulfonated with sulfonation fractions f = 0.26 and 0.52 of the available sites. The polymer was dissolved in different ratios of D_{12}-cyclohexane and D_7-1-Propanol (f_{pro}= 0.10, 0.15, 0.20, 0.30, 0.35, 0.40, 0.70, 0.80, 0.90 and 1.00) to get 1% (w/w) polymer solutions. All the deuterated solvents were obtained from Cambridge Isotope Laboratories, Inc., USA and were used as received.

SANS EXPERIMENT

SANS measurements were carried out at room temperature on the General-Purpose Small Angle Neutron Scattering (GP-SANS) at High Flux Isotope Reactor (HFIR) at Oak Ridge National Laboratory.[38] The data were collected at two different detector configurations: 2 m and 18.5 m to capture a broad momentum transfer vector ($q = 0.005 - 0.6$ Å^{-1}), $q = 4\pi\sin(\theta)/\lambda$, where 2θ is the scattering angle and λ is the wave length of the monochromatic neutron beam and $\lambda = 4.65$ Å. Scattering patterns were recorded for the copolymer solutions, empty cell, and all solvent combinations of d_{12}-cyclohexane and d_7-propanol. The scattering of solvents and empty cell was subtracted from the data. Data were normalized to a calibrated, standard porosil-B[38] and corrected for their transmission to obtain absolute intensity. Data were recorded on 2-dimensional detectors and integrated into one dimensional scattering patterns using the standard data reduction procedures in Mantid[23, 38] and SPICE[23, 38] software packages available at GP-SANS instrument.

SANS Data Analysis

Initial estimates of the scattering length densities (SLD) of core and corona were calculated by the chemical formula and the bulk densities of different blocks. SLD of the different mixtures of d_{12}-cyclohexane and d_7-1-propanol were calculated by SLD mixing rules and the volume fractions. The SLD of t-BPS, PEP, PSS, pure cyclohexane and propanol are given in Table 3.1.

Component	Neutron SLD × 10^{-6} (Å^{-2})
t-BPS	0.71
PEP	-0.3
PSS	1.69
D7-Propanol	5.48
D12-cyclohexane	6.72

Table 3.1: Neutron SLD values for pure compounds

The average dimensions of the scattering objects were initially estimated by calculating the radius of gyration R_g from the Guinier approximation for spherical particles,[39-42]

$$I(q) = SLD^2V^2 \exp\left(-\frac{1}{3}q^2R_g^2\right) \qquad (3.1)$$

where I(q) is the measured intensity, V is the volume of the particle, q is the momentum transfer vector. The Guinier approximation is valid for dilute and homogeneous solutions, where particles in the system scatter independently and are randomly orientated.

The initial analysis determined the slope of the scattering profile at intermediate q range. In this region, the scattering intensity I(q) scales with q as $I(q) \sim q^{-\alpha}$ where α is a scaling exponent[39–42] that point to the overall shape of the aggregate in this q region. A full analysis in terms of core Gaussian shell models of different symmetries was used. These form

factors for core-shell assemblies were used because they account for the interface between the core and the corona was developed by Paterson[43, 44] and have been successfully used to capture core shell assemblies of polymers in selective solvents. The model allows for mixing the core and corona capturing interfacial stabilities that often drive phase transitions in micellar systems. The fitting routines are given in numerous SANS analysis packages. These packages available at NIST.[45] Here SAS*fit*[46] version 0.93.5 were used. Best fits were obtained by minimizing χ^2. The average χ^2 for our fits were 1.4 where $\chi^2 = 1$ is an excellent fit.

RESUTS AND DISCUSSION

SANS patterns of 1 Wt% pentablock with f = 0.26 and 0.52 in cyclohexane:propanol solutions with propanol fractions f_{pro} from 0.1 to 1.0 are presented in Figure 1 over extended q range capturing the aggregates as well as their internal structure. I(q) as a function of q is presented in a and c and the corresponding Kratky representation $q^2I(q)$ is plotted versus q are shown in b and d. The Kratky representation distinguishes changes that take place on the length scale of the core dimensions from chain conformation. In the lower sulfonation regime, the patterns are relatively featureless with a shoulder at q~ 0.01 $Å^{-1}$, which corresponds to 600 Å in real space. For the higher sulfonating levels, the patterns consist

of a well-defined signature at q~0.03 $Å^{-1}$, which is corresponds to ~ 200 Å in real space.

As most of the corona is highly swollen, as shown in Figure 1c and d inserts, the scattering

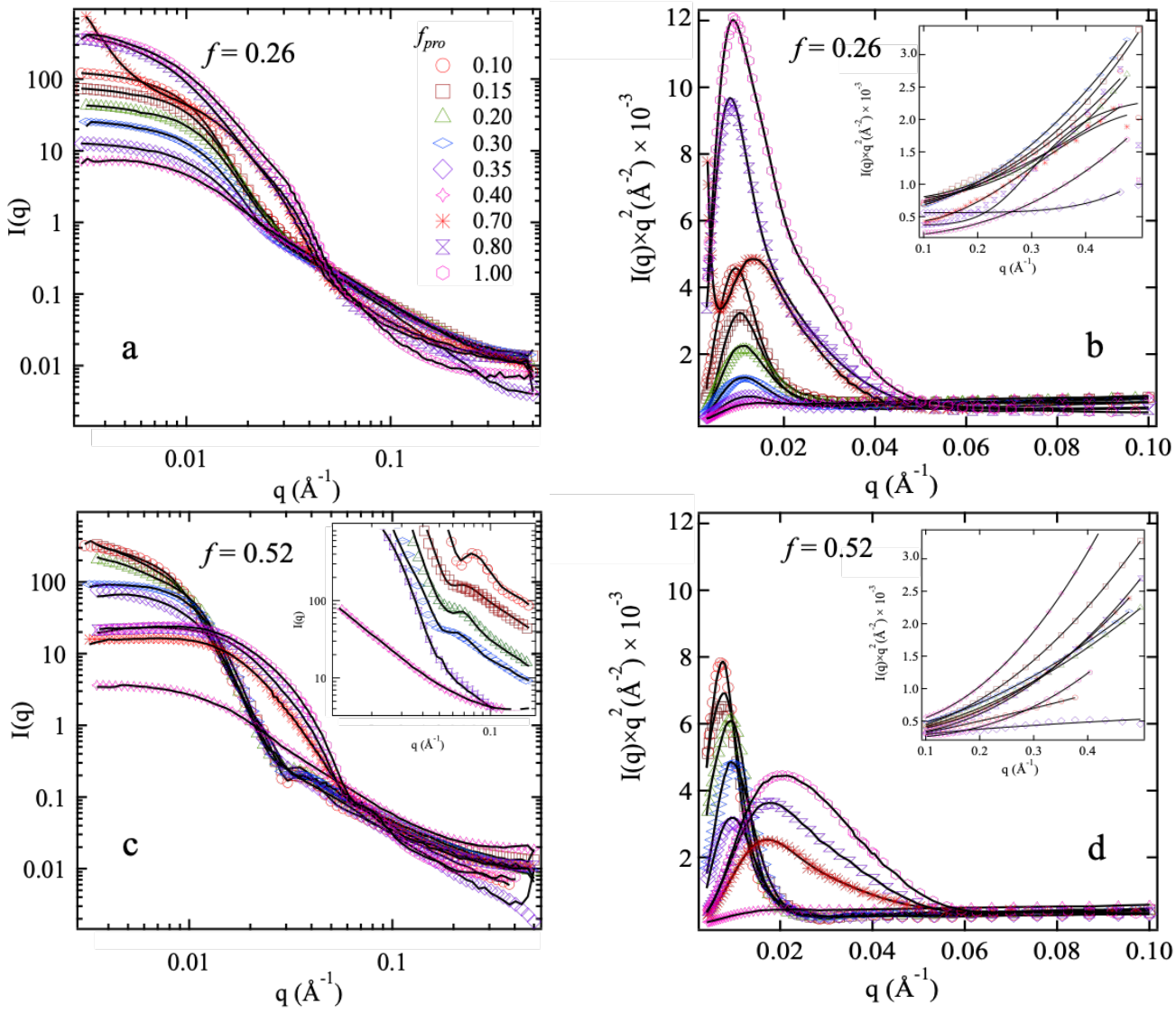

Figure 3.1: SANS profile of 1%wt solutions of pentablock at different propanol fractions a) f = 0.26, b) Kratkey plot f = 0.26; c) f = 0.52 and d) Kratky plot f = 0.52 at room temperature. The inserts in b and d correspond to the high q region in the Kratky plots. Data are marked by the indicated symbols and fitting to distinctive core-shell models as discussed in the text.

intensity captures well the core packing and its interface with the corona. With increasing propanol fraction, two distinctively different regimes are observed for both sulfonation levels: I_{max} decreases up to approximately $f=0.4$ and then increases, as shown in Figure 2a. I_{max} at q=0.007 Å^{-1} exhibits the same trends as the calculated values using a Guinier analysis.[41, 42] Concurrently, signatures that correspond to the corona (q = 0.01 Å^{-1}) initially shift to higher q values, broaden and then practically dimmish, where the scattering functions capture concentration fluctuations rather than well-defined aggregates. Upon further increase in propanol however, similar features are developed, now at smaller dimensions (higher q values). This behavior is captured in the Kratky plots in Figure 1b,d. These data suggest that the PB exhibits a phase transition with a reentrant micellar phase as a function of propanol concentration, driven by the distribution of propanol between the blocks.

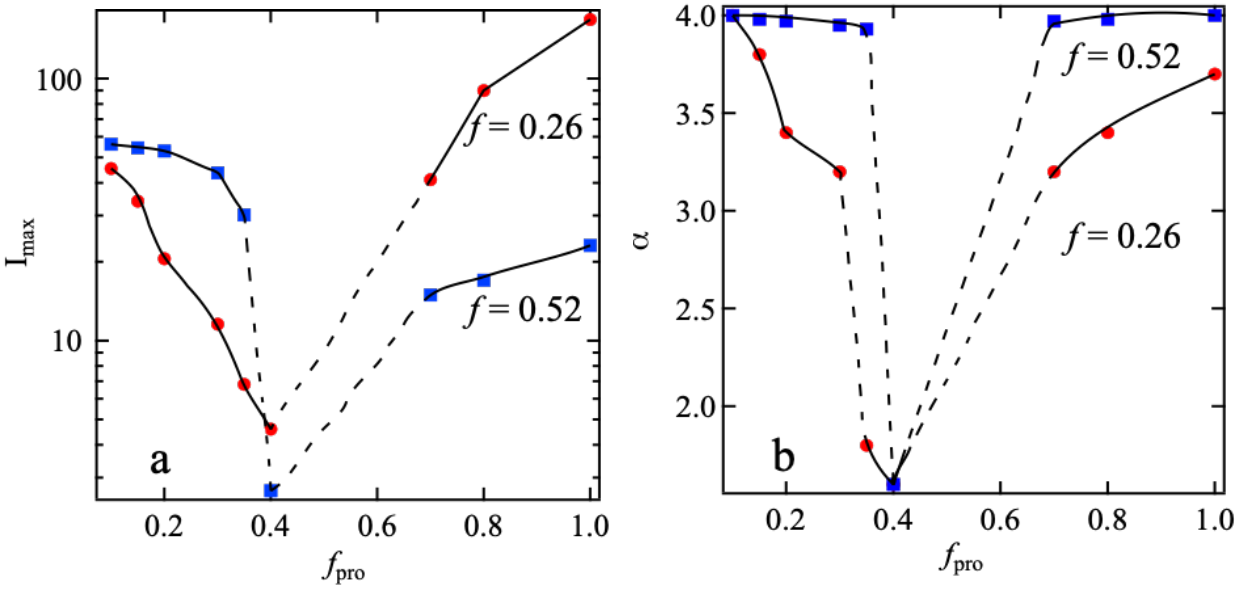

Figure 3.2: a) I_{max}(q)of scattering at q=0.007 Å^{-1} b) Power law exponent α of the scattering profiles at intermediate q as a function of propanol fraction.

In the intermediate q range, I(q) provides further insight into the shape of the micelles.[41, 42] In this range, $I(q) \sim q^{-\alpha}$ where α characteristics of the shape of the scattering object. Here α varies from 4, typical of a spherical object, to 1, typical for elongated cylindrical or rod-like object, and then again to 4 as propanol is added to the system, as shown in Figure 2b. These initial findings suggest that spherical aggregates, formed in cyclohexane, evolve into elongated assemblies with increasing propanol content, and break up. With further increase in propanol content, spherical objects are detected.

Detailed structure of the micelles was obtained though fitting I(q) to form factors of assemblies with a core-shell (corona) morphology with a dense core and a Gaussian corona.[34] Guided by the values of α, the form factor was varied from spherical to elliptical and finally to cylindrical before the micelles dissociates. Radius of the core R_{core} and radius of gyration of the corona Rg,corona are shown in Figure 3.3. The symmetry of the core-

Sulfonation	f_{pro}	**Form factor**	R_{short}(Å)	R_{long}(Å)
f= 0.26	0.2	elliptical core	88	105
	0.3	elliptical core	79	115
	0.35	elliptical core	72	124
	0.4	cylindrical core	75	167
f= 0.52	0.4	cylindrical core	64	152

Table 3.2: The dimensions extracted from the fitting the data to elongated

shell micelle is indicated by different symbols. For elongated structures, the smaller values of R_{core} are plotted and the longer dimensions are presented in Table 3.2.

At the intermediate propanol fractions, where the micelles are disrupted, strong scattering is observed, however the patterns are not consistent with any one well defined structure, while the system remains visually optical translucent and homogenous. This is consistent with scattering of large swarms that are a mix of worm like structures and simple concentration fluctuations but do not yield clear dimensions. R_{core} and R_g of the corona decreases with increasing propanol fraction up to ~0.4% of propanol. For the $f = 0.26$, the micelles are re-formed and both the radius of the core and R_g of the coronal increase with increasing propanol fraction. For $f = 0.52$, R_{core} and $R_{gcorona}$ remain small as the propanol fraction increases.

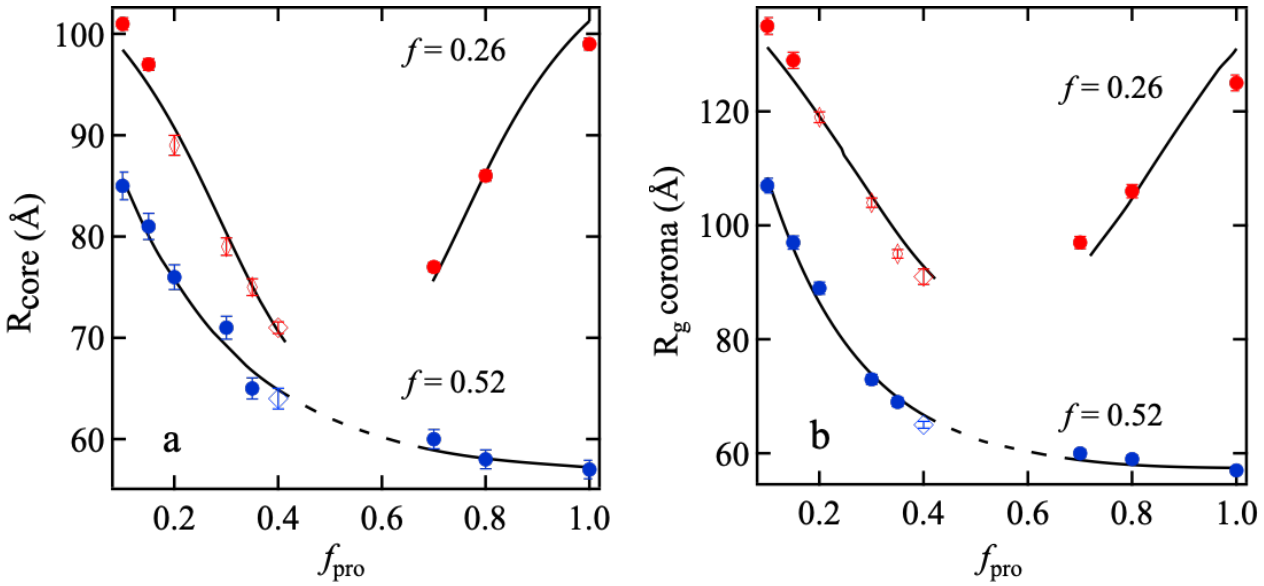

Figure 3.3: Data extracted from core-shell models fitting a) radius of the core b) radius of gyration of corona for $f = 0.26$ (red) and $f = 0.52$ (blue). Results for spherical core (circles), elliptical core (diamonds) and cylindrical core (squares).

In cyclohexane, the PSS segments segregates into the core with limited number of solvent molecules, whereas the PEP and t-BPS reside in the corona with the PEP highly swollen.[34, 36] Propanol changes not only the polarity of the solvent but the degree of solvation of the

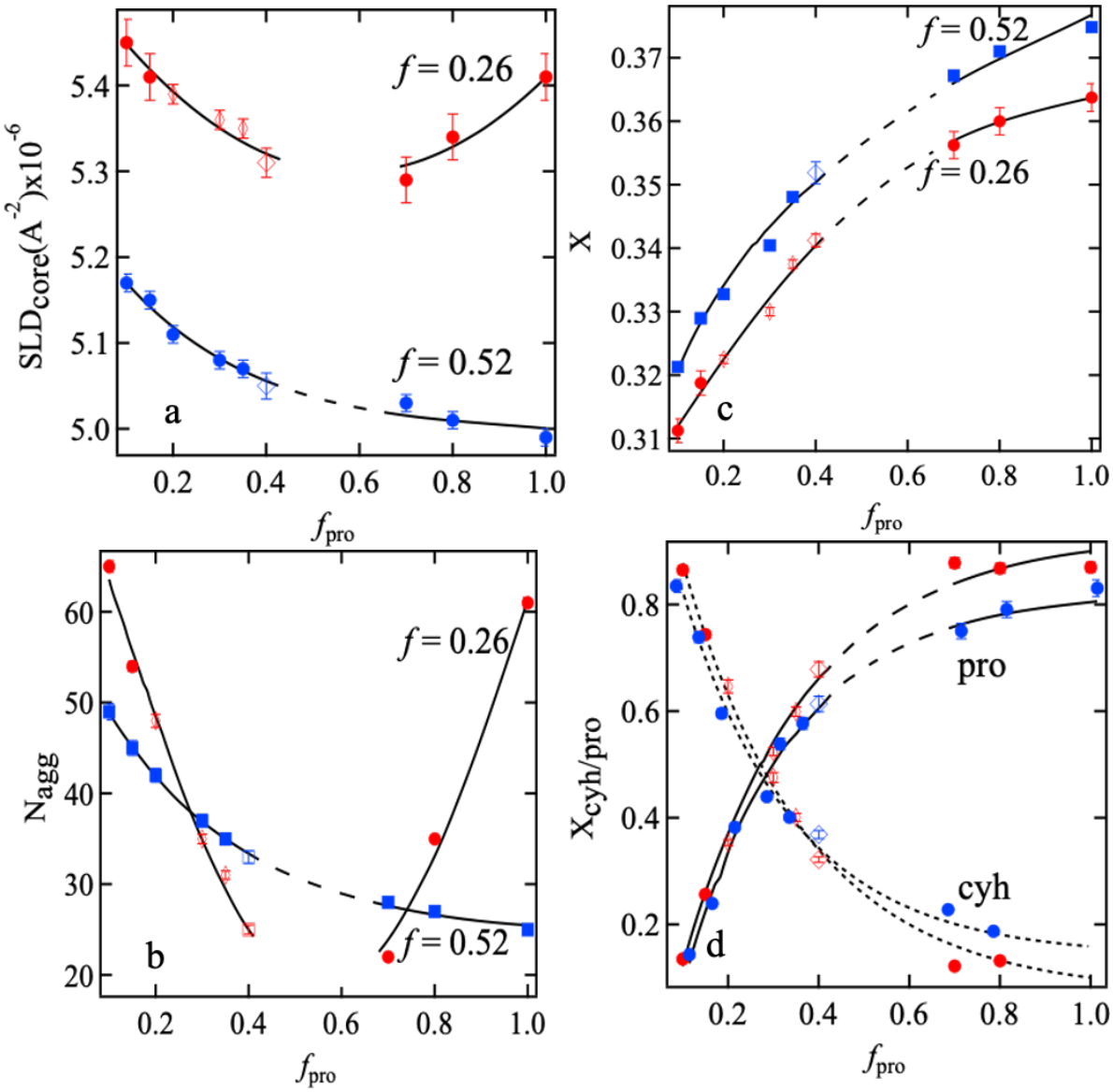

Figure 3.4: a) Scattering length density of core, b) aggregation number, c) total solvent fraction in the core as a function of propanol fractions, and d) relative fractions of cyclohexane and propanol for $f = 0.26$ (red) and $f = 0.52$ (blue). Results for spherical core (circles), elliptical core (diamonds) and cylindrical core (squares).

core and the degree of collapse of the hydrophobic blocks as well as the interfacial energy at the core-corona interface. These three factors determine the energetics that govern the stability of the micelles.

The SLD of the core, aggregation number and fraction of solvents in the core, as extracted from the analysis, are presented in Figure 4 along with the calculated ratio of cyclohexane to propanol in the core. With increasing propanol fraction, R_{core} and the core SLD decrease. As both solvents are deuterated, the decrease of the SLD of the core captures the number of PSS segments that assemble in the center of the aggregate, providing a measure of the aggregation number. For both sulfonation levels, the number of polymer molecules in the aggregate initially decreases, however as the reentrant phase evolves, the aggregation number increases for the lower sulfonation fraction but remains low for the higher sulfonation fraction. For $f_{pro} = 0.1$, cyclohexane is most prevalent in the core while only small amounts of propanol are in the core. However, with increasing f_{pro}, propanol constitutes the majority of the solvent in the core while cyclohexane if present only in trace amounts. This transition occurs after $f_{pro} \sim 0.4$ where cyclohexane is still dominated in the bulk.

At lower sulfonation fraction the core is more sparsely packed and swollen, whereas for higher sulfonation levels the core is denser. As propanol is added, the assemblies become more elongated until they break up. The delicate balance of the solubility of blocks in becomes more intricate since the PSS block is hardly soluble in cyclohexane but only partially soluble in propanol, whereas PEP and t-BPS are soluble in propanol to different

degrees. This balance is reflected in the degree of intermixing of the core and the corona,[46] as extracted from the analysis shown in Figure 3.5.

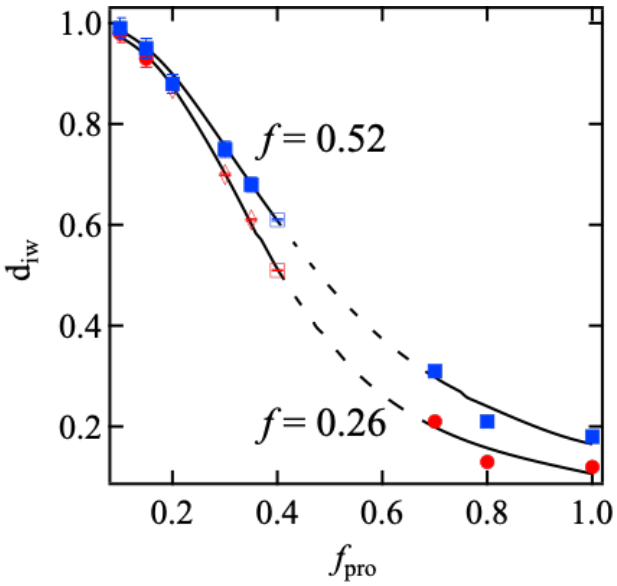

Figure 3.5: The degree of interpenetration d_{iw} of the core and the corona as extracted from the analysis with $d_{iw} = 1$ being fully segregated.

In cyclohexane, the PSS is segregated to the core where the PEP assumes a highly swollen configuration. Propanol is driven to the PSS and PEP segments, however with significant affinities. The PEP segments remain Gaussian, but slightly less swollen. The t-BPS segments are only slightly affected. With increasing propanol fraction, it resides predominately at the core-corona interface. As a result, the presence of propanol drives a shape transformation but does not invert the micelles.

Similar to charged diblock co-polymers, the free energy of a micelle of a polymer can be described in terms of $F = F_{core} + F_{corona} + F_{interface.}$, where the dimensions of the core are obtained by minimization of F. F_{core} includes a component that accounts for the elasticity of the chain, ionic clustering and solvation energy.[47] F_{corona} for a first approximation

consists predominantly of elastic stretching energy and confinement entropy. At the boundary of the core and the corona the interfacial energy per chain is approximated by $F_{int} \sim \frac{a^3 N}{R}\ \gamma d_{int}$ and is determined by the surface tension γ, the Kuhn length a, the number monomers per chain N and the radius of the chain R, and the dimensionality of the assembly, plainer, cylindrical and spherical, d_{int} = 1, 2 and 3 respectively.[48] This simplistic geometrical consideration however is complicated by the presence of ionic clusters. However, with increasing propanol fraction, and increase in interfacial width d_{iw} as shown in Figure 3.5, the interfacial tension is strongly affected, driving instabilities that result is a micellar transition. This simplistic model only provides a context for realizing the complex set of interactions that drive the micelles of ionizable co-polymers.

The association of cyclohexane and propanol with polar and non-polar segments of the

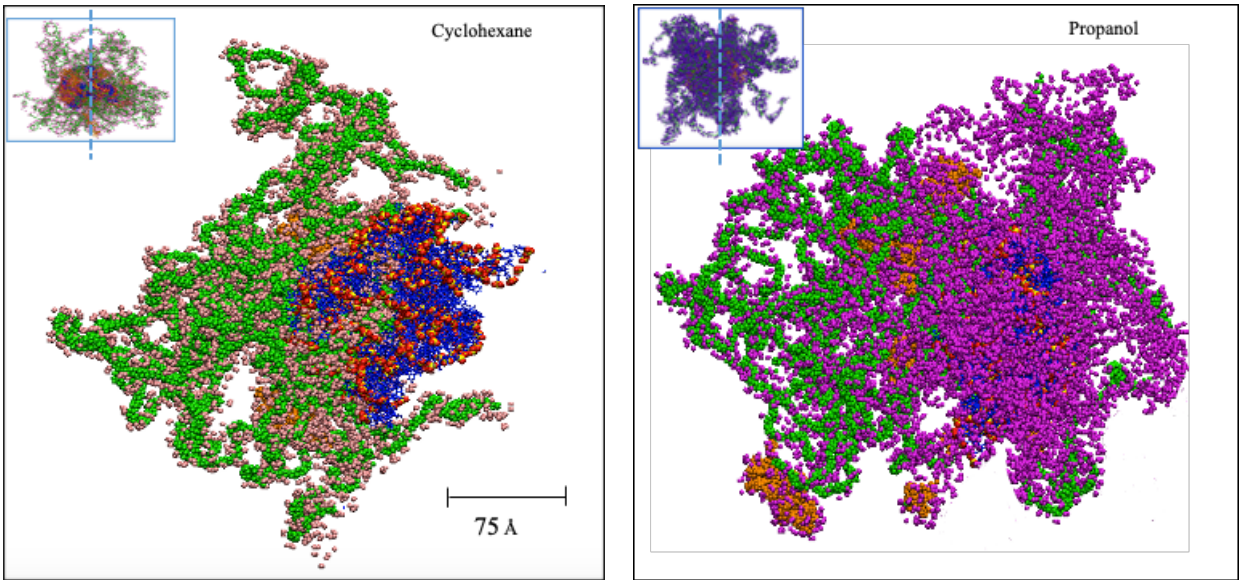

Figure 3.6: Cross section of micelles and the associated solvents of micelles of 5 pentablock chains for f = 0.55 in cyclohexane and propanol. Insert represent the whole micelle. Green PEP blocks, orange t-BPS blocks, blue PSS blocks, red oxygen, yellow sulfur, gray sodium, pink cyclohexane, and purple propanol.

blocks is captured by molecular dynamics simulations. Figure 3.6 visualizes micelles formed by five pentablock chains with f=0.55 in cyclohexane and propanol and associated solvents within 5Å of the polymer chains.[49] The micelles are equilibrated for 100 ns. Both polymer and solvents are modeled by OPLS-AA[50, 51] force field and simulated using the LAMMPS[52] software package. These simulations show that cyclohexane reside predominantly in the PEP segment while the propanol occupy multiple sites and affects the interfacial energies.

CONCLUSIONS

The effects of solvent polarity on the assemblies formed by an ABCBA pentablock co-polymer were probed by small angle neutron scattering, as propanol is added to cyclohexane. These solvents are fully miscible. We find that similar to van der Waals block co-polymers in selective solvents, core-Gaussian shell aggregates are formed with ionic blocks in the core of the micelles in both cyclohexane and propanol. In cyclohexane with low propanol fractions, the PSS segregates to the core, forming tight a ionic network with some interstitial space, as was previously observed.[34] Cyclohexane is a good solvent for PEP resulting in a highly swollen corona. The t-BPS block resides in the corona and is only slightly swollen. The highly incompatible nature of the blocks and the multiple sites available for propanol drives a transition from a spherical to an elongated micelle and then to a transitional region where large swarms with increasing of propanol fraction. In contrast to van der Waals polymers, at higher propanol fractions spherical assemblies are formed but with a smaller number of polymer molecules and significantly higher portion of solvent

in the core. Concurrently, though PEP segments are soluble in propanol, the corona becomes more condensed in comparison with cyclohexane, predominantly due to solubility difference of the PEP in the 2 solvents The structure of the micelles at high propanol fractions is surprising and reflects the effects of the balance between high incompatibility of the ionic segments with the rest of the blocks and the interaction of the propanol with each of the blocks. The attraction of the ionizable groups drives the formation of an ionic core, where the affinity of the propanol to the ionic segment results in a swollen core. Propanol which partitions to both the core and the corona reduces the core-corona interfacial energy, breaking the micelles into swarms. Increasing the propanol fraction also impacts the packing of the corona. Though the hydrophobic segments are soluble in propanol, they are less soluble than in cyclohexane, thus forming a denser corona. In this region, the propanol resides in the core, at the interface and in the corona. As a result, the core-corona interface is broader.

The insight obtained here offers a glimpse into the formation of micelles of ionizable block co-polymers in the high segregation regime and demonstrated the complexity of assemblies where the solvents occupy multiple distinctive sites. Further the results show the significance of the interfacial region between the blocks.

ACKNOWLEDGMENTS

This work was supported by the NSF Grant No. DMR-1611136. The SANS measurements conducted using the GP-SANS at ORNL's high flux isotope reactor (HFIR) neutron source was sponsored by the Scientific user facilities division, Office of Basic Energy Sciences,

U.S. Department of Energy. Travel to Oak Ridge National Laboratory to carry out this work was supported by a Travel Fellowship from the DOE-EPSCoR Grant to the University of Tennessee, Grant No. DE-FG02-08ER46528. The numerical simulations were performed under the supervision of Dr. Gary S. Grest, in part, at the Center for Integrated Nanotechnologies, an Office of Science User Facility operated for the U.S. Department of Energy (DOE) Office of Science at Sandia National Laboratories (Contract DE-NA-0003525). and at the Palmetto cluster, which is part of the supercomputer facility at Clemson university. The authors would also like to thank Dr. Dipak Aryal for valuable guidance on the numerical simulations.

REFERENCES

1. Li, C.; Li, Q.; Kaneti, Y. V.; Hou, D.; Yamauchi, Y.; Mai, Y. Self-assembly of copolymers towards mesoporous materials for energy storage and conversion systems. *Chemical Society Reviews* **2020,** 49 (14), 4681-4736.
2. Chakrabarty, A.; Teramoto, Y. Scalable Pickering Stabilization to Design Cellulose Nanofiber-wrapped Block Copolymer Microspheres for Thermal Energy Storage. *ACS Sustainable Chemistry & Engineering* **2020,** 8 (11), 4623-4632.
3. Soltannia, B.; Islam, M. A.; Cho, J.-Y.; Mohammadtabar, F.; Wang, R.; Piunova, V. A.; Almansoori, Z.; Rastgar, M.; Myles, A. J.; La, Y.-H. Thermally stable core-shell star-shaped block copolymers for antifouling enhancement of water purification membranes. *Journal of Membrane Science* **2020,** 598, 117686.

4. Bhushan, B., Bioinspired Water Desalination and Water Purification Approaches Using Membranes. In *Bioinspired Water Harvesting, Purification, and Oil-Water Separation*, Springer: 2020; pp 161-174.

5. Chen, S. H.; Willis, C.; Shull, K. R. Water transport and mechanical response of block copolymer ion-exchange membranes for water purification. *Journal of Membrane Science* **2017,** 544, 388-396.

6. Razavi, B.; Abdollahi, A.; Roghani-Mamaqani, H.; Salami-Kalajahi, M. Light-, temperature-, and pH-responsive micellar assemblies of spiropyran-initiated amphiphilic block copolymers: Kinetics of photochromism, responsiveness, and smart drug delivery. *Materials Science and Engineering: C* **2020,** 109, 110524.

7. Zou, Y.; Zhou, X.; Zhu, Y.; Cheng, X.; Zhao, D.; Deng, Y. sp2-Hybridized carbon-containing block copolymer templated synthesis of mesoporous semiconducting metal oxides with excellent gas sensing property. *Accounts of chemical research* **2019,** 52 (3), 714-725.

8. Bar-Cohen, Y.; Anderson, I. A. Electroactive polymer (EAP) actuators—background review. *Mechanics of Soft Materials* **2019,** 1 (1), 5.

9. Wong, C. K.; Qiang, X.; Müller, A. H.; Gröschel, A. H. Self-Assembly of block copolymers into internally ordered microparticles. *Progress in Polymer Science* **2020,** 102, 101211.

10. Eisenberg, A. Clustering of ions in organic polymers. A theoretical approach. *Macromolecules* **1970,** 3 (2), 147-154.

11. Eisenberg, A.; Hird, B.; Moore, R. A new multiplet-cluster model for the morphology of random ionomers. *Macromolecules* **1990,** 23 (18), 4098- 4107.

12. Antony, P.; De, S. K. Ionic thermoplastic elastomers: a review. *Journal of Macromolecular Science, Part C: Polymer Reviews* **2001,** 41 (1-2), 41-77.

13. Wang, X.; Goswami, M.; Kumar, R.; Sumpter, B. G.; Mays, J. Morphologies of block copolymers composed of charged and neutral blocks. *Soft Matter* **2012,** 8 (11), 3036-3052.

14. Lodge, T. Characterization of polymer materials by scattering techniques, with applications to block copolymers. *Microchimica Acta* **1994,** 116 (1-3), 1-31.

15. Lodge, T. P. Block copolymers: past successes and future challenges. *Macromolecular chemistry and physics* **2003,** 204 (2), 265-273.

16. Villaluenga, I.; Chen, X. C.; Devaux, D.; Hallinan, D. T.; Balsara, N. P. Nanoparticle- driven assembly of highly conducting hybrid block copolymer electrolytes. *Macromolecules* **2015,** 48 (2), 358-364.

17. Loo, W. S.; Jiang, X.; Maslyn, J. A.; Oh, H. J.; Zhu, C.; Downing, K. H.; Balsara, N. P. Reentrant phase behavior and coexistence in asymmetric block copolymer electrolytes. *Soft matter* **2018,** 14 (15), 2789-2795.

18. Senapati, S.; Darling, R. J.; Loh, D.; Schneider, I. C.; Wannemuehler, M. J.; Narasimhan, B.; Mallapragada, S. K. Pentablock copolymer micelle nanoadjuvants enhance cytosolic delivery of antigen and improve vaccine efficacy while inducing low inflammation. *ACS Biomaterials Science & Engineering* **2019,** 5 (3), 1332-1342.

19. Park, M. J.; Balsara, N. P. Phase behavior of symmetric sulfonated block copolymers. *Macromolecules* **2008,** 41 (10), 3678-3687.

20. Shim, J.; Bates, F. S.; Lodge, T. P. Superlattice by charged block copolymer self-assembly. *Nature communications* **2019,** 10 (1), 1-7.

21. Shim, J.; Bates, F. S.; Lodge, T. P. Bicontinuous microemulsions in partially charged ternary polymer blends. *ACS Macro Letters* **2019,** 8 (9), 1166- 1171.

22. Willis, C. L.; Handlin Jr, D. L.; Trenor, S. R.; Mather, B. D., Sulfonated block copolymers, method for making same, and various uses for such block copolymers. Google Patents: 2010.

23. Wignall, G. D.; Littrell, K. C.; Heller, W. T.; Melnichenko, Y. B.; Bailey, K. M.; Lynn, G. W.; Myles, D. A.; Urban, V. S.; Buchanan, M. V.; Selby, D. L. The 40 m general purpose small-angle neutron scattering instrument at Oak Ridge National Laboratory. *Journal of Applied Crystallography* **2012,** 45 (5), 990-998.

24. Huang, F.; Largier, T. D.; Zheng, W.; Cornelius, C. J. Pentablock copolymer morphology dependent transport and its impact upon film swelling, proton conductivity, hydrogen fuel cell operation, vanadium flow battery function, and electroactive actuator performance. *Journal of Membrane Science* **2018,** 545, 1-10.

25. Geise, G.; Freeman, B.; Paul, D. Characterization of a sulfonated pentablock copolymer for desalination applications. *Polymer* **2010,** 51 (24), 5815-5822.

26. Fan, Y.; Zhang, M.; Moore, R. B.; Cornelius, C. J. Structure, physical properties, and molecule transport of gas, liquid, and ions within a pentablock copolymer. *Journal of Membrane Science* **2014,** 464, 179-187.

27. Choi, J.-H.; Willis, C. L.; Winey, K. I. Effects of neutralization with Et3Al on structure and properties in sulfonated styrenic pentablock copolymers. *Journal of membrane science* **2013,** 428, 516-522.

28. Choi, J.-H.; Kota, A.; Winey, K. I. Micellar morphology in sulfonated pentablock copolymer solutions. *Industrial & engineering chemistry research* **2010,** 49 (23), 12093- 12097.

29. Lundberg, R.; Makowski, H. Solution behavior of ionomers. I. Metal sulfonate ionomers in mixed solvents. *Journal of Polymer Science: Polymer Physics Edition* **1980,** 18 (8), 1821-1836.

30. Meng, D.; Wang, Q. Solvent response of diblock copolymer brushes. *The Journal of chemical physics* **2009,** 130 (13), 134904.

31. Truong, P. V.; Black, R. L.; Coote, J. P.; Lee, B.; Ardebili, H.; Stein, G. E. Systematic Approaches To Tailor the Morphologies and Transport Properties of Solution-Cast Sulfonated Pentablock Copolymers. *ACS Applied Polymer Materials* **2018,** 1 (1), 8-17.

32. Ertem, S. P.; Caire, B. R.; Tsai, T. H.; Zeng, D.; Vandiver, M. A.; Kusoglu, A.; Seifert, S.; Hayward, R. C.; Weber, A. Z.; Herring, A. M. Ion transport properties of mechanically stable symmetric ABCBA pentablock copolymers

with quaternary ammonium functionalized midblock. *Journal of Polymer Science Part B: Polymer Physics* **2017,** 55 (7), 612-622.

33. Huang, F.; Zheng, W.; Tahmasbi Rad, A.; Nieh, M. P.; Cornelius, C. J. The role of TEOS-TIP within a pentablock ionomer: Morphology, physical properties, and ion transport. *Journal of Polymer Science Part B: Polymer Physics* **2017,** 55 (7), 575-586.

34. Etampawala, T. N.; Aryal, D.; Osti, N. C.; He, L.; Heller, W. T.; Willis, C. L.; Grest, G. S.; Perahia, D. Association of a multifunctional ionic block copolymer in a selective solvent. *The Journal of chemical physics* **2016,** 145 (18), 184903.

35. Aryal, D.; Etampawala, T.; Perahia, D.; Grest, G. S. Phase Behavior of a Single Structured Ionomer Chain in Solution.*Macromolecular Theory and Simulations* **2014,** 23 (9), 543-549.

36. Aryal, D.; Grest, G. S.; Perahia, D. Soft nanoparticles: nano ionic networks of associated ionic polymers. *Nanoscale* **2017,** 9 (6), 2117-2122.

37. Mineart, K. P.; Ryan, J. J.; Appavou, M.-S.; Lee, B.; Gradzielski, M.; Spontak, R. J. Self-Assembly of a Midblock-Sulfonated Pentablock Copolymer in Mixed Organic Solvents: A Combined SAXS and SANS Analysis. *Langmuir* **2019,** 35 (4), 1032-1039.

38. Littrell, K.; Atchley, K.; Cheng, G.; Melnichenko, Y.; Wignall, G. General purpose small-angle neutron scattering instrument on HFIR Oak Ridge. *Neutron news* **2008,** 19 (3), 20-21.

39. Roe, R.-J.; Roe, R., *Methods of X-ray and neutron scattering in polymer science*. Oxford University Press New York: 2000; Vol. 739.

40. Pynn, R. The Mathematical Foundations of Neutron Scattering. *Neutron Scatt. Prim* **1990**, 28-31.

41. Jackson, A. J. Introduction to small-angle neutron scattering and neutron reflectometry. *NIST Center for Neutron Research* **2008**, 1-24.

42. Hammouda, B. Probing Nanoscale Structures: The SANS Toolbox (2009). *NIST Center for Neutron Research* **2008**.

43. Pedersen, J. S.; Gerstenberg, M. C. Scattering form factor of block copolymer micelles. *Macromolecules* **1996,** 29 (4), 1363-1365.

44. Pedersen, J. S. Form factors of block copolymer micelles with spherical, ellipsoidal and cylindrical cores. *Journal of Applied Crystallography* **2000,** 33 (3), 637-640.

45. Kline, S. R. Reduction and analysis of SANS and USANS data using IGOR Pro. *Journal of applied crystallography* **2006,** 39 (6), 895-900.

46. Breßler, I.; Kohlbrecher, J.; Thünemann, A. F. SASfit: a tool for small-angle scattering data analysis using a library of analytical expressions. *Journal of applied crystallography* **2015,** 48 (5), 1587-1598.

47. Ohnsorg, M. L.; Ting, J. M.; Jones, S. D.; Jung, S.; Bates, F. S.; Reineke, T. M. Tuning PNIPAm self-assembly and thermoresponse: roles of hydrophobic end-groups and hydrophilic comonomer. *Polymer Chemistry* **2019,** 10 (25), 3469-3479.

48. Netz, R. Micellar morphologies of charged diblock-copolymers. *EPL (Europhysics Letters)* **1999,** 47 (3), 391.

49. Senanayake, M.; Aryal, D.; Grest, G. S.; Perahia, D. Response of Ionizable Block Copolymer Assemblies to Solvent Polarity: A Molecular Dynamics Study. (in preparation).

50. Jorgensen, W. L.; Madura, J. D.; Swenson, C. J. Optimized intermolecular potential functions for liquid hydrocarbons. *Journal of the American Chemical Society* **1984,** 106 (22), 6638-6646.

51. Jorgensen, W. L.; Maxwell, D. S.; Tirado-Rives, J. Development and testing of the OPLS all-atom force field on conformational energetics and properties of organic liquids. *Journal American Chemical Society* **1996,** 118 (45), 11225-11236.

52. Plimpton, S. Fast parallel algorithms for short-range molecular dynamics. *Journal computational physics* **1995,** 117 (1), 1-19.

CHAPTER FOUR

RESPONSE OF IONIZABLE BLOCK COPOLYMER ASSEMBLIES TO SOLVENT POLARITY: A MOLECULAR DYNAMICS STUDY

Abstract

Ionizable co-polymers associate in solutions where ionic cluster formation often drives assembly. The response of ionic clusters affects the driving forces for assemblies, where the larger incompatibility between the blocks, the more distinctive the response to solvent stimuli. Here, using atomistic molecular dynamics simulations, we follow the response of micelles formed by a symmetric pentablock copolymer, that consists of a randomly sulfonated polystyrene center tethered to polyethylene-r-propylene block, terminated by poly (t-butyl styrene). The three blocks response differently in each solvent depending on their polarity. In cyclohexane, the ionic blocks form a collapsed conformation while the non-polar blocks form a swollen corona. In propanol and THF, the ionic block is swollen, while the non-ionic blocks are slightly collapsed. With increasing sulfonation, the ionic blocks form a more stable ionic core with cyclohexane associating around the dense ionic core while THF and propanol penetrate into the core.

Introduction

Ionizable block co-polymers, which consist of ionic blocks covalently bonded to one or more non-ionic segments, are at the center of many current and potential application such as clean energy,[1, 2] separation devices[3, 4] and bio-medical science[5, 6]. Combining ionizable blocks which can facilitate transport of water and ions with van der Waals blocks that can provide mechanical stability opens up numerous possibilities for wide range of new materials. Because of the long-range electrostatic interactions, the ionic segments interaction much stronger than the non-ionic segments which has a strong affect the bulk and interfacial characteristics of the macromolecules. As a result of the strong electrostatic interaction, these materials often have a very high glass transition temperature T_g, making them a challenge to process by melt extrusion. Finding a common solvent for the different blocks can also be a challenge as the ionic blocks are miscible in polar solvents which the non-ionic segments often are not. The balance the solvation of soluble blocks and aggregation of insoluble blocks often lead to the formation of long-lived micelles in solution. These micellar assemblies are then directly transferred into the membrane and control the functionality of the membrane.[7, 8] As the blocks are highly incompatible, they exhibit distinctive affinities to different solvents.

Here, we probe the response of a symmetric pentablock co-polymer with a sulfonated polystyrene (PSS) center tethered to polyethylene-r-propylene (PEP) and terminated by poly(t-butyl styrene) (t-BPS) to different solvents. This polymer was designed by Kraton™. The PSS block controls the transport of ions and water, while the PEP blocks provide flexibility and the t-BPS blocks enhance mechanical stability. Due to

high T_g of the PSS blocks, solvent casting is one of the only ways to process this polymer industrially. In non-polar solvents, this pentablock forms micelles with spherical and elliptical symmetries[9, 10] with the PSS blocks residing at the core of the micelle surrounded by the PEP segments. The t-BPS blocks are distributed across the hydrophobic regions with a slight preference to the PSS interface. These micellar assemblies formed in the solution are directly transferred into the membrane and control the functionality of the membrane. As the blocks are highly incompatible, they exhibit distinctive affinities to different solvents.

Choi et al.[9] first showed by x-ray scattering and STEM that in cyclohexane/heptane mixtures, these pentablocks form spherical aggregates with an inner ionic core and outer non-ionic corona. Using small angle neutron scattering, Etempawala et al.[10] showed using small angle neutron scattering that a cyclohexane and heptane mixture these pentablock copolymers form ellipsoidal core-shell micelles with the PSS block in the core and Gaussian decaying chains of swollen PEP and t-BPS in the corona. With increasing solution concentration, they found that the size of the micelle, the thickness of the corona, and the aggregation number increase, while the solvent fraction in the core decreases. Aryal et al.[11] carried out molecular dynamics (MD) simulations of this pentablock in water and in a cyclohexane/heptane mixture. They found that the core of the aggregates consists of a network of PSS with the hydrophobic blocks partially intertwined in the core but predominantly residing in a highly swollen corona. In water, the PSS blocks reside largely at the water-polymer interface, while in a mixed solution of cyclohexane and heptane, a more tightly packed ionic network is formed. The ionic network serves as a long-lived

skeleton of the assembled nanoparticle where the hydrophobic blocks are able to migrate in and out of this structure depending on the nature of the solvent. The importance of the solution structure of these micelles on the properties of solvent casted membranes was studied by Huang et al.[7] They observed that a random distribution of discrete sulfonated domains in membranes casted from a cyclohexane_heptane solution while an ordered pentablock morphology consisting of lamella and hexagonally packed ion groups were observed in films cast from a THF solution.

Here, we the probed response of micellar assemblies of this pentablock for sulfonation level *f* from 0.15 to 0.55 in three solvents: cyclohexane, THF and propanol by using fully atomistic MD simulations. We observed that the pentablock aggregates into core-shell micelles structures in all three solvents. The ionic core and the non-polar corona response differently to the three solvents depending on their polarity. These finding can be integrated into synthesis more efficient transport membranes where shape of the nano aggregates present in the membrane is tuned by the quality of the solvent used in membrane casting.

Model and Methodology

The sulfonation level and molecular weight of our simulated polymers were chosen to be match previous experimental[9, 10] and computational studies.[11-13] The molecular weight of each chain is ~50,000 g/mol with a weight percent (wt%) of the center atactic PSS block is ~40%, each of the randomly substituted PEP blocks is ~20%, and each of the t-BPS blocks is ~10%. The counterion is Na^+. The polystyrene center block was randomly

sulfonated to a sulfonation level of f = 0.15, 0.30 and 0.55. The three solvent systems, cyclohexane, tetrahydrofuran (THF) and propanol, were chosen to match the industrially used solvents to cast the films as well as to cover the broad spectrum of solvent polarity. Previous experimental studies[10] have shown that number of polymer molecule per micelle formed in non-polar solvent varies from 25-70 depending on the concentration of the polymer solution. However, it is known that critical micelle concentration of ionic block copolymer can be extremely low[14]. The number of polymer molecules per micelle for this study were chosen to be 5 pentablock chains by considering these factors as well as the computational time required to equilibrate the systems. These simulations give insight into the effect of solvent polarity on the local packing and structure of the micelles which can be translated into controlling the structure of solvent casted membranes.

Molecular dynamics simulations of multi-chains of ionic pentablock were carried out using the Large-Scale Atomic/Molecular Massively Parallel Simulator (LAMMPS).[15] The pentablock chains and solvent molecules are modelled using the Optimized Potentials for Liquid Simulations All Atoms (OPLS-AA) force fields developed by Jorgensen et al.[16, 17] with updated parameters for the polyethylene-r-propylene block.[18] All Lennard-Jones interactions are cutoff at r_c = 1.2 nm. Coulomb interactions are treated with long-range particle−particle particle-mesh algorithm (PPPM)[19] Ewald with a real space cutoff of 1.2 nm and a precision of 10^{-4}.

The pentablock molecules and three solvents were constructed using Polymer builder and Amorphous Cell modules of Materials Studio®. Following the aggregation of polymers molecules to form micelles in dilute solvent is very challenging computational due to large system size and the slow diffusion of the chains. Therefore, we used a different route to form the micelles[11] in which the five polymer chains were first collapsed into a spherical micelle in an implicit poor solvent and then merged with the solvent. This was done by placing the chains with a large spherical cavity which was slowly reduced in radii

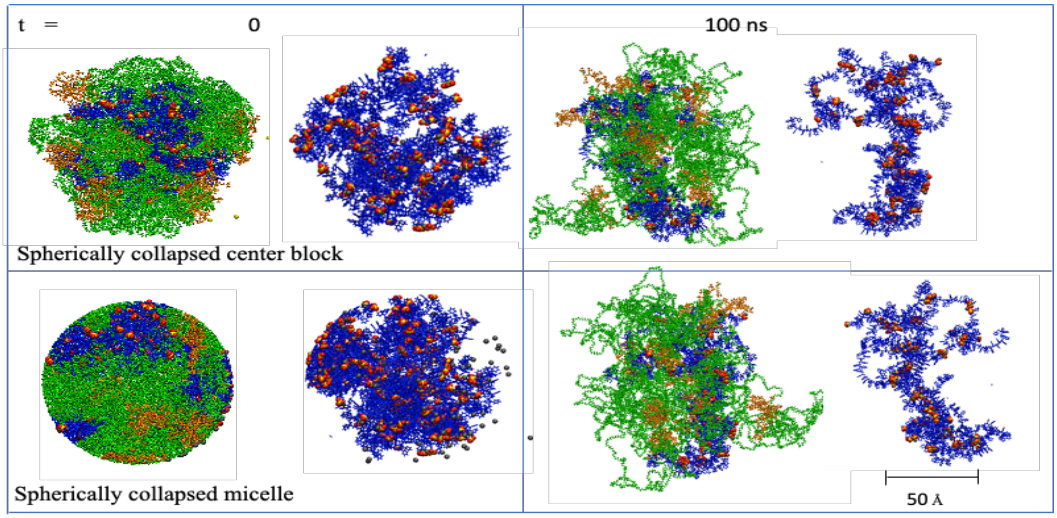

Figure 4.1. Visualization micelles with sulfonation fraction $f = 0.15$ as made (left panel) by compressing the ionic blocks (top) and whole system (bottom) in implicit poor solvent. Right panel corresponds to the micelles after 100 ns in propanol at 500 K. In each frame the entire micelle and the ionic center blocks are shown. The solvent molecules are removed for clarity. The t-BPS block is shown in orange, the PEP in green, polystyrene in blue, oxygen atoms in red, sulfur atoms in yellow and sodium counterions in gray.

until the interior of the micelle reached melt density (in LAMMPS this was done using the 'fix indent' command[20]). We tested two case. In the first, the five polymer chains were compressed to form a spherical aggregate as shown in the bottom row of Figure 4.1. Motivated by previous experimental[9, 10] and computational[11] work that found that the ionic blocks form the core of the micelle, we also make the initial micelles by compressing only the ionic center blocks to form a dense core as shown in the upper row of Figure 1. Separately we equilibrated systems of 97,200 cyclohexane molecules, 83,500 THF molecules and 120,000 propanol molecules in a cubic simulation cell with periodic boundary conditions. After making a cavity in the center of each solvent system large enough to accommodate the collapsed micelle, the micelle and solvent were merged and equilibrated at constant pressure $P = 0$. The final dimensions of the simulation were ~ 30 nm for cyclohexane and propanol and 26.0 nm for THF. The systems were then run a constant volume at a temperature of $T = 500$ K for at least 100 ns. The temperature was

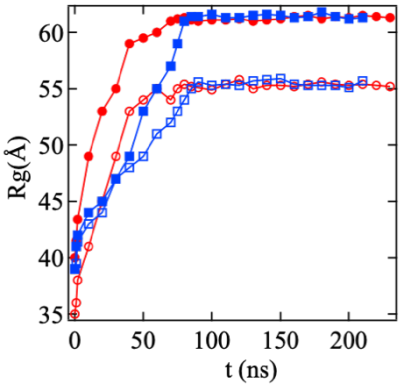

Figure 4.2. Radius of gyration R_g of the micelle (open) and the ionic blocks (solid) as a function of time for $f = 0.15$ in propanol. Red circles correspond to spherically compressing the center blocks and blue squares correspond to compressing the whole system to form the micelles.

maintained by coupling the system weakly to a thermostat with a damping time of 100 ps. After 100 ns, both ways of making the micelles rearranged into similar structures as shown in Figure 1 (right panels) for the micelles in propanol. The time for the two starting states to reorganize was determined by calculating the radius of gyration R_g as function of time for the whole micelle and for the ionic segments as shown in Figure 2. These results show that the size of the micelle as well as that of ionic segments reach a steady state after approximately 100 ns. Similar times were observed for the micelles in cyclohexane and THF. In subsequent discussions, results are presented for the micelles formed by compressing the ionic blocks, though the two give very similar results.

Results

As seen in Figure 4.3, the three blocks respond to the three solvents differently. In cyclohexane, which is non-polar and a good solvent for the non-ionic segments, ionic blocks rearrange at low sulfonation fraction (f = 0.15), while maintaining its overall spherical shape of the micelle. With increasing sulfonation, the ionic blocks condense forming a spherical core, while the non-polar t-BPS and PEP blocks, which are soluble in cyclohexane, the non-ionic blocks forming the corona. In THF, which is more polar and a common solvent for both the ionic and non-ionic segments, the ionic blocks reorganize into a more swollen, extended structure for low sulfonation. For the highest sulfonation fraction (f = 0.55), the ionic blocks form a collapsed aspherical core with the non-ionic blocks forming an extended corona. In propanol, which is polar and good solvent for both ionic and non-ionic blocks, the ionic blocks form a swollen, extended structure for low *f,*

which collapses into a dense, spherical core for large *f*. In contrast to cyclohexane and THF, the non-ionic blocks are more collapsed in propanol.

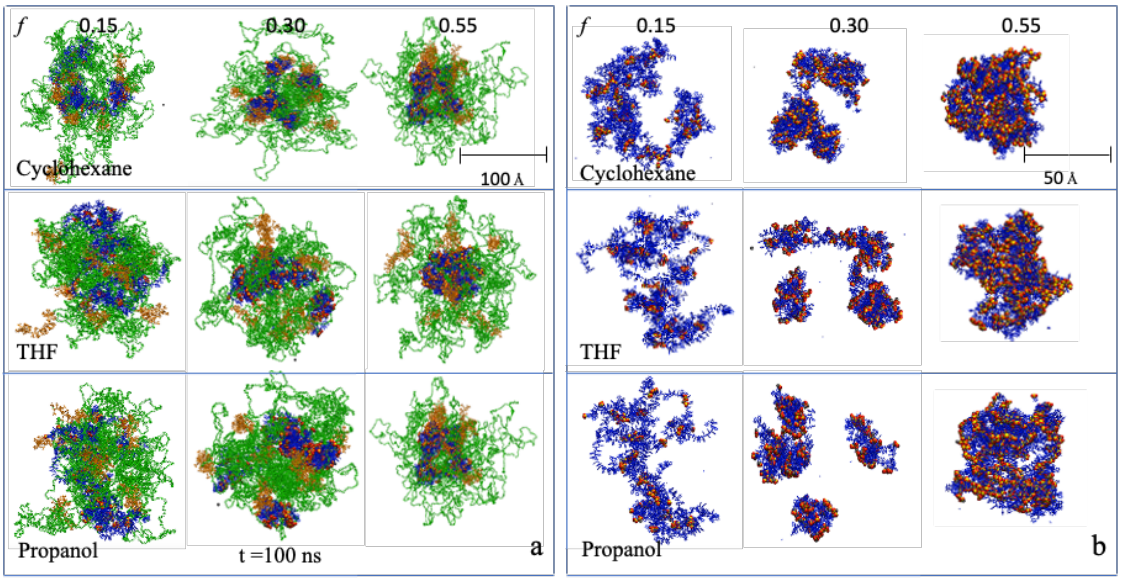

Figure 4.3. Visualization of a) the micelle and b) the ionic center blocks in cyclohexane (top), THF (center) and propanol (bottom) for $f = 0.15$, 0.30 and 0.55 at 500 K. The solvent molecules are removed for clarity. The t-BPS block is shown in orange, the PEP block in green, polystyrene in blue, oxygen atoms in red, and sulfur atoms in yellow.

spherical shape of the micelle. With increasing sulfonation, the ionic blocks condense forming a spherical core to the micelle for $f = 0.55$. The non-polar t-BPS and PEP blocks, which are soluble in cyclohexane, the non-ionic blocks forming the corona. In THF, which is more polar and a common solvent for both the ionic and non-ionic segments, the ionic blocks reorganize into a more swollen, extended structure in low sulfonation. With the highest sulfonation fraction ($f = 0.55$), the ionic blocks form a collapsed aspherical core

with the non-ionic blocks forming an extended corona. In propanol, which is polar and good solvent for both ionic and non-ionic blocks, the ionic blocks form a swollen, extended structure for low *f,* which collapses into a dense, spherical core for large *f*. In contrast to cyclohexane and THF, the non-ionic blocks are more collapsed.

The nano scale aggregation of these pentablocks was further resolved by probing the static structure factor S(q). Computationally, S(q) is given by $S(q) = \sum_{i,j=1}^{N} b_i b_j \langle \exp[i\boldsymbol{q}.(\boldsymbol{r_i} - \boldsymbol{r_j})] \rangle / \sum_{i=1}^{N} b_i^2$,

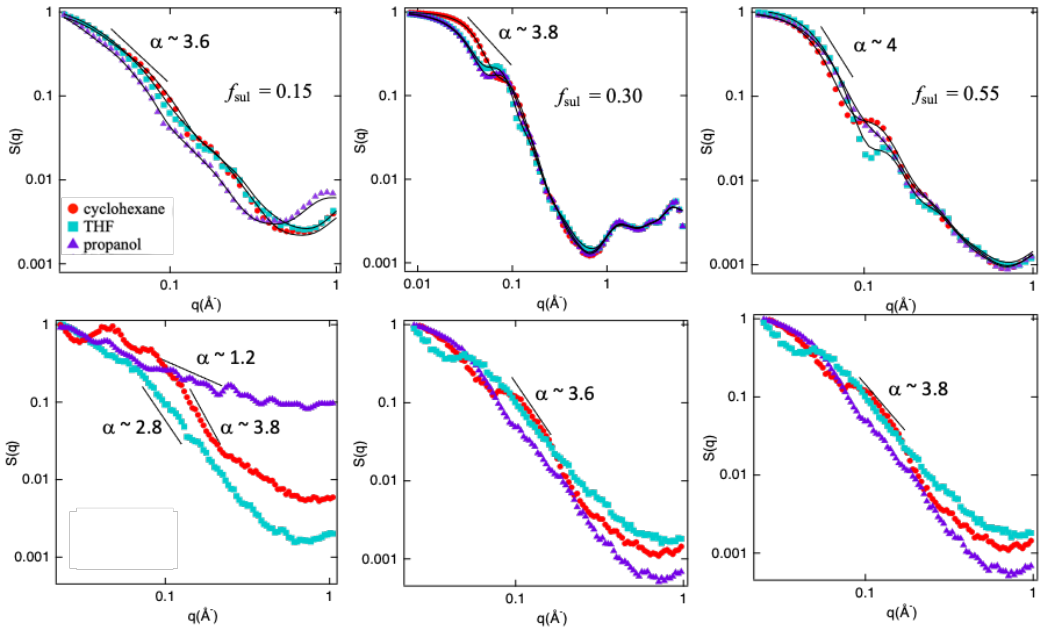

Figure 4.4. Static structure factor *S(q)* as function of wave vector *q* for the micelle (top) and for the ionic blocks (bottom) in cyclohexane (red circles), THF (blue squares) and propanol (purple triangles) for different sulfonation fractions *f* = 0.15 (right), *f* = 0.30 (center), *f* = 0.55 (left). Solid lines correspond best fits to the core-shell model.

where b_i are the scattering lengths and $\boldsymbol{r_i}$ the position of atom i. Using the scattering lengths b_i for neutrons[21, 22], $S(q)$ for entire micelle and for the ionic blocks is shown in Figure 4. All the results are averaged over 200 configurations with 500 random $\boldsymbol{q}$ vectors for each q.

The secondary peak in $S(q)$ at low q is a direct measure of how well-defined the structure of a micelle is. For $f = 0.15$, $S(q)$ does not have a well-defined peak at very q, indicative of the diffuse nature of the micelle, particularly the core which is the strongest scatter. However, with increasing sulfonation, the low q peak $S(q)$ is clearly seen for all three solvents which indicates the formation of a more well-defined aggregate. The effective size of the micelle is given by $d = 2\pi/q_{peak}$, which for $f = 0.30$ and $f = 0.55$ corresponds to $d = 7.9$ nm and 5.2 nm, respectively.

At intermediate q regime, $S(q)$ scales as $q^{-\alpha}$. The value of α depends on the shape of the aggregate. For a sphere, $\alpha = 4$, for a Gaussian chain $\alpha = 2$ and for a cylinder $\alpha = 1$. As seen from the fits in Figure 4.3, α increases from 3.6 to 4.0 as the sulfonation level f increases. This indicates that the micelle become more spherical as f increases, consistent with the visual observations shown in Figure 2. The static structure factor $S(q)$ of just the ionic blocks shows a significant solvent dependency for $f = 0.15$. In cyclohexane $\alpha = 3.8$, which suggests a more spherical aggregate. With increasing solvent polarity α decreases. In propanol, $\alpha \sim 1$ which illustrate the more elongated structure of the ionic blocks for $f = 0.15$. However, for higher sulfonation $\alpha \sim 4$ for all solvents as the ionic blocks form a more spherical core.

Further, insight into the structure was obtained by fitting $S(q)$ for the entire micelle to core-shell form factors[23, 24]. In an ideal core-shell mode, the surface of the core is smooth

and well defined, and the shell is homogeneously distributed around the core. But with the presence of three different blocks which has different flexibility and interactions, there is some intermixing of the core and corona. The model has a correlation term between core and corona which allows for this intermixing. Also, an elliptical or spherical core fit was used depending on the value of α. For $f = 0.15$, the data for $S(q)$ is best fit with an elliptical core-shell model with high degree of intermixing of core and the corona. For $f = 0.30$, spherical-core shell model gave the best fit with significant intermixing of core and corona while $f = 0.55$, the best fit is for a spherical core-shell model with very little intermixing of ionic blocks in the core and the non-ionic blocks in corona. These fits are consistent with the visible observations that for the higher sulfonation levels, core is more homogeneous and spherical.

The distribution of the atoms within the micelles and the ionic blocks are captured as radial density profile as a function of distance from the center of mass of the micelle for the $f = 0.15$ and 0. 55 are shown in Figure 4.5. These mass density profiles support the visual observations of the micelles shown in Figure 4.2 and reveal further details about the aggregates. In all three solvents, the overall density and of the ionic blocks are more diffusive for $f = 0.15$ but much larger with a sharper interface for $f = 0.55$. The radius of the micelle is largest (~ 9 nm) for cyclohexane is ~90 Å and decreases as the polarity of the solvent increases. For $f = 0.55$, the overall size of the micelle is very similar for all three solvents. The solvent density shows that while all three solvent penetrate the core, there is about twice as much propanol and THF in the core than cyclohexane.

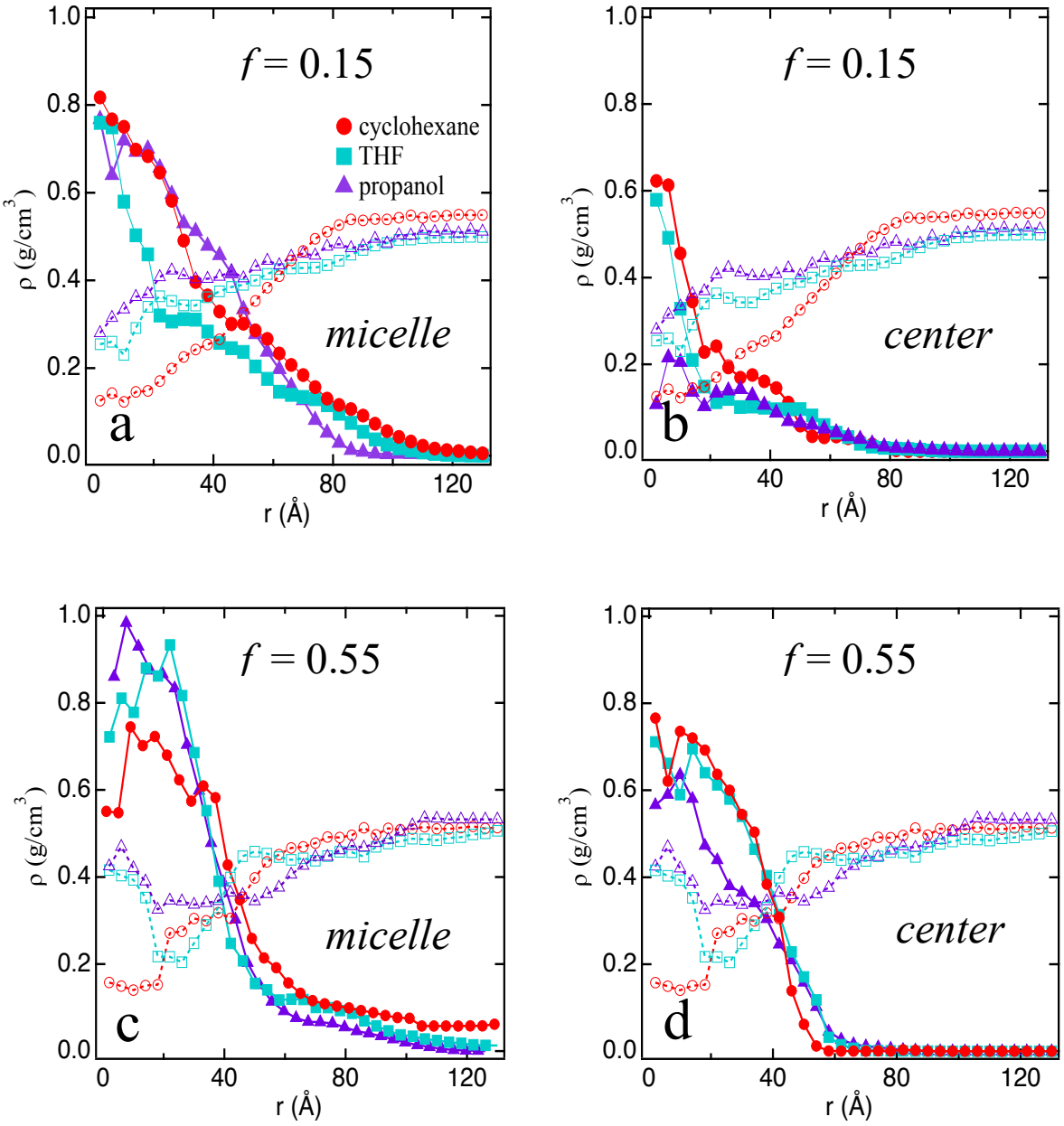

Figure 4.5. Radial density as function distance r from the center of mass of (a) micelle and (b) ionic blocks for $f = 0.15$ and (c) micelle and (d) ionic blocks for $f = 0.55$ (solid symbols) in cyclohexane, THF and propanol. Open symbols are the solvent density.

The ionic groups of the center block aggregate into clusters. For $f = 0.15$ average cluster size is ~ 4 in cyclohexane and decreases ~ 2 for the more polar solvents. Here two SO_3^-

groups are considered to be in the same cluster if two sulfur atoms are separated by a distance of 0.7 nm or less. For the highest sulfonation fraction $f = 0.55$, the average cluster size increases to ~20 for propanol and THF and 24 for cyclohexane. The effects of solvent polarity on cluster formation in ionic core is further explored by probing the association of the solvent molecules with the ionic groups. Figure 6 illustrates the association of cyclohexane and propanol molecules for $f = 0.15$ and $f = 0.55$. For low sulfonation fraction, both all three solvent molecules associate with the ionic groups. However, more propanol

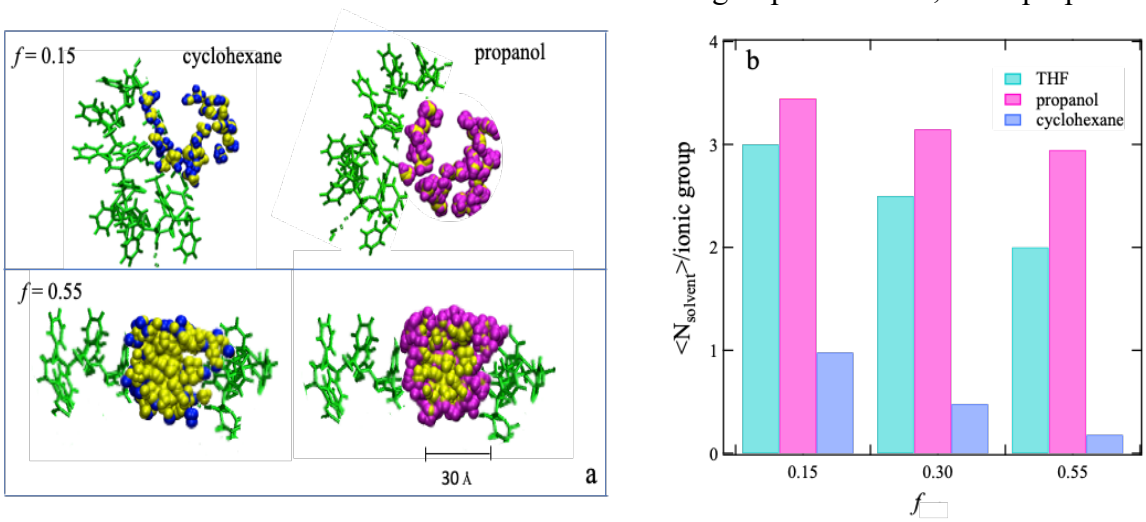

Figure 4.6. a) Example of association of cyclohexane (blue) and propanol (pink) with ionic groups for $f = 0.15$ (top) $f = 0.55$ (bottom). A cross section of the ionic blocks is shown. Yellow corresponds to the sulfur atoms, green represents part of the backbone and the phenyl rings. b) Number of solvent molecules per ionic group associated for with an ionic group for different sulfonation levels.

and THF molecules are associated with the ionic groups at about the same level as for low sulfonation fractions. In contrast, cyclohexane is largely excluded from the core. The THF

and propanol molecules which penetrate into the core, weaken the ionic interaction, resulting in a slightly swollen ionic core compared to cyclohexane (Figure 5b).

Conclusions

Here using molecular dynamics simulations, we studied the of solvent polarity on the structure of micelles made structured ionic block copolymers. We found that the micelles formed from this pentablock copolymer response differently depending on the polarity of the solvent. In cyclohexane, the ionic blocks form a collapsed conformation while non-polar blocks form a swollen state. In contrast to cyclohexane, in propanol and THF the ionic blocks are more swollen and non-polar blocks slightly more collapsed. With increasing sulfonation, ionic blocks condense to form a more stable ionic core. Cyclohexane associated around the dense ionic core while THF and propanol penetrated into the core.

Acknowledgements

We gratefully acknowledges NSF Grant No. DMR-1611136. This research used resources at the National Energy Research Scientific Computing Center (NERSC), a U.S. Department of Energy Office of Science User Facility operated under Contract No. DE-AC02-05CH11231. This work was made possible in part by advanced computational resources deployed and maintained by Clemson Computing and Information Technology. This work was performed, in part, at the Center for Integrated Nanotechnologies, a U.S. Department of Energy and Office of Basic Energy Sciences user facility. Sandia National

Laboratories is a multimission laboratory managed and operated by National Technology and Engineering Solutions of Sandia LLC, a wholly owned subsidiary of Honeywell International Inc., for the U.S. Department of Energy's National Nuclear Security Administration under Contract DE-NA0003525.

References

1. Adhikari, S.; Pagels, M. K.; Jeon, J. Y.; Bae, C., Ionomers for Electrochemical Energy Conversion & Storage Technologies. *Polymer* **2020,** *211*, 123080.
2. Li, Y.; Van Cleve, T.; Sun, R.; Gawas, R.; Wang, G.; Tang, M.; Elabd, Y. A.; Snyder, J.; Neyerlin, K. C., Modifying the Electrocatalyst–Ionomer Interface via Sulfonated Poly (ionic liquid) Block Copolymers to Enable High-Performance Polymer Electrolyte Fuel Cells. *ACS Energy Letters* **2020,** *5* (6), 1726-1731.
3. Wang, S.; Yang, L.; He, G.; Shi, B.; Li, Y.; Wu, H.; Zhang, R.; Nunes, S.; Jiang, Z., Two-dimensional nanochannel membranes for molecular and ionic separations. *Chemical Society Reviews* **2020,** *49* (4), 1071-1089.
4. Fam, W.; Mansouri, J.; Li, H.; Chen, V., Improving CO2 separation performance of thin film composite hollow fiber with Pebax® 1657/ionic liquid gel membranes. *Journal of membrane science* **2017,** *537*, 54-68.
5. Lu, B.; Zhou, G.; Xiao, F.; He, Q.; Zhang, J., Stimuli-responsive poly (ionic liquid) nanoparticles for controlled drug delivery. *Journal of Materials Chemistry B* **2020,** *8* (35), 7994-8001.

6. Gao, L.-f.; Lin, X.; Hai, X.; Chen, X.-w.; Wang, J.-h., Polymeric Ionic Liquid-Based Fluorescent Amphiphilic Block Copolymer Micelle for Selective and Sensitive Detection of p-Phenylenediamine. *ACS applied materials & interfaces* **2018,** *10* (49), 43049-43056.

7. Huang, F.; Largier, T. D.; Zheng, W.; Cornelius, C. J., Pentablock copolymer morphology dependent transport and its impact upon film swelling, proton conductivity, hydrogen fuel cell operation, vanadium flow battery function, and electroactive actuator performance. *J. Mem. Sci.* **2018,** *545*, 1-10.

8. Madathil, K.; Lantz, K. A.; Stefik, M.; Stein, G. E., Effects of Trace Water on Self-Assembly of Sulfonated Block Copolymers During Solution Processing. *ACS App. Poly. Mat.* **2020**.

9. Choi, J.-H.; Kota, A.; Winey, K. I., Micellar Morphology in Sulfonated Pentablock Copolymer Solutions. *Ind. Eng. Chem. Res.* **2010,** *49* (23), 12093-12097.

10. Etampawala, T. N.; Aryal, D.; Osti, N. C.; He, L.; Heller, W. T.; Willis, C. L.; Grest, G. S.; Perahia, D., Association of a Multifunctional Ionic Block Copolymer in a Selective Solvent. *J. Chem. Phys.* **2016,** *145*, 184903.

11. Aryal, D.; Grest, G. S.; Perahia, D., Nano Ionic Networks: Association of Structured Ionic Polymers in Solution. *Nanoscale* **2016,** *9*, 2117-2122.

12. Aryal, D.; Etampawala, T.; Perahia, D.; Grest, G. S., Phase Behavior of a Single Structured Ionomer Chain in Solution. *Macromolecular Theory and Simulations* **2014,** *23*, 543-549.

13. Aryal, D.; Perahia, D.; Grest, G. S., Solvent controlled ion association in structured copolymers: Molecular dynamics simulations in dilute solutions. *J. Chem. Phys.* **2015,** *143*, 124905.

14. Letchford, K.; Burt, H., A review of the formation and classification of amphiphilic block copolymer nanoparticulate structures: micelles, nanospheres, nanocapsules and polymersomes. *European journal of pharmaceutics and biopharmaceutics* **2007,** *65* (3), 259-269.

15. Plimpton, S., Fast parallel algorithms for short-range molecular dynamics. *J. Comp.Phys.* **1995,** *117*, 1-19.

16. Jorgensen, W. L.; Madura, J. D.; Swenson, C. J., Optimized Intermolecular Potential Functions for Liquid Hydrocarbons. *J. Am. Chem. Soc.* **1984,** *106*, 6638-6646.

17. Jorgensen, W. L.; Maxwell, D. S.; TiradoRives, J., Development and testing of the OPLS all-atom force field on conformational energetics and properties of organic liquids. *J. Am. Chem. Soc.* **1996,** *118*, 11225-11236.

18. Murzyn, K.; Bratek, M.; Pasenkiewicz-Gierula, M., Refined OPLS all-atom force field parameters for n-pentadecane, methyl acetate, and dimethyl phosphate. *J. Phys. Chem. B* **2013,** *117*, 16388-16396.

19. Hockney, R. W.; Eastwood, J. W., *Computer Simulation Using Particles* Adam Hilger-IOP, Bristol: 1988.

20. LAMMPS webpage: http://lammps.sandia.gov.

21. Jackson, A. J., Introduction to small-angle neutron scattering and neutron reflectometry. *NIST Center for Neutron Research* **2008**, 1-24.

22. Hammouda, B., Probing Nanoscale Structures: The SANS Toolbox (2009). *NIST Center for Neutron Research* **2008**.

23. Pedersen, J. S.; Gerstenberg, M. C., Scattering form factor of block copolymer micelles. *Macromolecules* **1996,** *29* (4), 1363-1365.

24. Pedersen, J. S., Form factors of block copolymer micelles with spherical, ellipsoidal and cylindrical cores. *Journal of Applied Crystallography* **2000,** *33* (3), 637-640.

CHAPTER FIVE

INTERFACIAL RESPONSE OF STRUCTURED IONOMER THIN FILMS

Abstract

Ionic block co-polymers with distinctive block characteristics display the diversity crucial for design of macromolecules for targeted applications. From the energy-water nexus to biotechnology, controlling the interrelation between interfacial response and bulk behavior of these polymers remains a challenge. Here we probe a symmetric block co-polymer with a sulfonated polystyrene center tethered to polyethylene-r-propylene and terminated by poly(t-butyl styrene) at the interface with water, propanol and THF using molecular dynamics simulations. We find that the interfacial width at the water interface decreases, exposing more ionizable groups whereas the interfacial width for the propanol and THF systems increases and is dominated by hydrophobic blocks. Water molecules associate predominantly with the ionic blocks while propanol and THF reside in both the ionic and non-ionic segments. The composition and topology of the interfaces reflect the response of the individual segments to the solvents; nevertheless, they are strongly coupled with the solvent effects on the ionic clusters.

Introduction

Ionizable polymeric membranes are in the core of the energy-water nexus and transcend numerous biotechnology applications, where they facilitate ion transport across interfaces. [1-3] Their technological promise has driven immense efforts to tether ionizable segments that enable transport to van der Waals polymers, incorporating the rich phase diagrams that co-polymers offer with the transport ability of ionic polymers.[4]

Incorporating ionizable groups into van der Waals co-polymers introduces long range electrostatic interactions that affect the bulk and interfacial characteristics of the macromolecules. Additionally, these ionic segments impact the interactions of the polymer with solvents which are often an integral part of many technologies. Although tailoring ionic polymers chemistry and topology to targeted application provides a promising approach to molecular engineering, their interfaces, particularly in presence of solvents, remain largely uncontrolled. Manifestation of interfacial dynamics is a time lag observed between the onset of exposure of polymers such as polystyrene sulfonate (PSS), PFSIs and Nafion™ to solvents and the actual onset of diffusion. [5-7] This delay has been attributed to the time it takes for the interface to rearrange and transport channels to form. However molecular insight to understanding the dynamics at the interface and formation of transport channels, is yet to be realized. The challenge lies in the structured nature of the co-polymers whose blocks are highly segregated and each block has a markedly different affinity and response at interfaces with solvents. The intricate relation between the multiple blocks of ionizable co-polymers results in a broad range of fundamental new macromolecular behavior.

Controlling the response of a structured, ionizable co-polymer to solvents at films interfaces and at internal boundaries requires molecular level insight of the evolving interfacial structures in these films. Here using fully atomistic classical molecular dynamics (MD) simulations, we probe the interfacial regions of structured ionic block co-polymers at the boundary with solvents.[8] We find that though the interfacial region often rearranges in contact with solvents, unlocking ionic clusters is critical to the polymer

response to solvents and their overall structural adaptation.

Specifically, we probe interfacial dynamics of a model ionizable pentablock co-polymer with a randomly sulfonated polystyrene (PSS) tethered symmetrically to two non-polar blocks of poly(ethylene-r-propylene) (PEP) terminated by two poly(t-butyl styrene) blocks (t-BPS). This polymer was designed by Kraton™ with the rational that tethering mechanical stabilizing groups symmetrically around an ionizable block will lead to ion and water transporting channels surrounded by mechanically stablizing groups. The blocks are in the high segregation limit and exhibit distinctive affinities to most common solvents. The intriguing structure and potential technological uses of this co-polymer have driven numerous studies of solutions[9-14] and membranes[15-22] of this pentablock. These studies provide the first insight into the interrelation of the polymer with solvents and set the foundation for the choice of systems probed herein. This pentablock forms micelles in non-polar solvents with spherical and elliptical symmetries.[10-11] The PSS blocks reside at the core surrounded by the PEP segment. The t-BPS is distributed across the hydrophobic regions with a slight preference to the PSS interface. A direct molecular insight was attained by MD simulations by Aryal et al.[23] who found that in contrast to spherical micelles formed by non-ionic block co-polymers, the core of the aggregates consists of a network of PSS. The hydrophobic blocks are partially intertwined in the core but predominantly reside in a highly swollen corona. In high dielectric constant solvents such as water, the PSS blocks reside largely at the water-polymer interface. The ionic networks within these micelles, however, are retained when the micelle is expose to solvents of different nature while the hydrophobic segments respond to changes in the solvent

environment.[11] These aggregates assemble into membranes where the shape, size and distribution of the ionic assemblies are strongly affected by the casting solvents and in turn affects the transport ability of the membranes.[14, 17]

The interface of membranes of this pentablock cast from numerous solvents is structured and consists of nano domains of all blocks. Using MD simulations Aryal et al.[8] showed that upon exposure to water, interfacial rearrangements take place, where the non-sulfonated segments are driven away from the water interface.

Building on the fundamental observations that the interface of the pentablock rearranges when exposed to water, we study the polymer-solvent interface response to water, propanol and THF. Three solvents were chosen with the rational of providing distinctive environments with direct impact on processing of the polymers into membranes and their operation within different applications. The response of the polymer films was followed for extended times to allow not only to capture the interfacial response but to follow the effects of solvents on the internal dynamics of the polymers. Figure 5.1 visualizes the polymer-solvent systems with the three solvents as made (t=0) and at 1000 ns. The response of thin films to vapors of these solvents is explored with the overarching goal of obtaining a molecular insight into transport across the membrane interface. We find that the interfacial response is a convoluted function of the interaction of each of the blocks with the solvents and is strongly affected by the ionic network.

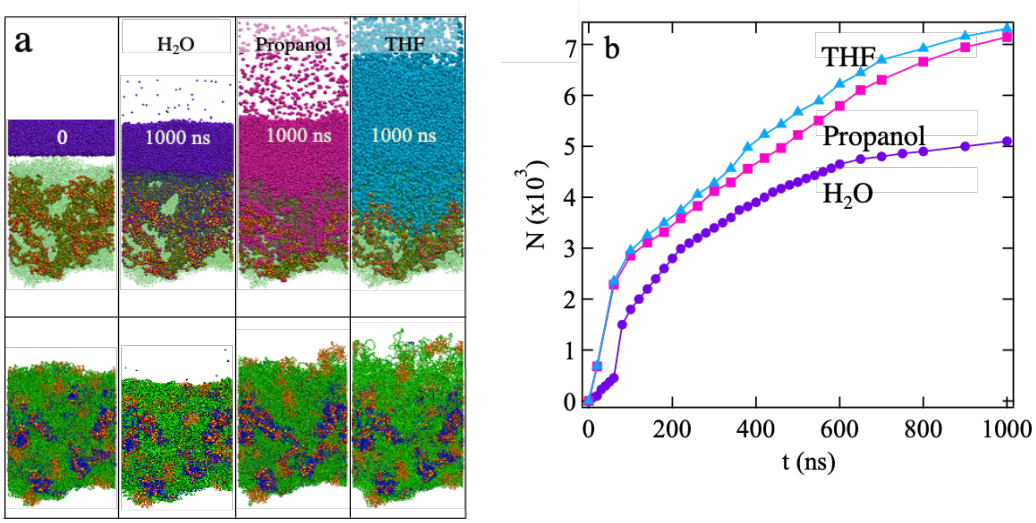

Figure 5.1 a) Visualization of the solvent/membrane systems with water, propanol and THF after 1000 ns for $f = 0.55$ at 400 K. The top images depict the solvents where some of the polymer molecules are plotted in a semi-transparent mode. The lower images correspond to the polymer molecules and the solvent molecules are removed for clarity. The image at time $t = 0$ corresponds to the membrane and water layer prior to direct exposure. The t-butyl polystyrene block is shown in orange, ethylene-propylene block in green, polystyrene block in blue, oxygen atoms in red, sulfur atoms in yellow, propanol and THF atoms in pink, and water molecules in violet. b) Number of solvent molecules N in the membrane as a function of time t for water propanol, and THF.

Methodology

The pentablock, propanol and THF were built using the Polymer Builder and Amorphous Cell modules in Accelrys Materials Studio©. All three were modeled using All Atoms Optimized Potential for Liquid Simulations (OPLS-AA) force fields developed by Jorgensen et al.[24-25] with updated parameters for the polyethylene-r-propylene block.[26]

Water molecules were modeled using the TIP4P/EW model.[27] All Lennard-Jones interactions are cutoff at r_c = 1.2 nm. Coulomb interactions are treated with long-range particle−particle particle-mesh algorithm (PPPM)[28] Ewald with a real space cutoff of 1.2 nm and a precision of 10^{-4}.

The polymer membrane contained thirty pentablock chains, each with a molecular weight ~50,000 g/mol. The total weight percent (wt%) of the center atactic PSS block is ~40%, each of the randomly substituted PEP blocks is ~20%, and each of the t-BPS blocks is ~10%. The counterion is Na^+. The polystyrene center block was randomly sulfonated to a sulfonation level of f = 0.55. The membrane thickness is ~ 17 nm with a cross-sectional area L_x x L_y = 16 nm x16 nm. The length of simulation cell perpendicular to the film L_z = 40 nm to allow space for the solvent. A smooth, repulsive walls, modeled by a purely repulsive 9-3 LJ potential, were placed at the upper and lower edge of the simulation cell to keep the molecules from crossing directly from one side of the membrane to the other. The simulation cell is periodic in the x and y directions. Three systems of 64,000 water molecules, 23,700 propanol and 23,500 THF molecules were equilibrated in a cell with dimensions L_x and L_y matching that of the pentablock film. A slab of 6 nm thick water, 14 nm thick propanol and THF were cut from the bulk simulation and placed in contact with one surface of the pentablock film as shown in Figure 1. A a small space was left between the top of the solvent films and the upper wall as seen in Figure 1 to facilitate formation of a vapor. Since water, propanol and THF evaporate into this gap, the diffusion into the membrane is under ambient pressure. For more details see Aryal et al.[8]

All simulations were carried out using the LAMMPS MD code. The Newton equations of motions were integrated using a velocity-Verlet algorithm. The reference system propagator algorithm (RESPA)[29] with multi-time scale integrator and a time step of 1.0 fs for the bond, angle, dihedral, van der Waals interactions, and direct interactions part of the electrostatic interactions was used. For the long-range electrostatic interactions, a time step of 2.0 fs was used. The temperature of the system was maintained with a Langevin thermostat with a damping time of 0.1 ps. After the water, propanol and THF slabs are placed in contact with the polymer, each system was run at constant volume for 1000 ns.

Results

The visualization of water, propanol and THF -membranes systems is presented in Figure 1a, 1000 ns after exposure to the solvents. These exceedingly long times are comparable with segmental dynamics of non-ionic polymer melts and allow the solvent molecules to transverse the membranes. Upon exposure of the films to water, propanol and THF notable different procceses take place at the interface as observed in the bottom panel of Figure 1a. Water drive retraction and packing of the hydrohobic chains at the interfaces, exposing some of the ionic segments, whereas at the interface with propanol or THF the hydrophobic blocks are swollen by the solvents. However, some sulfonated segments reside at the interface with all three solvents. The images show that propanol and THF reside in all blocks in contrast to water that is located predominantly in the sulfonated one, pointing to different transport pathways for each of the solvents.

The number of solvent molecules in the membrane as a function of exposure time is shown in Figure 5.1b. For water, an initial slow onset is observed where rearrangements take place and expose the sulfonated groups to the solvents. These results for the early times are consistent with those observed in MD simulations by Aryal et al.[8] and experimentally by neutron reflectivity by He et al. for other inomers.[6] In contrast, propanol and THF rapidly diffuse into the membranes and the hydrophobic blocks swell. At long exposure times all three solvents drive rearrangements of the ionic clusters. A top view of the interfaces for the three solvents is presented in Figure 5.2a. The surface of the dry film is dominated by hydrophobic groups as shown at *t=0.*

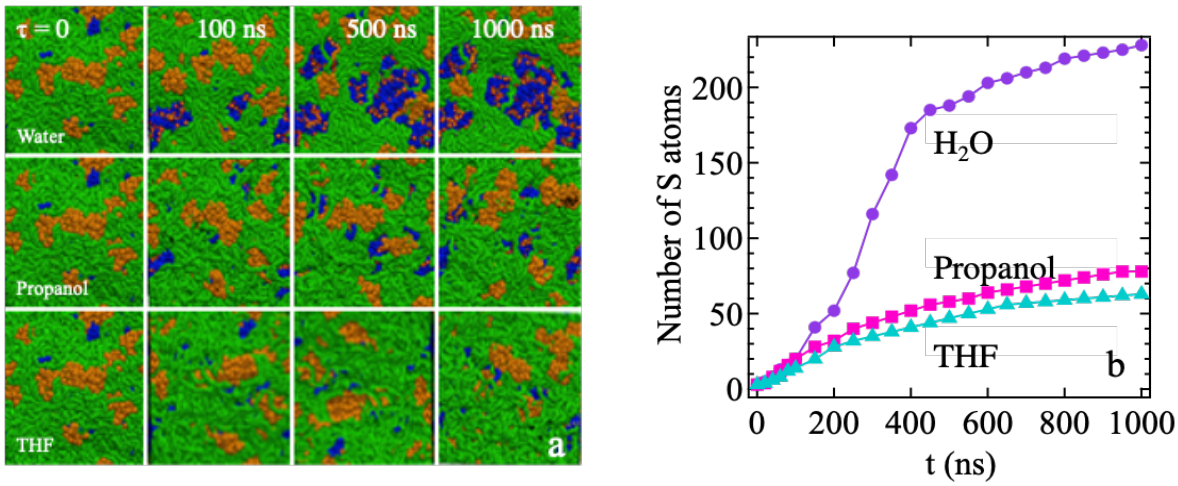

Figure 5.2. a) Top view of the polymer-solvent interface at the indicated simulation times. The t-BPS block is shown in orange, PEP block in green, polystyrene block in blue, oxygen atoms in red, and sulfur atoms in yellow. b) Number of sulfur atoms at the polymer-solvent interface as a function of time for water, propanol, and THF.

In contact with water, the hydrophobic segments retract from the interface exposing more ionic groups, whereas in THF and propanol the hydrophobic groups initially swell. At later times however, the ionic groups migrate to the interface. This interfacial response in water is consistent with previous observations of Aryal el al.[23] who showed that in micellar solutions of the pentablock, the hydrophobic segments retract in presence of water while dominating the interface with cyclohexane, whereas the ionic blocks form a network that remains stable. For all solvents however, the number of sulfonated groups that reside at the interface increases with exposure time as shown in Figure 2b. The number of additional sulfur atoms at the polymer-water interface is four times larger than at the polymer-propanol and THF interfaces after 1000 ns.

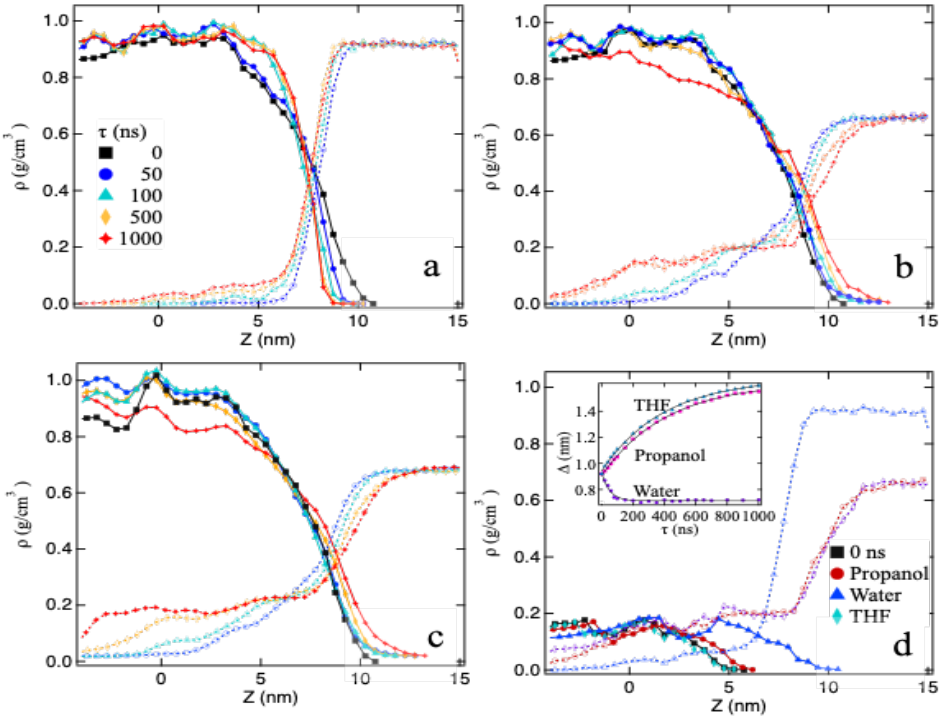

Figure 5.3. Mass density of the polymer films at the interface with a) water b) propanol and c) THF as a function of distance z from center of membrane at different exposure times

along with the profiles of the corresponding solvents. d) the density profile of the ionic block prior to exposure (neat) and at 1000 ns after exposure to the three solvents. Insert presents the time evolution of interfacial width for the 3 solvents. Full symbols represent the polymer density and open symbols the solvents.

The response of the polymer film to the different solvents was further explored following the time evolution of the density of membrane exposed to the three solvents. The interfacial profiles, measured from the center of the film, perpendicular to the interface, presented in Figure 5.3 a-c, clearly show that the polymer exhibits a sharp interface with water while the interface with propanol and THF are significantly broader. In bulk, the ionic clusters dominate the dynamics of the polymers. To corelate the interfacial dynamics with the ionic clusters network, the density profiles for PSS were extracted and are shown are shown in Figure 5.3d. These profiles reveal that with increasing exposure time to water the PSS blocks migrate towards the interface. In comparison, only small changes are noticeable in the location of the PSS for films exposed to propanol and THF.

The interfacial widths of the films capture the inherent roughness of the polymer boundaries and the degree of swelling. The interfacial width Δ was calculated by fitting the interfacial region to an error function $erf(z/\sqrt{2}\Delta)$. The interfacial widths for the three solvents are shown in the inert of Figure 5.3-d. For water, the interfacial width decreases with time of exposure while in propanol and THF, it increases, though the rate of change decreases after ~500 ns.

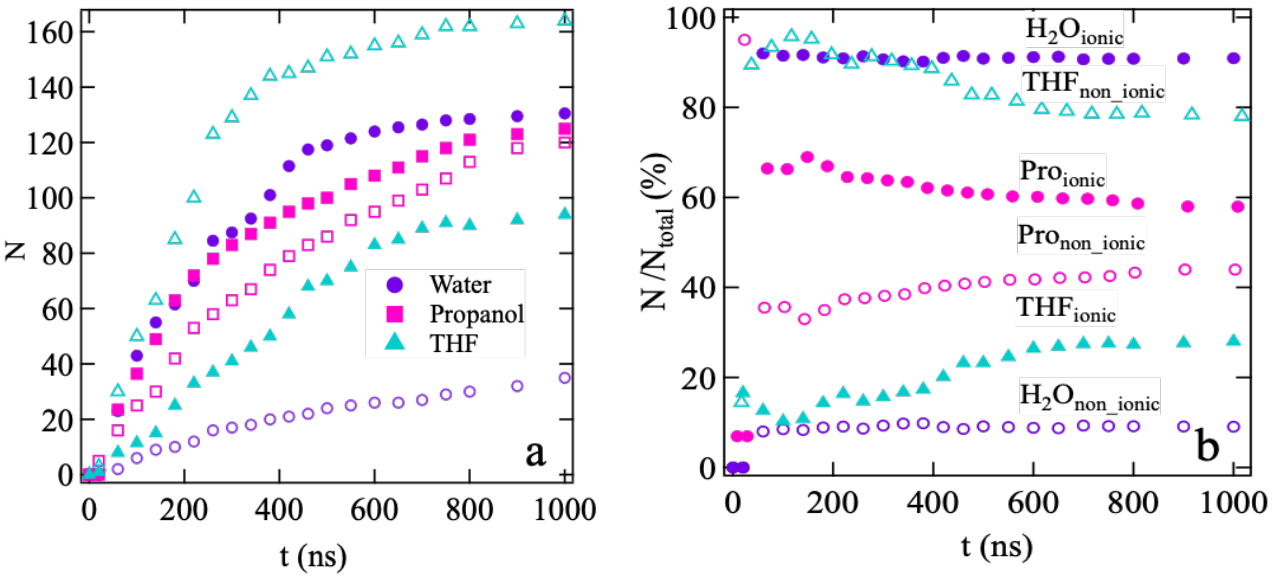

Figure 5.4. a) The uptake of solvent in the PSS (full symbols) and the t-BPS and PEP blocks (open symbols) in a 4nm thick slab at the center of the film and b) the percentage of solvent molecules in the different blocks.

With a clear distinction in the interfacial characteristics of the polymer exposed to water, propanol and THF, we further probed the solvent distribution as a function of time for a 4nm slab in the center of the film. Figure 4a captures the number of solvent molecules that reside in this slab in both the ionic and non-ionic blocks. With increasing exposure time, all three solvents diffuse into the film and reach a steady state at the center. Most of the water molecules reside in the PSS blocks. In contrast, significant amounts of THF reside in the hydrophobic region, with yet a notable number are associated with the PSS block. The propanol however is distributed across both regions. The fraction of solvent molecules in each of the blocks is shown in Figure 4b, where the time dependence of the

percentage of the number of each of the solvent molecules in the center slab is plotted. Hardly any changes are observed for the water distribution with time. At early times significant amount of THF resides in the hydrophobic blocks, however as time progresses, some of the THF molecules migrate into the hydrophilic regions. Even at the initial stage the propanol, resides in both ionic with a slight preference to the ionic regime. With increasing time, the difference is reduced. We note that though THF and propanol reside in all segments, the ionic networks are retained, though are changing in size and shape. These results are consistent with our solution studies[23] that have shown that in propanol the micelles expand and change shape but do not break and the sulfonated blocks remain in the core.

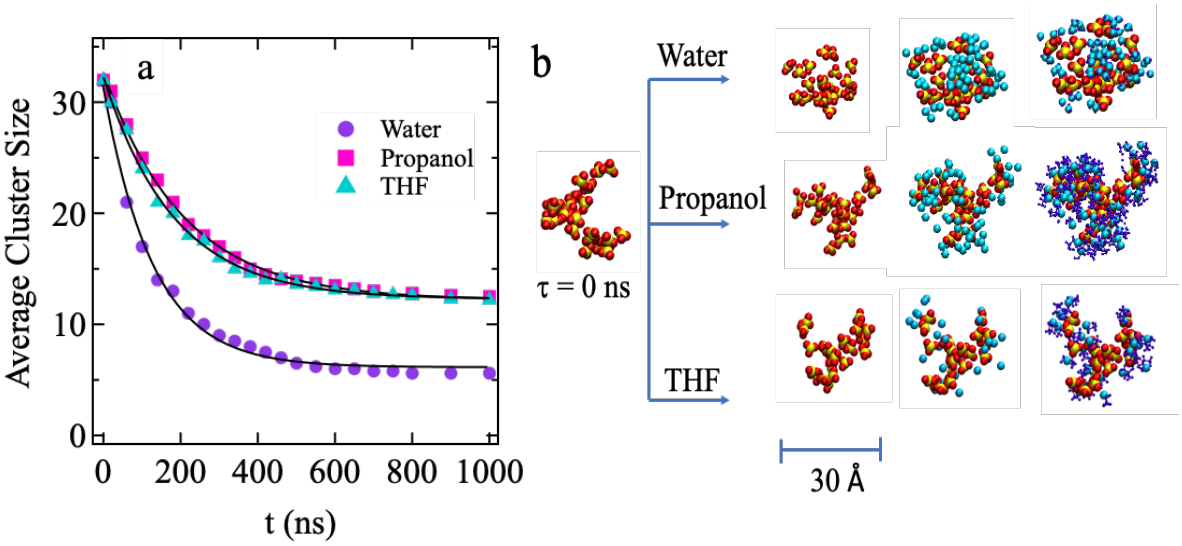

Figure 5.5. a) Average cluster size in a 4 nm thick slab at the center of membrane as function of time for water, propanol, and THF. b) Illustration of breakup of ionic network into small ionic clusters in water, propanol and THF.

The correlation of the solvent distribution among the blocks with the ionic clusters characteristics was explored by calculating changes in the average cluster size with time in this center slab. Ionic clusters are defined by assuming that any two sulfur atoms that are separated by less than 0.6 nm, are in the same ionic cluster. The closest distance between two sulfur is a cluster is 0.46 nm. The average cluster size in the 4 nm thick slab at the center of membrane as a function of time is shown in Figure 5a. Similar results for the cluster size distribution are obtained with cutoff distance 0.5 or 0.7 nm.

For all three solvents, the average cluster size decreases with increasing number of solvent molecules, where the most pronounced effect is in water compared to propanol and THF. The cluster dimensions do not change any further after the solvent saturates the membrane. To calculate the degree of association of solvent molecules with the ionic clusters, we define a sphere around each sulfur atoms of radius 0.7 nm. If any atom in a solvent molecule is within any sphere around a sulfur atom, it is counted as being associated with an ionic cluster, otherwise it is counted as being associated with the other two blocks. The number of solvent molecules directly associated with the sulfonated groups is markedly different for water and propanol as demonstrated in Figure 5b. The association pattern of the solvent molecules with the ionic clusters is attributed to both the polarity of the solvents and the size of the solvent. Nevertheless, the clusters in solvents with lower dielectric constants are larger compared to water.

Conclusions

This study offers an insight into response structured ionic block copolymers films to solvents of different polarities including water, propanol and THF. The interface of the

dry membrane is dominated by the aliphatic domains. With exposure to water, the interfaces rearrange; hydrophobic segments retract, exposing more hydrophilic groups and the interface becomes smoother. At the interface with propanol and THF, the hydrophobic segments swell, and fewer ionic groups reside at the interface compared to water. While propanol and THF penetrate the membrane at a higher rate than water, their distribution in the different blocks is markedly different. Water penetrates the film predominantly through the PSS domains, while propanol and THF reside in all blocks. All three solvents strongly effect the of size and distribution of the ionic clusters. The overall response of the film is strongly affected by the network of ionic clusters that change in size and continuity with solvent penetration.

Acknowledgements

DP gratefully acknowledges NSF Grant No. DMR-1611136. This research used resources at the National Energy Research Scientific Computing Center (NERSC), a U.S. Department of Energy Office of Science User Facility operated under Contract No. DE-AC02-05CH11231. This work was made possible in part by advanced computational resources deployed and maintained by Clemson Computing and Information Technology. This work was performed, in part, at the Center for Integrated Nanotechnologies, a U.S. Department of Energy and Office of Basic Energy Sciences user facility. Sandia National Laboratories is a multimission laboratory managed and operated by National Technology and Engineering Solutions of Sandia LLC, a wholly owned subsidiary of Honeywell International Inc., for the U.S. Department of Energy's National Nuclear Security Administration under Contract DE-NA0003525. The authors knowledge valuable

discussions with Carl Willis, Marc Charendoff and Robert Banning at Kraton Polymers LLC.

REFERENCES

1. Adhikari, S.; Pagels, M. K.; Jeon, J. Y.; Bae, C., Ionomers for Electrochemical Energy Conversion & Storage Technologies. *Polymer* **2020**, 123080.
2. Li, D.; Park, E. J.; Zhu, W.; Shi, Q.; Zhou, Y.; Tian, H.; Lin, Y.; Serov, A.; Zulevi, B.; Baca, E. D., Highly quaternized polystyrene ionomers for high performance anion exchange membrane water electrolysers. *Nature Energy* **2020**, 1-8.
3. Long, X.; Deng, C.; Xiao, G.; Cheng, F.; Zhou, Y.; Zhao, L.; Cai, L.; Chen, J.; Du, J., Electrochemical Sensors with Antifouling Properties for Sensitive Detection of Isoproturon Based on Glassy Carbon Electrode Modified with Nafion Membrane. *Int. J. Electrochem. Sci* **2020,** *15*, 4964-4977.
4. Park, M. J.; Balsara, N. P., Phase behavior of symmetric sulfonated block copolymers. *Macromolecules* **2008,** *41* (10), 3678-3687.
5. Zawodzinski Jr, T. A.; Derouin, C.; Radzinski, S.; Sherman, R. J.; Smith, V. T.; Springer, T. E.; Gottesfeld, S., Water uptake by and transport through Nafion® 117 membranes. *Journal of the electrochemical society* **1993,** *140*, 1041-1047.
6. He, L. L.; Smith, H. L.; Majewski, J.; Fujimoto, C. H.; Cornelius, C. J.; Perahia, D., Interfacial Effects on Water Penetration into Ultrathin Ionomer Films: An in Situ Study Using Neutron Reflectometry. *Macromolecules* **2009,** *42*, 5745-5751.

7. Zhao, Q.; Majsztrik, P.; Benziger, J., Diffusion and interfacial transport of water in Nafion. *The journal of physical chemistry B* **2011,** *115* (12), 2717-2727.

8. Aryal, D.; Agrawal, A.; Perahia, D.; Grest, G. S., Structured Ionomer Thin Films at Water Interface: Molecular Dynamics Simulation Insight. *Langmuir : the ACS journal of surfaces and colloids* **2017,** *33* (41), 11070-11076.

9. Choi, J.-H.; Kota, A.; Winey, K. I., Micellar Morphology in Sulfonated Pentablock Copolymer Solutions. *Ind. Eng. Chem. Res.* **2010,** *49* (23), 12093-12097.

10. Griffin, P. J.; Salmon, G. B.; Ford, J.; Winey, K. I., Predicting the solution morphology of a sulfonated pentablock copolymer in binary solvent mixtures. *J. Polym. Sci. B Polym, Phys,* **2016,** *54*, 254-262.

11. Etampawala, T. N.; Aryal, D.; Osti, N. C.; He, L.; Heller, W. T.; Willis, C. L.; Grest, G. S.; Perahia, D., Association of a Multifunctional Ionic Block Copolymer in a Selective Solvent. *J. Chem. Phys.* **2016,** *145*, 184903.

12. Mineart, K. P.; Jiang, X.; Jinnai, H.; Takahara, A.; Spontak, R. J., Morphological Investigation of Midblock-Sulfonated Block Ionomers Prepared from Solvents Differing in Polarity. *Macro. Rapid Comm.* **2015,** *36*, 432-438.

13. Mineart, K. P.; Ryan, J. J.; Appavou, M.-S.; Lee, B.; Gradzielski, M.; Spontak, R. J., Self-Assembly of a Midblock-Sulfonated Pentablock Copolymer in Mixed Organic Solvents: A Combined SAXS and SANS Analysis. *Langmuir : the ACS journal of surfaces and colloids* **2019,** *35*, 1032-1039.

14. Madathil, K.; Lantz, K. A.; Stefik, M.; Stein, G. E., Effects of Trace Water on Self-Assembly of Sulfonated Block Copolymers During Solution Processing. *ACS App. Poly. Mat.* **2020**.

15. Fan, Y.; Zhang, M.; Moore, R. B.; Cornelius, C. J., Structure, physical properties, and molecule transport of gas, liquid, and ions within a pentablock copolymer. *J. Mem. Sci.* **2014,** *464*, 179-187.

16. Laprade, E. J.; Liaw, C. Y.; Jiang, Z.; Shull, K. R., Mechanical and microstructural characterization of sulfonated pentablock copolymer membranes. *J. Polym. Sci. B Polym, Phys,* **2015,** *53*, 39-47.

17. Huang, F.; Largier, T. D.; Zheng, W.; Cornelius, C. J., Pentablock copolymer morphology dependent transport and its impact upon film swelling, proton conductivity, hydrogen fuel cell operation, vanadium flow battery function, and electroactive actuator performance. *J. Mem. Sci.* **2018,** *545*, 1-10.

18. Truong, P. V.; Shingleton, S.; Kammoun, M.; Black, R. L.; Charendoff, M.; Willis, C.; Ardebili, H.; Stein, G. E., Structure and properties of sulfonated pentablock terpolymer films as a function of wet–dry cycles. *Macromolecules* **2018,** *51*, 2203-2215.

19. Akhtar, F. H.; Vovushua, H.; Villalobos, L. F.; Shevate, R.; Kumar, M.; Nunes, S. P.; Schwingenschlögl, U.; Peinemann, K.-V., Highways for water molecules: Interplay between nanostructure and water vapor transport in block copolymer membranes. *J. Mem. Sci.* **2019,** *572*, 641-649.

20. Filice, S.; Mazurkiewicz-Pawlicka, M.; Malolepszy, A.; Stobinski, L.; Kwiatkowski, R.; Boczkowska, A.; Gradon, L.; Scalese, S., Sulfonated Pentablock Copolymer Membranes and Graphene Oxide Addition for Efficient Removal of Metal Ions from Water. *Nanomaterials* **2020,** *10*, 1157.

21. Thomas, E. R.; Jain, A.; Mann, S. C.; Yang, Y.; Green, M. D.; Walker, W. S.; Perreault, F.; Lind, M. L.; Verduzco, R., Freestanding self-assembled sulfonated pentablock terpolymer membranes for high flux pervaporation desalination. *J. Mem. Sci.* **2020,** *613*, 118460.

22. Colón-Ortiz, J.; Patel, S. Y.; Berninzon, A.; Gabounia, G.; Landers, J. M.; Neimark, A. V., In-situ growth and characterization of metal oxide nanoparticles within block-copolymer polyelectrolyte membranes. *Coll. Surf. A Physicochem. Eng. Aspects* **2020,** *601*, 125028.

23. Aryal, D.; Grest, G. S.; Perahia, D., Nano Ionic Networks: Association of Structured Ionic Polymers in Solution. *Nanoscale* **2016,** *9*, 2117-2122.

24. Jorgensen, W. L.; Madura, J. D.; Swenson, C. J., Optimized Intermolecular Potential Functions for Liquid Hydrocarbons. *J. Am. Chem. Soc.* **1984,** *106*, 6638-6646.

25. Jorgensen, W. L.; Maxwell, D. S.; TiradoRives, J., Development and testing of the OPLS all-atom force field on conformational energetics and properties of organic liquids. *J. Am. Chem. Soc.* **1996,** *118*, 11225-11236.

26. Murzyn, K.; Bratek, M.; Pasenkiewicz-Gierula, M., Refined OPLS all-atom force field parameters for n-pentadecane, methyl acetate, and dimethyl phosphate. *J. Phys. Chem. B* **2013,** *117*, 16388-16396.

27. Horn, H. W.; Swope, W. C.; Pitera, J. W.; Madura, J. D.; Dick, T. J.; Hura, G. L.; Head-Gordon, T., Development of an improved four-site water model for biomolecular simulations: TIP4P-Ew. *J. Chem. Phys.* **2004,** *120*, 9665-9678.

28. Hockney, R. W.; Eastwood, J. W., *Computer Simulation Using Particles* Adam Hilger-IOP, Bristol: 1988.

29. Tuckerman, M.; Berne, B. J.; Martyna, G. J., Reversible Multtiple Time Scale Molecular Dynamics. *J. Chem. Phys.* **1992,** *97*, 1990-2001.

CHAPTER SIX

EFFECTS OF INTERACTION STRENGTH OF ASSOCIATING GROUPS ON LINEAR AND STAR POLYMERS DYNAMICS.

Abstract

The addition of even a small number of associating groups has dramatic effects on the mobility and viscoelastic response of polymer melts. The associating group aggregate forming a polymer network, whose lifetime depends on the strength of the interaction between the associating groups. Here, using molecular dynamics simulations, we probe the effects of associating groups on the structure and dynamics of linear and star polymer melts and blends, where both the associating groups and the topology affect the properties of the system. The polymer chains are modeled by a bead-spring model and the associating groups are incorporated in the form of associating beads with an interaction strength between then that is varied from 1-20 k_BT. As the strength of the interaction between associating groups increases the aggregate into clusters of increasing size. These cluster act as crosslinkers which slow the chain mobility. Blends of chains with and without associating groups macroscopically phase separation even for relatively weak interaction between the associating groups.

1. Introduction

Associating groups in polymers drive their structure in melts and in solutions and has remarkable effects on their properties including mechanical properties and viscoelastic response. Associative complexes are driven by a broad range of interactions from hydrogen bonding and π-π interactions to long lived assemblies such as ionic clusters in

polymers. Hydrogen bonding and π-π interactions are typically pairwise association whose strength depend on the polarizability of the association groups and steric effects. Association of ionizable groups however are formed by multiple groups and exhibit a hierarchical assembly process in which multiples are first formed where tight ionic species are tightly arranged in a charge balanced manner.[1] The multiples form ionic clusters, where cohesion of these clusters affects the structure and dynamics of polymers and their function. It has long been realized that ionic clusters determining the structure and dynamics of ionic polymers.[2] However, the interrelation of the strength of interactions of the association groups, fundamental to formation of clusters, and their correlations with the overall structure and dynamics of the polymers is yet to be resolved. In contrast to hydrogen bonds and π–π stacking, ionic assemblies are dominated by long range electrostatic interactions of multiple associative groups that affect the delicate energy balance with the elasticity of the chain.[2-4]

Associating polymers are in the core of many applications where ion transport is an integrated part of their function. These include polymers for energy generation and storage, the water economy as well as bio technology.[4-6] The ionizable groups aggregate into long-lived clusters which serve as physical cross-linkers and in parallel, facilitate transport. The shape, size and cohesion of these clusters and the interrelation with the overall structure and dynamics of the polymers remain an open question despite immense efforts. This is due in part to the fact that the nature of the ionic clusters including internal packing of the ionic groups, and the overall size and shape of the clusters result from a delicate balance between numerous factors including factors that stem from the ionic groups including

electrostatic interactions, size of the ionic groups, size and charge of counterions, coupled with polymeric characteristics such as stiffness of the polymer backbone, chain architecture and polarity of their surroundings. Numerous computational studies have focused on resolving the daunting task of resolving the effects of separate factors.[7-12] Among these are studies by Hall and co-workers who imbedded charges on coarse grained models and studies their effects on the structure.[9, 10] The current study uses molecular dynamics (MD) simulations to derive the relation between the strength of the associating groups and the polymer characteristics.

To understand the assembly process of the ionic clusters, the complexity of the system is reduced by using a coarse-grained bead spring model in which the associating groups are incorporated in the form of associating beads along the backbone. We target a range of interchain interactions of up to ~ $20k_BT$ that is sufficient for the polymers to associate, but the chains are not locked by the long-range electrostatic interactions. Specifically, we study linear and 3-arm star in which the interaction strength between associating bead is varied in melts of pristine polymers and blends. Melts of pristine polymers are probed with the goal to resolve cluster size dependence on the interactions with the associating groups and determine the interrelation between cluster characteristics and polymer dynamics polymer dynamics. Increasing complexity, blends of associative and non-associative polymers are then studied, probing the interrelation between cluster formation and phase segregation.

In their recent study, Carrillo et al.[13] showed using small-angle neutron scattering and MD simulations that while interchain associations are important in a melt, intrachain

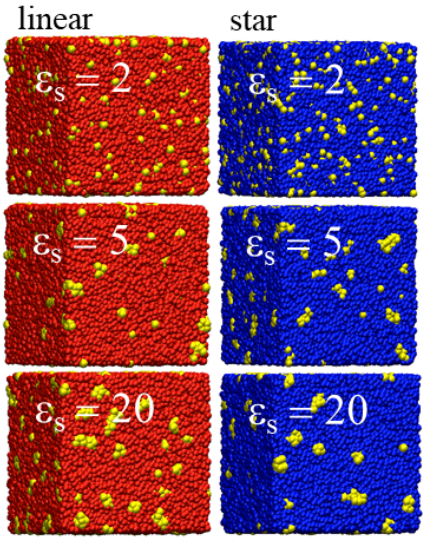

Figure 6.1. Images of a melt of 500 chains chain contains 100 beads of linear (red) and star (blue) polymers with 5 associating groups (yellow) per chain for three values of the interaction strength between associating groups ε_s = 2, 5 and 20 at t=10^7 τ.

association cannot be neglected in determining the static structures of associating polymers. They showed that even moderate association strength and degree of functionality, the chains are contracted and deviate from the standard random walk structure. This leads to intrachain loops which are not included in any dynamic theories of associating polymers. We find a similar reduction in the radius of gyration of the chains. We also show that the number of unique chains contributing to a cluster decreases as the size of the associating group aggregate increases and that there are fewer unique chains and hence more intrachain associations for 3-arm star polymer compared to linear chains. Figure 1 visualizes melts of linear and star polymers for increasing interaction strengths of the associating beads, demonstrating the ability of the chains to associate and form clusters at very low association strength.

Though a vast amount of knowladge has been obtained on the associating polymer melts and solutions, little is known about blends of associating polymers, though they are of immense

technological significant, particularly understanding the formation of ionic-nonionic interfaces within membranes. Polymer blends are usually described in terms of an effective interaction parameter χ, which describes the relative strength of the interactions between the monomers on different chains.[14] For a blend of two chains of the same length N, the blend is miscible if $\chi < \chi_c$ and immiscible for $\chi > \chi_c$ where χ_c is the critical value of χ. In Flory-Huggins theory $\chi_c N = 2$. However, the factors that affect blending of nearly identical polymers in which one contains a fraction of strongly interacting associating groups along the backbone, which is often critical to formation of stable interfaces in device applications, have not been resolved. While van der Waals polymers and identical ionizable ones hardly interpenetrate in thin films, the effects of the association strength on the degree of segregation is not known. Further it is unknown how the miscibility depends on the interrelation of chain architecture and the strength of the interaction between associating groups. Here we present results for blends of linear and star polymers in which half of the chains contain associating groups and half do not. We show that even for relatively weak interaction between the associating groups, these blends are immiscible.

2. Methodology

Molecular dynamics simulations were performed using the Kremer-Grest coarse-grained model in which the polymer chains are treated as beads (monomers) of mass m and diameter σ connected by a non-extensible spring.[15] We studied melts of 500 chains of linear and three arm star polymers, each with 100 beads per chain. For blends, each system contained 2000 chains with and 2000 chains without associating beads. Two types of beads were used, non-associating groups (type 1) and associating groups (type 2). A pair of monomers of type α and β separated by a distance r interact with a Lennard-Jones potential,

$$U_{\alpha\beta}(r) = \begin{cases} 4\varepsilon_{\alpha\beta}\left[\left(\frac{\sigma}{r}\right)^{12} - \left(\frac{\sigma}{r}\right)^{6}\right] & r \le r_{cut} \\ 0 & r > r_{cut} \end{cases} \quad (6.1)$$

with cutoff r_{cut} =2.5σ. The non-associating groups interact with strength ε_{11}. The associating beads interact with strength $\varepsilon_{22} \geq \varepsilon_{11}$. The cross term is set to $\varepsilon_{12} = \varepsilon_{11}$. W studied systems where the dimensionless ratio of the strength of the associating and non-associating groups $\varepsilon_s = \varepsilon_{22}/\varepsilon_{11}$ varies from 1 to 20. As all the systems were simulated at a temperature $T = \varepsilon_{11}/k_B$, the strength of the interaction between associating beads corresponds to 1 to 20 k_BT. Five associating groups are randomly distributed on each chain. The potential between connected beads is defined by the finitely extensible nonlinear elastic potential with a spring constant $k = 30\varepsilon/\sigma^2$ and a maximum bond extension parameter of $R_o = 1.5\sigma$.[15] The entanglement length $N_e \sim 84$ for the linear, homopolymer melt.[16, 17]

The simulations are carried out using the Large Scale Atomic Molecular Massively Parallel Simulator (LAMMPS) software.[18] Melts of linear chains of length 100 were prepared following the procedure described by Auhl et al.[19] For the star polymers, linear chains of length 67 were first prepared after which a strand of length 33 beads was added to the center bead. The linear-star blends were made by randomly placing the two types of chains in the simulation cell. The equations of motion were integrated with a time step at $\delta t = 0.01\tau$, where $\tau = (m\sigma^2/\varepsilon_{11})^{1/2}$ is the standard time unit for a Lennard-Jones fluid. The temperature was set to $T = \varepsilon_{11}/k_B$ using a Langevin thermostat with a damping time constant of 10τ to maintain temperature.[20, 21] For reference, for a homopolymer (ε_s=1) of linear chain

melt, the glass transition temperature $T_g \sim 0.43\ \varepsilon_{11}/k_B$.[22] After the systems were equilibrated at pressure $P = 0$ with $\varepsilon_s = 1$, five beads on each chain were randomly changed to type 2 and the simulations run for an additional 1 million steps at constant pressure after which the systems were run at constant volume. The final density ρ is all cases is $\rho \sim 0.89\sigma^3$. All systems were run for at least 1 billion time steps or 10^7 τ.

The static structure factor *S(q)*, which computationally is given by

$$S(q) = \sum_{i,j=1}^{N} b_i\, b_j \langle exp[i\boldsymbol{q}.(\boldsymbol{r_i} - \boldsymbol{r_j})]\rangle / \sum_{i=1}^{N} b_i^2 \qquad (6.2)$$

where b_i is the scattering length for monomer *i.* Due to the periodic boundary conditions, the wavevectors $\boldsymbol{q}$ are limited to $\boldsymbol{q} = \frac{2\pi}{L}\ (n_x, n_y, n_z)$, where *L* is the length of the simulation cell and n_x, n_y and n_z are integers. The structure factor *S(q)* for the associating groups is obtained by setting b_i=1 for each associating bead (type 2) and $b_i = 0$ for the non-associating beads (type 1). For blends of chains with and without associating groups, we measured the structure factor *S(q)* of two types of polymers, which provides information on miscibility. These two structure factors are obtained by setting $b_i = 1$ for one type of chain and $b_i = 0$ for the other to provide maximum contrast between the two types of chains. Excess scattering in *S(q)* at low *q* is indicative of phase separation.

3. Results and Discussion

A-Melts The evolution of the assembly of the associating groups was probed following switching on the interaction ε_s between associating groups. The average cluster size N_c was calculated as a function of time and is shown in Figure 2a. Two associating group beads are considered to be in the same cluster if they are separated by a distance of

1.5 σ or less. Similar results are obtained for cutoff distances of 1.4 and 1.6 σ. The average cluster size N_c increases with time and reaches a steady value after 0.4 to 1.0 x10^6τ depending on the strength of the associating groups. The stronger the interaction, the larger the clusters

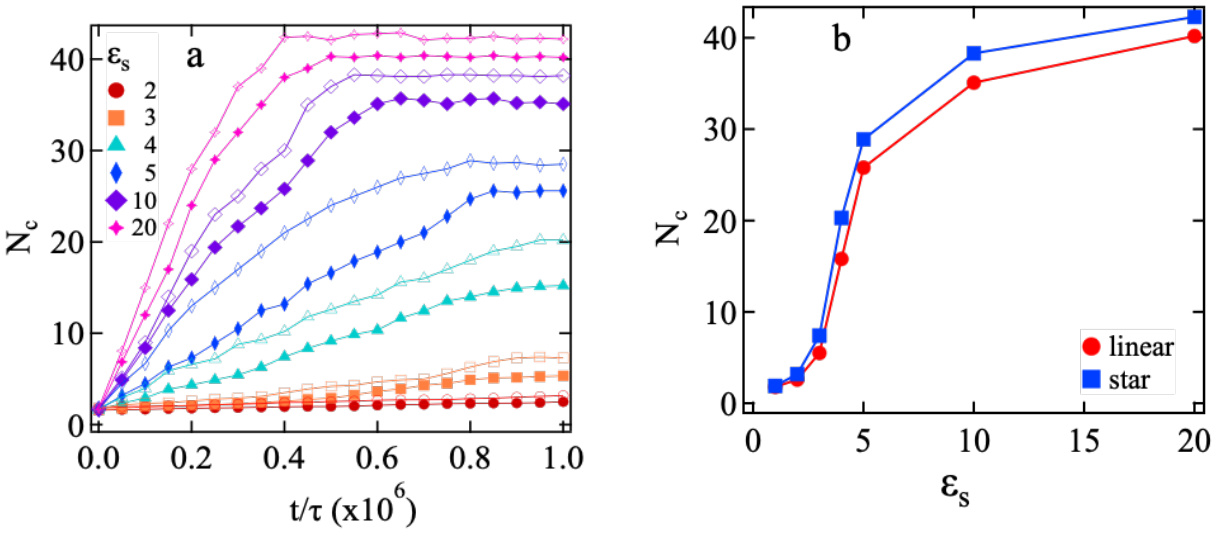

Figure 6.2. a) Average cluster size N_c as a function of time at the indicated six values of the associating group strength ε_s for linear (bold) and star (open) polymer melts. b) Average cluster size as function of ε_s. Results for chains of 100 beads with 5 associating groups per chain.

are, and they form faster. N_c averaged over the last half of the run is shown in Figure 2b where increasing the interaction strength between associating groups from ε_s = 1 to 5, results in a steep increase in the average cluster size N_c. For larger ε_s, the increase in N_c with ε_s is more gradual. This is attributed to constraints on packing from the non-associating beads.

Experimentally, one strong signature of the clustering of associating groups is seen in static structure factor *S(q)* measured by neutron scattering. Results for *S(q)* for the associating groups for linear and star melts are shown in Figure 3 for six values of the associating

group interaction strength ε_s. The results are averaged over 200 configurations taken from the last $2\text{x}10^6\,\tau$ of the run. As ε_s increases the peak at low q increases in intensity indicative of the formation of clusters of associating groups. The onset of this low q signature is at $q \sim 1\sigma^{-1}$ occurs for $\varepsilon_s > 3$ for linear chains and for $\varepsilon_s > 2$ for the star polymers. The difference of the two chain architectures result in a higher peak intensity for a given ε_s for star polymers than for linear chains. The characteristic distance $d = 2\pi/q$ for the first peak $\sim 6\sigma$ corresponds to an average distance between associating group clusters. The formation of clusters was illustrated in the images shown insets of Figure 3. The intensity and width

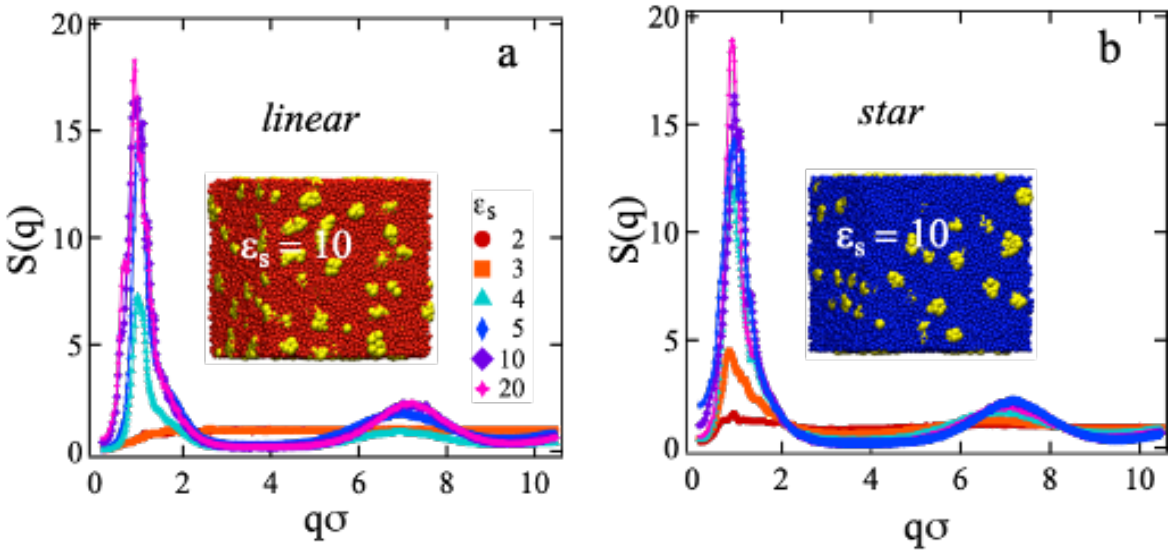

Figure 6.3. Static structure factor *S(q)* of the associating groups as a function of wave vector q of (a) linear and (b) star polymer melts for six values of the interaction strength ε_s between associating groups. The inset shows images of the system at $t = 10^7\,\tau$ for $\varepsilon_s = 10$. The associating groups shown in yellow and non-associating groups in red (linear) and blue (star).

of S(q) for different ε_s values show that foe $\varepsilon_s = 2$ the associating centers are only weakly correlated spatially while for stronger ε_s they form well defined correlations that increase

with increasing cluster size. The secondary structure in S(q) at $q{\sim}6\sigma^{-1}$ is a signature of local monomer packing of the associating groups which increases with increasing ε_s.

To separate the intra and inter molecular contributions to the associating group clusters, we measured the number of unique polymer chains N_{uc} in a cluster of size N_c. The

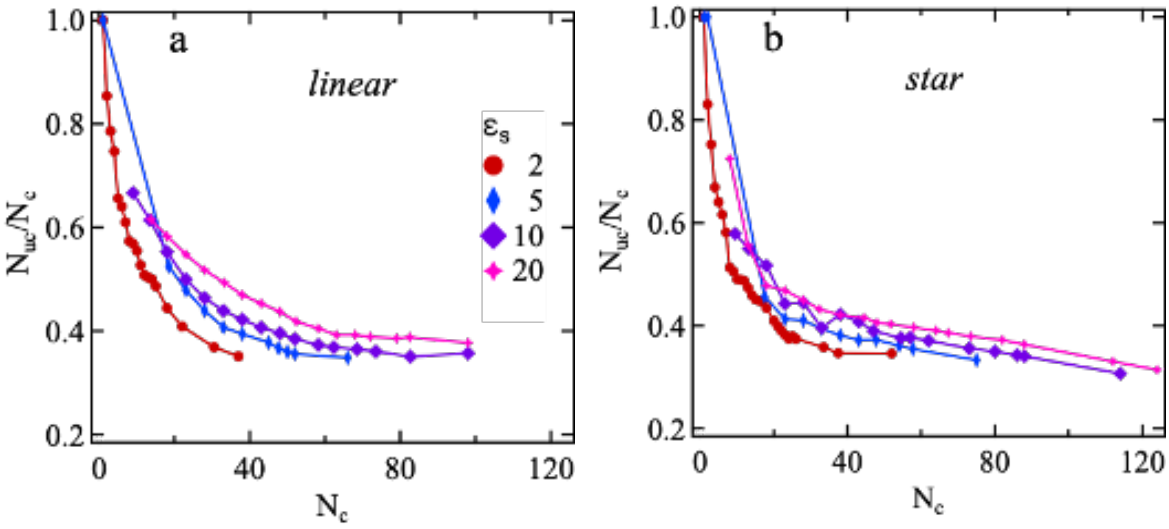

Figure 6.4. Number of unique chains N_{uc} in a cluster divided by the cluster size N_c as a function of cluster size for (a) linear (b) star melts for four values of ε_s.

significance of inter versus intra-chain associations of significance because several reasons. The associating groups incur different elastic forces depending on the number tethered chains, affecting cluster stability.[3] Further the clusters serve as anchoring points to different chains, where the degree and affecting their dynamics. The fraction of unique chains in a cluster decreases with increasing cluster size for both linear and star melts as shown in Figure 4. For the smallest clusters which are formed for small ε_s, the association is predominately between chains (interchain) where $N_{uc}/N_c \sim 1$. As the cluster size increases, the average number of unique chains contributing to a specific cluster decreases as

intrachain associations become more prevalent. In other words, the larger clusters consist of more association within one chain compared to smaller clusters.

For larger clusters in the linear chain melts, each chain contributes on average 2.5 associating groups to a cluster, which is about half the number of associating groups on each chain. The number of intrachain association affects the dimensions of individual chains as is reflected in the mean squared average radius of gyration $<R_g^2>$ presented in

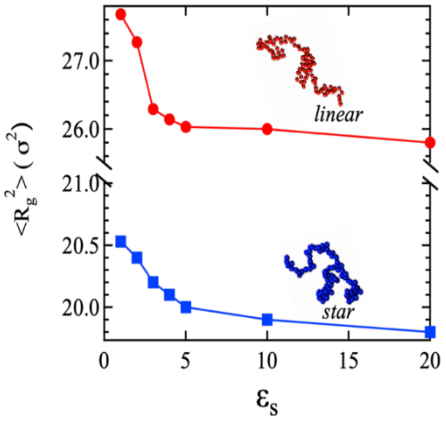

Figure 6.5. Mean squared radius of gyration $<R_g^2>$ of the polymer chains as a function of interaction strength ε_s of the associating groups for linear (red circle) and star (blue square) melts.

Figure 5. The increase in the number of intra chain contributions leads to a decrease in the chains as ε_s (and the correspondingly the average cluster size) increases. For the linear chains, this decrease in $<R_g^2>$ saturates for $\varepsilon_s > 5$, consistent with the observation shown in Figure 4a that N_{uc}/N_c is approximately constant for the larger clusters. For the star polymers, the fraction of the unique chains in a cluster of the same size is lower than for linear melts and continues to decrease as the cluster size increases. The larger clusters for the star polymers contain more intramolecular associating groups than for the linear chains,

which leads to further decrease in $R_g^2>$ as ε_s increases. The importance of intrachain associations and the reduction in $<R_g^2>$ with increasing strength ε_s of the associating beads is in agreement with previous neutron scattering and MD simulation results of Carrillo et al.[13]

The addition of even a small fraction of associating (ionic) groups is known experimentally to have a strong effect on the dynamics of the system attributed to cluster formation that act as crosslinks.[23, 24] Here the insight attained following N_{uc}/N_c as a

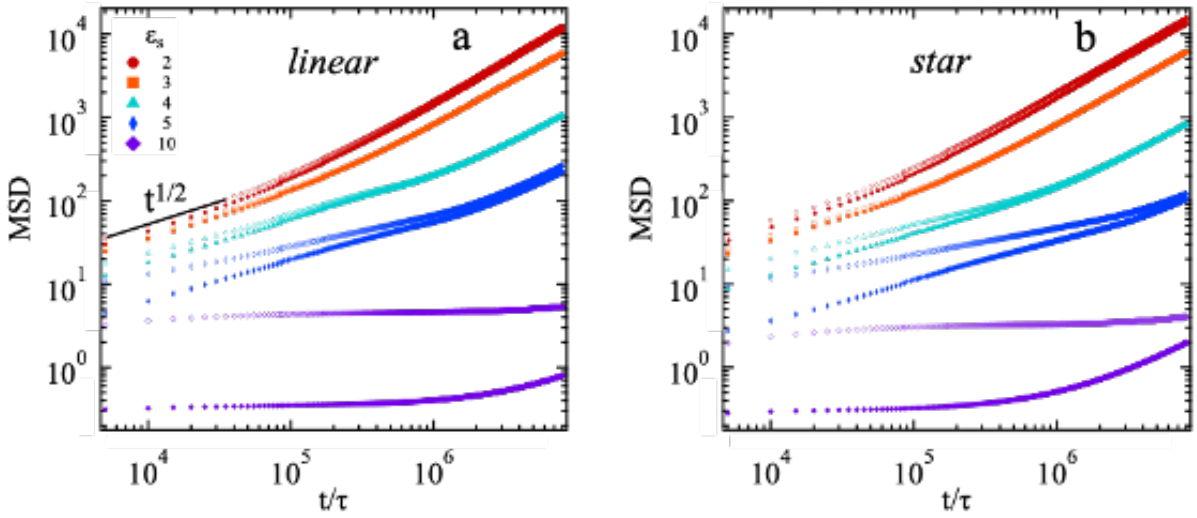

Figure 6.6. Mean square displacement (MSD) of the monomers in (a) linear and (b) polymer melts for ε_s = 2 (red circles), 3 (orange squares), 4 (light blue triangles), 5 (blue diamonds) and 10 (purple rhombi). Full symbols for associating beads and open symbols are for non-associating beads.

function of the association strength and its effects on the molecular dimensions offer a new understanding into the effects of cluster formation on dynamics. One way to capture dynamics is to calculate the mean squared displacement (MSD) $< (r_i(t) - r_i(0))^2 >$ of the monomers.[15] MSD values of the associating and non-associating beads for the linear

and star melts are shown in Figure 6 for five values of ε_s. MSD of non-associating chains (ε_s=1) overlap with those for ε_s = 2. As the chains are unentangled, the MSD for the linear, homopolymer follows Rouse $t^{1/2}$ dynamics[25, 26] at early time crossing over to the diffusive regime after the chain moves its own size. As ε_s increases the overall mobility of the chains clearly decreases as the associating beads act as instantaneous crosslinkers and dominate the mobility of the entire chain.[26] This is the case even though only 5 of the 100 beads on each chain are associating beads. Even for ε_s = 3, there is a measurable reduction in the mobility of both the associating and non-associating groups, which grows as ε_s increases. For $\varepsilon_s \leq 4$, the MSD shows Rouse-like $t^{1/2}$ dynamics at early times before crossing over to the diffusive t regime. For ε_s = 5, the motion of the two types of beads are significantly different even at very early time as the non-associating beads initially move faster than the associating beads. There is an intermediate region where the non-associating groups move slower than $t^{1/2}$ as their motion is constrained by that of the associating groups.

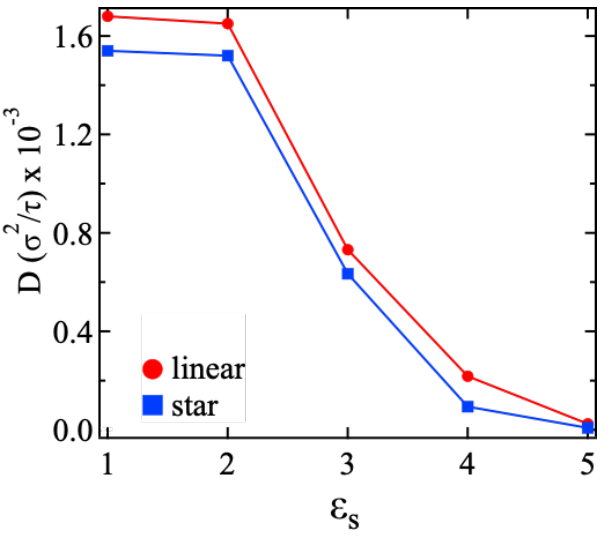

Figure 6.7. Diffusion constant D as a function of associating group strength ε_s for linear (red circles) and star (blue squares) melts.

The difference in associating group dominates and sets the time scale for motion of both types of beads. For $\varepsilon_s \leq 5$, the chains have moved several times their own size and reached the terminal diffusive regime where the MSD increases linearly with time. For these cases, we extract the diffusion coefficient $D = < (r_i(t) - r_i(0))^2 >/6t$ at late times. Results for D both the linear and star polymers as a function of ε_s are shown in Figure 7. As ε_s increases from 1 to 5, D decreases by roughly a factor of 180 with the linear chains always moving slightly faster than the star polymers. For $\varepsilon_s \geq 10$, the chains have not moved their own size during the time of the simulation (1 billion time steps), therefore *D* could not be measured. As the associating beads for $\varepsilon_s = 10$ and 20 have only moved a short distance, these two systems are kinetically trapped on the time scale of the simulations.

B. Blends With the understanding attained for pristine melts, we set resolve the characteristic of blending of polymers with and without associating groups. These systems

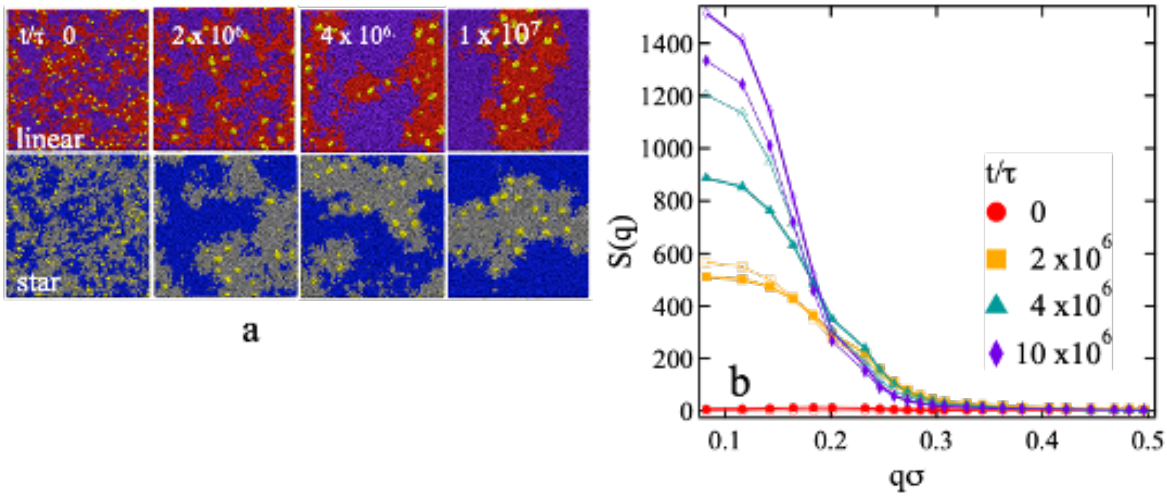

Figure 6.8. (a) Snapshots showing the time evolution of linear-linear (top) and star-star (bottom) blends in which half the chains contain associating groups and half do not for $\varepsilon_s = 5$. The associating groups are shown in yellow. (b) Static structure factor S(q) of the chains with associating groups for linear (full) and star (open) blends at different times. System contains 4000 chains.

would be defined by two competing interactions, those of the associating groups, coupled with enhances entropy. We probed 1:1 blends of linear polymer with and without associating beads and a similar blend of 3 arms stars with and without associating beads. The evolution of these blends is depicted in Figure 8 for a blend of 2000 chains of 100 beads with 5 associating groups per chain each interacting with strength $\varepsilon_s = 5$ and 2000 chains of 100 beads with no associating groups. The initial state if fully mixed with time the both systems clearly phase separate macroscopically into regions of chains with associating and without associating groups.

One signature of macroscopic phase separation is excess intensity of the static structure function *S(q)* scattered separately from of each the two components of the blend. This scattering that appears at low q values is shown in Figure 8-b. As expected for nearly

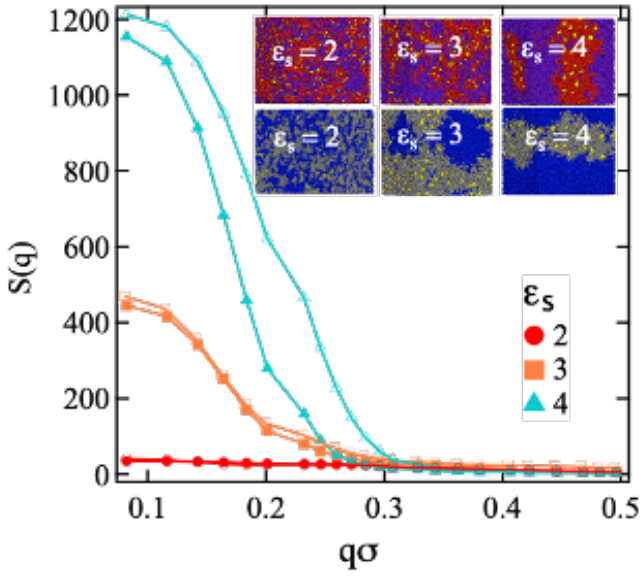

Figure 6.9. Coherent structure factor *S(q)* chains with associating groups for different ε_s at time $t = 10^7\tau$ for linear (full) and star (open) blends. Insert shows snapshots for the three systems at $t = 10^7\tau$.

incompressible systems,[27] *S(q)* for only the polymer chains with no associating groups is

the almost identical to that of the polymer with associating groups. The intensity at low q increases with time for both linear-linear and star-star blends, consistent with the visible observation of phase separation where the intensity of the low q signature of star-star blend is slightly stronger than the linear-linear blend.

The effect of varying the interaction strength ε_s between the associating groups on these blends is shown in Figure 9. For weak interaction between associating groups (ε_s = 2), both blends are miscible as is shown by no excess scattering at low q. However even for relatively small interaction strength between the associating groups ($\varepsilon_s \geq 3$) the blends macroscopically phase separation into regions with and without associating groups. For both ε_s = 3 and 4, the intensity at low q in *S(q)* increases with time similar to the results shown in Figure 8 for ε_s = 5. The insert of Figure 9 shows snapshots of the system at $10^7\tau$ where we see that the blend with ε_s = 2 is macroscopically miscible, with possibly some local segregation, while for larger interactions ($\varepsilon_s \geq 3$) chains with and without associating groups are immiscible even though the fraction of associating groups is small (5%) and their interaction strength is only a few k_BT.

Conclusions

The study has probed the effect of associative groups on melts of pristine polymers and their blends with linear and star architectures using molecular dynamics simulations. Polymer were modeled by bead-spring model and associating groups are incorporated randomly on the chains. As expected from studies of associative polymers, the associating group aggregate forming polymer networks. We show that even weak interactions between the associating groups are sufficient to drive association. By varying the strength of the

interaction between the associating groups, one can control the size of the aggregates and the mobility of the chains in melts. The overall mobility of the chains rapidly decreases as the associating beads act as instantaneous crosslinkers and dominate the motion of the entire chain. For interactions between associating groups of order 10 k_BT and larger, the system is kinetically trapped, forming a long-lived polymer network. The fraction of unique chains in a cluster decreases with increasing cluster size for both linear and star melts - this increase in the number of intra chain contributions leads to a decrease in the mean squared average radius of gyration.[13] Star polymer melts contain more intramolecular associating groups than for linear chains

Blends of chains with and without associating groups macroscopically phase separate even for a low concentration of weak (~$3k_BT$) associating groups – in the case studied here the fraction of associating groups on a chain is only 5%. This suggests that blending polymers with associating groups to the same polymer without associating groups will be difficult to achieve unless the strength of the associating groups is very weak. An interesting open question is whether chains with different factions of associating groups are miscible or not.

Acknowledgements

DP gratefully acknowledges DOE grant DE-SC007908. This research used resources at the National Energy Research Scientific Computing Center (NERSC), a U.S. Department of Energy Office of Science User Facility operated under Contract No. DE-AC02-05CH11231. This work was made possible in part by advanced computational resources deployed and maintained by Clemson Computing and Information Technology. This work

was performed, in part, at the Center for Integrated Nanotechnologies, a U.S. Department of Energy and Office of Basic Energy Sciences user facility.

Reference

1. B. Dreyfus, Macromolecules **18**, 284-292 (1985).
2. A. Eisenberg, Macromolecules **3**, 147-154 (1970).
3. A. Eisenberg, B. Hird and R. B. Moore, Macromolecules **23**, 4098-4107 (1990).
4. A. Eisenberg and J. Kim, (John Wiley and Sons, Inc, 1998).
5. B. P. Grady, Polym. Eng. Sci. **48**, 1029-1051 (2008).
6. L. Zhang, N. R. Brostowitz, K. A. Cavicchi and R. Weiss, Macromolecular Reaction Eng. **8**, 81-99 (2014).
7. M. Goswami, S. K. Kumar, A. Bhattacharya and J. F. Douglas, Macromolecules **40**, 4113-4118 (2007).
8. C. Wong and J. H. Clarke, J. Chem. Phys. **116**, 6795-6802 (2002).
9. L. M. Hall, M. E. Seitz, K. I. Winey, K. L. Opper, K. B. Wagener, M. J. Stevens and A. L. Frischknecht, J. Am. Chem. Soc. **134**, 574-587 (2012).
10. L. M. Hall, M. J. Stevens and A. L. Frischknecht, Macromolecules **45**, 8097-8108 (2012).
11. D. S. Bolintineanu, M. J. Stevens and A. L. Frischknecht, ACS Macro Lett. **2**, 206 (2013).
12. A. Agrawal, D. Perahia and G. S. Grest, Phys. Rev. E **92**, 022601 (2015).

13. J.-M. Y. Carrillo, W.-R. Chen, Z. Wang, B. G. Sumpter and Y. Wang, J. Phys. Comm. **3**, 035007 (2019).

14. M. Rubinstein and H. R. Colby, *Polymer Physics*. (Oxford University Press, 2003).

15. K. Kremer and G. S. Grest, J. Chem. Phys. **92**, 5057-5086 (1990).

16. S. K. Sukumaran, G. S. Grest, K. Kremer and R. Everaers, J. Polym. Sci. B Polym, Phys, **43**, 917-933 (2005).

17. R. S. Hoy, K. Foteinopoulou and M. Kröger, Phys. Rev. E **80**, 031803 (2009).

18. S. Plimpton, J. Comp.Phys. **117**, 1-19 (1995).

19. R. Auhl, R. Everaers, G. S. Grest, K. Kremer and S. J. Plimpton, J. Chem. Phys. **119**, 12718-12728 (2003).

20. T. Schneider and E. Stoll, Phys. Rev. B **17**, 1302-1322 (1978).

21. G. S. Grest and K. Kremer, Phys. Rev, A **33**, 3628-3631 (1986).

22. G. S. Grest, J. Chem. Phys. **145**, 141101 (2016).

23. R. Weiss and W.-C. Yu, Macromolecules **40**, 3640-3643 (2007).

24. R. Weiss and H. Zhao, J. Rheology **53**, 191-213 (2009).

25. P. E. Rouse, J. Chem. Phys. **21**, 1272-1280 (1953).

26. L. G. Baxandall, Macromolecules **22**, 1982-1988 (1989).

27. B. Hammouda, J. Non-Cystal. Solids **172**, 927-931 (1994).

CHAPTER SEVEN

SYNTHESIS AND CHARACTERIZATION OF BIOTIN SUBSTITUTED POLYPHENYLENE ETHYNYLENE

Abstract

Poly(phenylene ethynylene) derivatives substituted with biotin groups have tremendous potential applications in organic electronics and as biosensors. Herein, we synthesized the PPE which has biotin substituted side arms and compared it with PPEs lacking biotin groups. Our results show that the extinction coefficient for absorption of light in the UV region of the spectrum is lower for the PPE derivative having biotin groups in the side chains. The presence of biotin side groups also influences aggregation of PPE, as reflected in a decrease in critical micelle concentration in THF. Our AFM results illustrate that PPE with no biotin group forms isolated extended structures on films, whereas PPE with biotin forms an extended network.

Introduction

Poly(*p*-phenylene-ethynylene) (PPE) derivatives have remarkable fluorescence and semiconducting properties[1]. These distinctive properties allow PPEs to serve in many different organic based electronics[2, 3] and sensory applications[4, 5]. Unfortunately, the rigid hydrophobic conjugated backbone make PPEs water insoluble, which prevents the PPEs from being broadly applicable, especially in biological applications[6]. Tremendous effort has been taken to resolve this challenge as exemplified by the synthesis of PPEs with less rigid backbones, such as poly(*o*-phenylene ethynylene)s[7]. One other approach is to change

the interchain interactions by modifying the side chain functional groups [8]. This approach resolves the aggregation challenge while it may also resolve the challenge of biocompatibility depending on the nature of the functional group. Novel synthetic strategies have the capability of yielding PPEs with different functional groups in the side chains to include groups which are biocompatible such as biotin[9].

It is well know that PPE aggregation in aqueous media can be carefully tuned to result in organic nanoparticles, that have their own broad application space[10]. The electro-optical response of these types of nanoparticles depends on conjugation length, which is in turn affected by the chemistry of both backbone and side groups. Conjugation length depends on the relative orientation of phenyl rings with respect to each other, thus controlling the structural and dynamic properties of both extended PPEs as well as of composite nanoparticles. For example PPEs with dinonyl side groups form complex fluids in toluene at relatively high concentrations where the structure of the PPEs changes from a gel phase to molecular solution with increasing temperature[11]. Small angle neutron scattering (SANS) has shown at higher temperature that PPE molecules are extended and MD simulation has shown that this extended structure is the most stable one in solution[12].

While PPEs with general functional groups are widely synthesized and intensively studied, PPEs with bio-compatible groups remains an underexplored area of research. In the current study, we focus on synthesis of PPEs with biotin-substituted side arms and study their structural properties in aqueous and non-aqueous solutions. Biotin is a co-enzyme which has a strong binding capability with many important enzymes including

streptavidin and avidin[13]. Understanding of structure of biotin substituted PPEs in solutions may open up a door to use PPEs in biological applications in deferent aspects.

Materials and Methods

All the reagents and solvents were purchased from Aldrich Chemicals Co., TCI America and Alfa Aesar. The solvents used in synthesis procedure was future purified by passing through alumina columns under N_2 atmosphere employing an MBRAUN solvent purification system. The solvents were used as received in extractions and purification techniques. The synthesis routes are summarized in Figure 7.1 to 7.4. monomers 1–7 and polymer 8 were synthesized by modifying previously reported protocols[14]. MBRAUN dry box or standard Schlenk techniques under N_2 atmosphere were used for air sensitive reaction procedures. Proton and carbon-13 NMR spectra were acquired at 25 ºC using either trimethylsilane or residual solvent peak as a reference on a Bruker Avance 500 spectrometer operating at 500 MHz for protons. The yields are reported either in gram or percent yield as appropriate.

Synthesis of PPEs

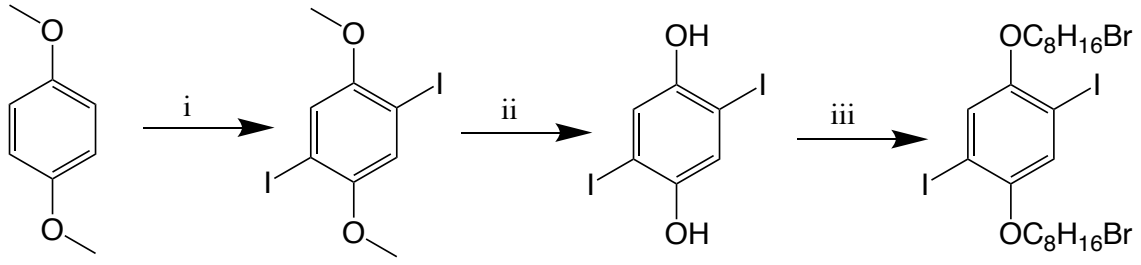

1 2 3 4

Figure 7.1. Synthesis of monomer 4: (i) ICl, CH_2Cl_2, reflux at for 24 hours; (ii) BBr_3, CH_2Cl_2 at –78 ºC, stir at RT for 24 hours; (iii) 1,8-dibromooctane, K_2CO_3, acetonitrile, reflux for 24 h at 50 ºC

Synthesis of 2,5-diido-1,4-dimethoxybenzene (2):

In a 250 mL round bottom flask 100 mL of methanol was cooled below 15 °C in an ice bath. Iodine monochloride (32 g, 0.2 moles) was added drop wise and stir about 30 min. Then 1,4methoxybenzene **(1)** (13g, 0.1mole) was added by maintaining the temperature bellow 15 °C. The mixture was allowed heated to room temperature and then refluxed 24h. Then reaction mixture was allowed to cool slowly which results white color crystals. The crystals were separated by vacuum filtration and washed with cold methanol. Formation of 2,4-diido-1,4-dimethoxybenzene **(2)** (13g, 60%) was confirmed by ^{1}H-NMR ($CDCl_3$, s-7.16, s-3.25).

Synthesis of 2,5-diido-1,4-dihydroxybenzene (3):

2,5-Diiodo-1,4- dimethoxybenzene (**2**, 11.0 g, 28.3 mmol) was dissolved in dichloromethane (150 mL) and cooled to −78 °C in dry ice and acetone. Boron tribromide (30 g), dissolved in dichloromethane (20 mL), was added dropwise. The resulting solution was allowed to reach room temperature while stirring overnight. The resulting reaction mixture was poured on ice and the obtained solid filtered. The residue was dried *in vacuo*. The crude was not pure to H-NMR. Final purification was done by crystallization from benzene/chloroform giving 7.70 g (48.9 mmol, 87 %) of the product.

Synthesis of 1,4-Bis(8-bromooctyloxy)-2,5-diiodobenzene (4):

2,5-diido-1,4-dihydroxybenzene (43.9 g, 0.121 mol) was added to a suspension of K_2CO_3 (50.2 g, 0.363 mol) in 500 mL of acetonitrile under N_2. 1,8-dibromooctane (98.74 g, 0.363 mol) was added dropwise using a syringe while mixture was stirring. The resulting mixture was reflux at 50 ºC for 24 hrs. After refluxing, 100 mL of hot toluene was added to the reaction mixture and solid residues were decanted off and the filtered solution and solvent was evaporated under reduced pressure. The resulted oily crude was dissolved in 3 mL of dichloromethane. This solution was added dropwise to the 500 mL of methanol in a cold water bath. The white solid (65.2 % yield) was collected. ^{1}H NMR ($CDCl_3$): δ 7.18 (s, 4H), 4.04 (t, 4H), 4.06 (t, 4H), 1.86-1.79 (m, 8H), 1.5-1.35 (m, 12H).

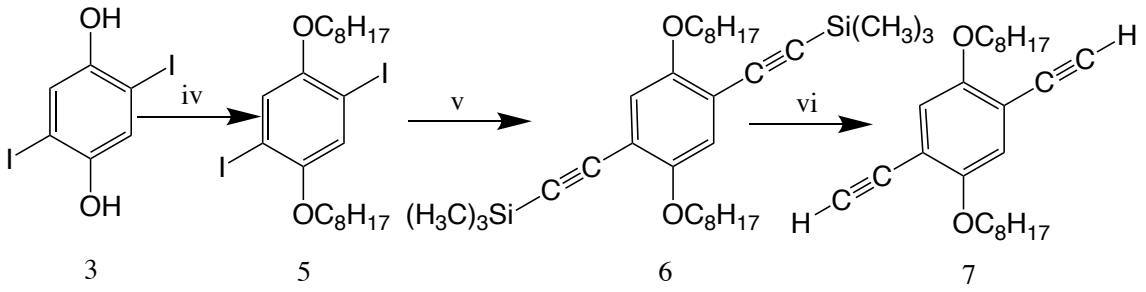

Figure 7.2. Synthesis of monomer 7. (iv) 1-bromooctane, K_2CO_3, acetonitrile, reflux for 24 hours at 50 °C. (v) Pd(PPh3), CuI, trisilyl acetylene, triethylamine, toluene, stir at 90 ºC for 24 hours. (vi) Methanol/THF, 5N NaOH, stir at RT for 3 hours.

Synthesis of 1,4-bisoctyloxy-2,5-diiodobenzene (5):

2,5-diido-1,4-dihydroxybenzene (43.9 g, 0.121 mol) was added to a suspension of K_2CO_3 (50.2 g, 0.363 mol) in 500 mL of acetonitrile under N_2. 1-bromooctane (70.12 g, 0.363 mol) was added dropwise using a syringe while mixture was stirring. The resulting mixture was reflux at 50 ºC for 24 hrs. After refluxing, 100 mL of hot toluene was added to the

reaction mixture and solid residues were decanted off and the filtered solution and solvent was evaporated under reduced pressure. The resulted oily crude was dissolved in 3 mL of dichloromethane. This solution was added dropwise to the 500 mL of methanol in a cold water bath. The white solid (71.2 % yield) was collected. ^{1}H NMR ($CDCl_3$): δ 6.82 (s, 4H), 3.9 (t, 4H), 4.06 (t, 4H), 1.86-1.70 (m, 4H), 1.5-1.30 (m, 16H), 0.9 (t,6H).

Synthesis of 1,4-bis[(trymethylsilyl)ethynyl]-2,5-bishocayloxybenzene (6).

1,4-bisoctyloxy-2,5-dibromobenzene (20.16 g, 34.4 mmol), trimethylsilylacetylene (13.5 g, 137.6 mmol), $Pd(PPh_3)4$, (4.77 g, 4.13 mmol), CuI (0.786 g, 4.13 mmol), diisopropylamine (55 mL) and toluene (100 mL) were added into a 250 mL pressure flask under the inert environment. The mixture was stirred at 90 ºC for 32 hours. Then reaction mixture was set to cool down to room temperature and added diethyl ether (200 mL). Then, the mixture was passed through silica gel. The filtrate was washed with saturated $NaHCO_3$ (3x200 mL), H_2O (200 mL) and 5-10 mol% HCl (100 mL). Resulted organic layer was rotor evaporated and collect the crude solid. To remove the phosphonium salts, the solid compound was re-dissolved in Hexane (100 mL) and passed through silica gel. The solution was rotor evaporated to get brownish orange solid. This solid was recrystallized in ethanol to yield Compound 5, as a pale yellow powder. (69.5% yield) ^{1}H NMR ($CDCl_3$): δ 6.85 (s, 2H), 3.90 (t, 4H), 1.83-1.75 (m, 4H), 1.54-1.33 (m, 16H), 0.89 (t, 6H), 0.25 (s, 18H).

Synthesis of 1,4-bis(ethynyl)-2,5-bisoctayloxybenzene (7).

1,4-bis[(trimethylsilyl)ethynyl]-2,5-bishocayloxybenzene (3.18 g, 6.05 mmol), tetrahydrofuran (40 mL), methanol (50 mL) and 20% NaOH (30 mL) were placed in a 500

mL three neck round bottom flask under N_2 and stirred at room temperature for 3 hours. Then, dimethyl ether (40 mL) was added to the flask. The organic layer was filleted out and washed with H_2O. Organic solvent was rotor evaporated to get the crude. The crude was purified by precipitation in methanol (30 mL) and filtered to yield off-white powder (82.5% yield). ^{1}H NMR ($CDCl_3$): 7.457 (2H,s), 3.9 (t, 4H), 2.760 (s, 2H), 1.53-1.33 (m, 16H), 1.81-1.76 (m, 4H), 0.85 (t, 6H).

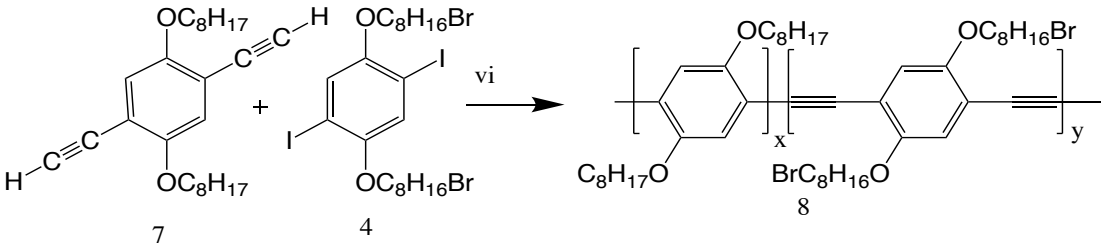

Figure 7.3. Synthesis of polymer 8a, 8b. (vii) $Pd(PPh_3)_2Cl_2$, CuI, triethylamine, DCM, reflux for 2 hours.

Synthesis of Polymer 8a (PPE-0Biotin).

Monomer 7 (0.38 g, 1.0 mmol), monomer 5 (0.58 g,1.0 mmol), $(Ph_2P)_2PdCl_2$ (3.48 mg, 4.47 μmol), CuI (0.85 mg, 4.2 μmol), diisopropylamine (8 mL) and dichloromethane (30 mL) were added into a 50 mL pressure vessel in the glove box. The mixture was heated at 40 ºC for 2 hours. Then the mixture was cooled to room temperature and diethyl ether (150 mL) was added. Following that mixture was washed with H_2O (100 mL). The resulted organic layer was extracted and solvent was evaporated under reduced pressure to get a brownish slurry. The crude was dissolved in minimum amount of dichloromethane (3 mL). This solution was added to methanol (100 mL) drop wise to yield polymer 8 as an orange

solid (0.72 g). ^{1}H NMR ($CDCl_3$): δ 7.04 (aromatic 4H), 4.06 (s, 8H), 1.87-1.29(m, 48H), 0.89 (t, 6H).

Synthesis of Polymer 8b (PPE-50Br).

Monomer 7 (0.38 g, 1.0 mmol), monomer 4 (0.74 g,1.0 mmol), $(Ph_2P)_2PdCl_2$ (3.48 mg, 4.47 μmol), CuI (0.85 mg, 4.2 μmol), diisopropylamine (8 mL) and dichloromethane (30 mL) were added into a 50 mL pressure vessel in the glove box. The mixture was heated at 40 ºC for 2 hours. Then the mixture was cooled to room temperature and diethyl ether (150 mL) was added. Following that mixture was washed with H_2O (100 mL). The resulted organic layer was extracted and solvent was evaporated under reduced pressure to get a brownish slurry. The crude was dissolved in minimum amount of dichloromethane (3 mL). This solution was added to methanol (100 mL) drop wise to

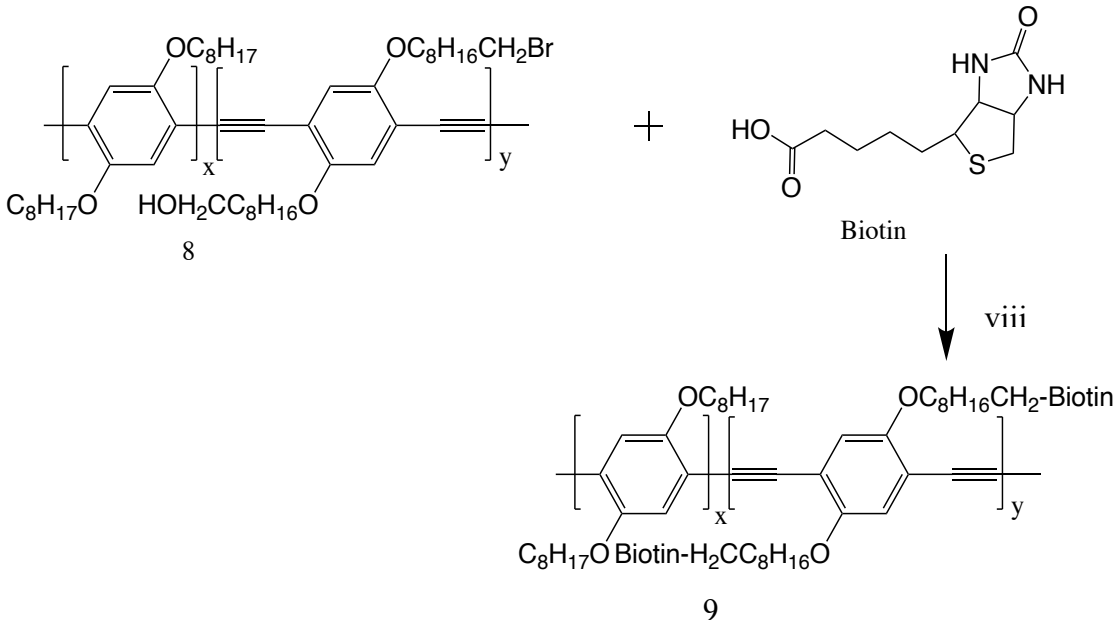

Figure 7.4. Synthesis of polymer 9. (viii) Biotin, K_2CO_3, DMF stir at 60 ºC for 72 hours, 1 *M* HCl workup

yield polymer 8 as an orange solid (0.92 g). ^{1}H NMR ($CDCl_3$): δ 6.93 (aromatic 4H), 4.03 (s, 8H), 3.39 (m, 4H), 1.86-1.28 (m, 48H), 0.88 (t, 6H).

Synthesis of Polymer 11 (PPE-50Biotin).

Polymer 10 (0.5 g) and biotin (0.24 g, 10 mmol) dissolved in DMF (10 mL) and potassium carbonate (1.38 g , 10 mmol) was added and mixture was stirred at 60 ºC for 72 hours. After cooling to room temperature HCl (1M, 10 mL) was added to the mixture and aqueous solution was extracted by DCM (3×20 mL) and the combined organic extract were dried over anhydrous Na_2SO_4 . The mixture was filleted and solvent was removed under reduced pressure to results polymer 11 ^{1}H NMR (D-THF): δ 6.93 (aromatic 4H), 6.08 (m, 2H), 4.02 (s, 8H), 3.37 (m, 4H), 1.92-1.23 (m, 64H), 0.88 (t, 6H).

Characterization of PPE

UV-vis absorption spectroscopy was used to probe the critical micelle concentration of PPE-50Biotin and PPE-0Biotin in THF. The absorption spectrum of PPE-50Biotin and

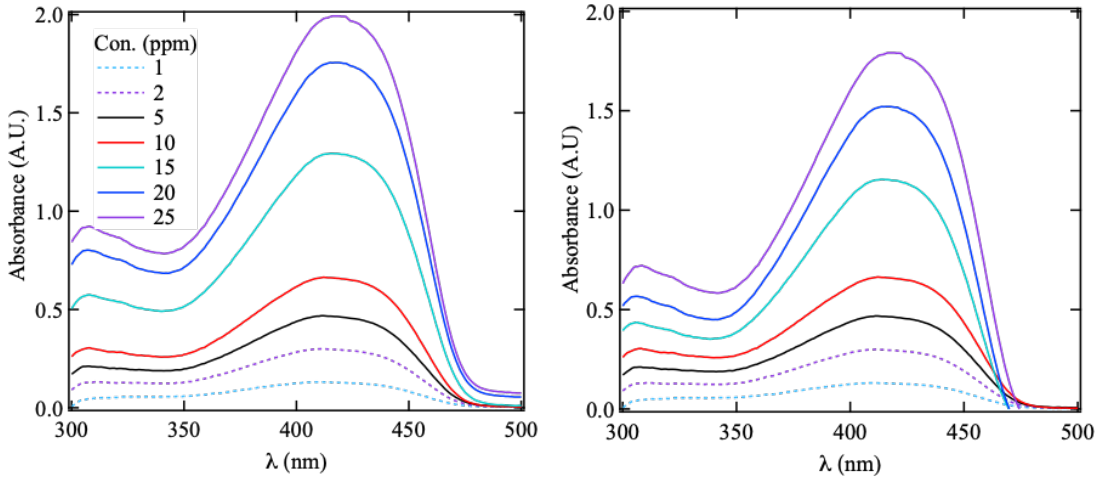

Figure 7.5. Absorption spectrum of a) PPE-0Biotin b) PPE-50Bitoin in THF for different concentrations

PPE-0Biotin is recorded as function of concentration and given in figure 7.5a and 7.5b. Absorption spectra show that PPE-0Biotin has higher absorption compared to PPE-50Biotin at similar concentrations. This result agrees with the disruption of biotin groups to the association of PPE which affect the conjugation length. This results were further characterized by probing the intensity of the spectrum as a function of the concentration at λ_{max} which is 420 nm and results is illustrated in Figure 7.6.

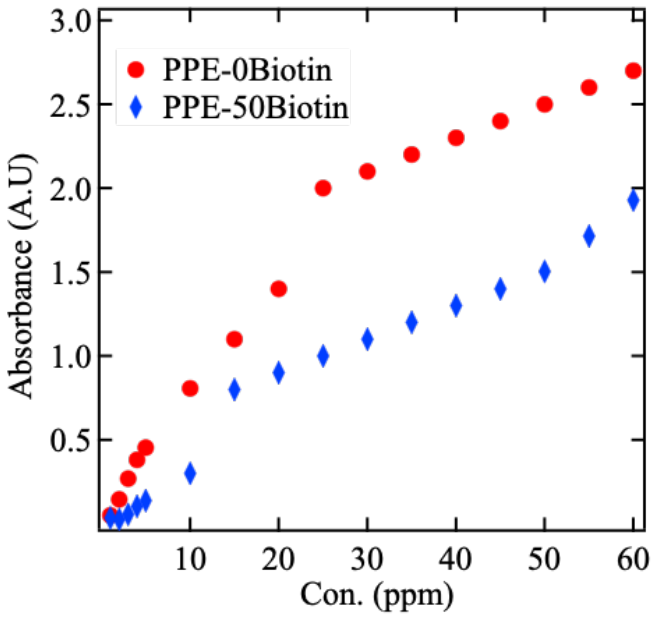

Figure 7.6. Absorption spectrum of PPE-0Biotin and PPE-50Bitoin in THF at 490 nm for different concentrations

Result shows that absorption intensity increases linearly for PPE-0Biotin up to 25 ppm and then it shows a big jump and increases linear again. We hypothesize that this jump is due to micellization of PPE in THF at 25 ppm. In contrast, PPE-50Biotin shows a jump at 15 ppm. This illustrate that cmc of PPE-50Biotin is lower than the absence of biotin. This agrees with the disruption of biotin groups to the aggregation of PPE in solutions.

The aggregation of biotin substituted PPE was further characterized by recoding the atomic force microscopic (AFM) images. Samples were prepared by using 50 ppm solutions of PPE-0Biotin and PPE-50Biotin in THF. A drop of PPE solution was put on clean silicon wafers and the solvent was permitted to evaporate under ambient conditions. Then the films were kept under the vacuum for 24 hours to make sure all the solvent was evaporated. Then AFM images were recorded using nanoscope atomic force microscope in tapping mode and the images for PPE-0Biotin and PPE-50Biotin is given in figure 7.7.

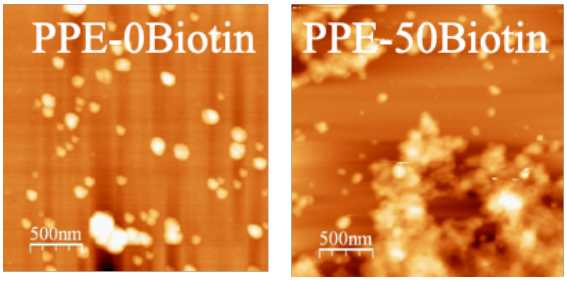

Figure 7.7. AFM height images of PPE-0Biotin and PPE-50Bitoin films casted by 50 ppm of polymer in THF.

AFM images show that PPE-0Biotin forms isolated extended structures. PPE forms extended confirmations in THF since it is a good solvent. However, the presence of biotin

groups causes the PPE to forms unstructured clumps. The stature and dynamics of these PPE will be characterized by SANS and QENS experiments.

Summary

We synthesized PPE derivatives with and without biotin substituted side groups. The properties of these PPE derivatives were characterized by UV-vis spectrometry and atomic force microscopy. We found that biotin groups lower the cmc of PPE. We found that PPE with biotin groups forms an extended network-like structure in polymer films.

Acknowledgement

I would like to thank Rhett Smith and Dr. Xiaoyan Yang from Clemson University for their valuable guidance throughout the synthesis of the polymers.

Reference

1. Bunz, U. H., Poly (aryleneethynylene) s: syntheses, properties, structures, and applications. *Chemical reviews* **2000,** *100* (4), 1605-1644.
2. Nie, J.; Wang, Z.; Huang, X.; Lu, G.; Feng, C., Uniform Continuous and Segmented Nanofibers Containing a π-Conjugated Oligo (p-phenylene ethynylene) Core via "Living" Crystallization-Driven Self-Assembly: Importance of Oligo (p-phenylene ethynylene) Chain Length. *Macromolecules* **2020,** *53* (15), 6299-6313.
3. Jagadesan, P.; Valandro, S.; Schanze, K., Ultrafast Photoinduced Electron Transfer in Conjugated Polyelectrolyte-Acceptor Ion Pair Complexes. *Materials Chemistry Frontiers* **2020**.

4. Zhou, Y.; Wang, J.; Li, X., Flexible room-temperature gas sensor based on poly (para-phenylene terephthalamide) fibers substrate coupled with composite NiO@ CuO sensing materials for ammonia detection. *Ceramics International* **2020**.

5. Braeken, Y.; Cheruku, S.; Seneca, S.; Smisdom, N.; Berden, L.; Kruyfhooft, L.; Penxten, H.; Lutsen, L.; Fron, E.; Vanderzande, D., Effect of Branching on the Optical Properties of Poly (p-phenylene ethynylene) Conjugated Polymer Nanoparticles for Bioimaging. *ACS Biomaterials Science & Engineering* **2019,** *5* (4), 1967-1977.

6. Swager, T. M.; Zheng, J., Poly (arylene ethynylene) s in chemosensing and biosensing. In *Poly (arylene etynylene) s*, Springer: 2005; pp 151-179.

7. Jones, T. V.; Blatchly, R. A.; Tew, G. N., Synthesis of alkoxy-substituted ortho-phenylene ethynylene oligomers. *Organic letters* **2003,** *5* (18), 3297-3299.

8. Lee, S. H.; Kömürlü, S.; Zhao, X.; Jiang, H.; Moriena, G.; Kleiman, V. D.; Schanze, K. S., Water-soluble conjugated polyelectrolytes with branched polyionic side chains. *Macromolecules* **2011,** *44* (12), 4742-4751.

9. Akbulut, H.; Guler, B.; Timur, S.; Yagci, Y., Synthesis, characterization and targeted cell imaging applications of poly (p-phenylene) s with amino and poly (ethylene glycol) substituents. *RSC Advances* **2015,** *5* (75), 60861-60869.

10. Tuncel, D.; Demir, H. V., Conjugated polymer nanoparticles. *Nanoscale* **2010,** *2* (4), 484-494.

11. Perahia, D.; Traiphol, R.; Bunz, U. H., From molecules to supramolecular structure: Self assembling of wirelike poly (p-phenyleneethynylene) s. *Macromolecules* **2001,** *34* (2), 151-155.

12. Maskey, S.; Pierce, F.; Perahia, D.; Grest, G. S., Conformational study of a single molecule of poly para phenylene ethynylenes in dilute solutions. *The Journal of chemical physics* **2011,** *134* (24), 244906.

13. Nguyen, T. T.; Sly, K. L.; Conboy, J. C., Comparison of the energetics of avidin, streptavidin, neutrAvidin, and anti-biotin antibody binding to biotinylated lipid bilayer examined by second-harmonic generation. *Analytical chemistry* **2012,** *84* (1), 201-208.

14. Etampawala, T., Neutron study of structured polymers at interfaces. **2013**.

CHAPTER EIGHT

SUMMARY

These studies focused on understanding the behavior of associating polymers including their assembly in different environments, using neutron scattering techniques coupled with molecular dynamics (MD) simulations. The main effort centered on the assembly of a multi-functional ionic polymers of the form ABCBA. The center block is a sulfonated polystyrene (PSS) (C) that enables transport tethered to, B, a polyethylene propylene (PEP) block, terminated by C, a t-butyl polystyrene (t-BPS) block. The aggregation of this polymer is driven by segregation of the ionizable block from the rest of the polymer as well as the interactions of each block with solvents.

- **Solvent tuning of structured ionic block co polymers: SANS insight**

In the third chapter, the effects of solvent polarity on the assemblies formed by an ABCBA pentablock co-polymer were probed by SANS, as propanol added to cyclohexane. We find that similar to van der Waals block co-polymers in selective solvents, core-Gaussian shell aggregates are formed with ionic blocks in the core of the micelles in both cyclohexane and propanol. In cyclohexane with low propanol fractions, the PSS segregates to the core, forming a tight ionic network with some interstitial space, as was previously observed. Cyclohexane is a good solvent for PEP resulting in a highly swollen corona. The t-BPS block resides in the corona and is only slightly swollen. The highly incompatible nature of the blocks and the multiple sites available for propanol drives a symmetry transitions from a spherical to an elongated micelle and then to a transitional region with large swarms with increasing of propanol fraction. In contrast to van der Waals polymers, at higher

propanol fractions spherical assemblies are formed but with a smaller number of polymer molecules and significantly higher portion of solvent in the core. The insight obtained here offers a glimpse into the formation of micelles of ionizable block co-polymers in the high segregation regime and demonstrated the complexity of assemblies where the solvents occupy multiple distinctive sites. Further the results show the significance of the interfacial region between the blocks.

- **Response of ionizable block copolymer assemblies to solvent polarity: a molecular dynamics study**

In the fourth chapter using MD simulations, we studied the effect of solvent polarity on the structure of micelles made structured ionic block copolymers. We found that the micelles formed from this pentablock copolymer response differently depending on the polarity of the solvent. In cyclohexane, the ionic blocks form a collapsed conformation while non-polar blocks form a swollen state. In contrast to cyclohexane, in propanol and THF the ionic blocks are more swollen and non-polar blocks slightly more collapsed. With increasing sulfonation, ionic blocks condense to form a more stable ionic core. Cyclohexane associated around the dense ionic core while THF and propanol penetrated into the core. This study provides for the first time a direct molecular insight into the distribution of solvents in micelles formed by ionizable co-polymers. This insight provides the fundamentals that govern the building blocks of these technologically important polymers.

- **Interfacial response of structured ionomer thin films**

The fifth chapter offers an insight into response structured ionic block copolymers films to solvents of different polarities including water, propanol and THF. In their many applications these polymers form membranes and interfacial effects play an important role. The interface of the dry membrane is dominated by the aliphatic domains. With exposure to water, the interfaces rearrange; hydrophobic segments retract, exposing more hydrophilic groups and the interface becomes smoother. At the interface with propanol and THF, the hydrophobic segments swell, and fewer ionic groups reside at the interface compared to water. While propanol and THF penetrate the membrane at a higher rate than water, their distribution in the different blocks is markedly different. Water penetrates the film predominantly through the PSS domains, while propanol and THF reside in all blocks. All three solvents strongly effect the of size and distribution of the ionic clusters. The composition and topology of the interfaces reflect the response of the individual segments to the solvents; nevertheless, they are strongly coupled with the solvent effects on the ionic clusters.

- **Effects of interaction strength of associating groups on linear and star polymers dynamics**

In sixth chapter, we provide a general insight into effects of associative groups on melts of pristine polymers and their blends with linear and star architectures using MD simulations. Polymer were modeled by bead-spring model and associating groups are incorporated randomly on the chains. As expected from studies of associative polymers, the associating group aggregate forming polymer networks. We show that even weak interactions between

the associating groups are sufficient to drive association. By varying the strength of the interaction between the associating groups, one can control the size of the aggregates and the mobility of the chains in melts. The overall mobility of the chains rapidly decreases as the associating beads act as instantaneous crosslinkers and dominate the motion of the entire chain. For interactions between associating groups of order 10 k_BT and larger, the system is kinetically trapped, forming a long-lived polymer network. The fraction of unique chains in a cluster decreases with increasing cluster size for both linear and star melts - this increase in the number of intra chain contributions leads to a decrease in the mean squared average radius of gyration. Star polymer melts contain more intramolecular associating groups than for linear chains

Blends of chains with and without associating groups macroscopically phase separate even for a low concentration of weak (~3k_BT) associating groups – in the case studied here the fraction of associating groups on a chain is only 5%. This suggests that blending polymers with associating groups to the same polymer without associating groups will be difficult to achieve unless the strength of the associating groups is very weak. An interesting open question is whether chains with different factions of associating groups are miscible or not.

- **Synthesis and characterization of biotin substituted polyphenylene ethynylene**

In the seventh chapter, we synthesized PPE derivatives with and without biotin substituted side groups. The properties of these PPE derivatives were characterized by UV-vis spectrometry and atomic force microscopy. We found that biotin groups lower the critical

micelle concentration of PPE and that PPEs with biotin groups forms an extended network-like structure in polymer films. These polymers will be probed in solutions and in their nanoparticulate phases.

APPENDIX

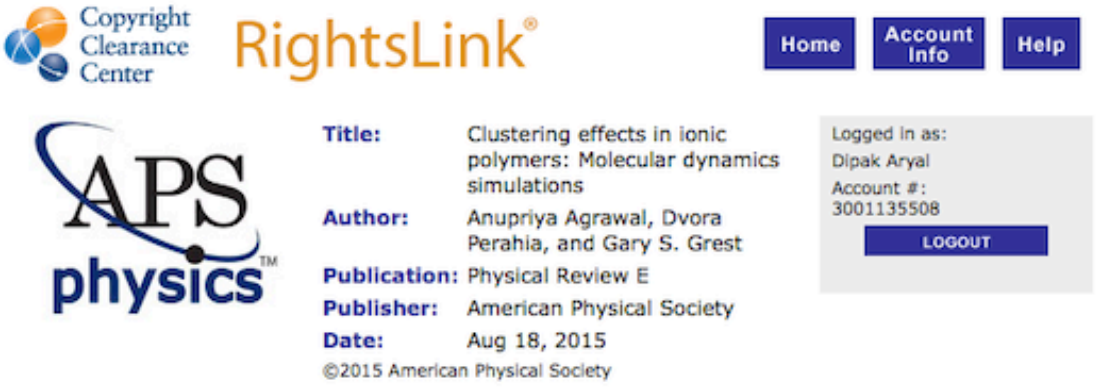

Review Order

Please review the order details and the associated terms and conditions.

No royalties will be charged for this reuse request although you are required to obtain a license and comply with the license terms and conditions. To obtain the license, click the Accept button below.

Licensed Content Publisher	American Physical Society
Licensed Content Publication	Physical Review E
Licensed Content Title	Clustering effects in ionic polymers: Molecular dynamics simulations
Licensed Content Author	Anupriya Agrawal, Dvora Perahia, and Gary S. Grest
Licensed Content Date	Aug 18, 2015
Licensed Content Volume	92
Type of use	Thesis/Dissertation
Requestor type	Student
Format	Electronic
Portion	chart/graph/table/figure
Number of charts/graphs/tables/figures	1
Portion description	Figure 1
Rights for	Main product
Duration of use	Life of Current Edition
Creation of copies for the disabled	no
With minor editing privileges	no
For distribution to	Worldwide
In the following language(s)	Original language of publication
With incidental promotional use	no
Lifetime unit quantity of new product	0 to 499
The requesting person/organization	Dipak Aryal/ Clemson University
Order reference number	

THE AMERICAN ASSOCIATION FOR THE ADVANCEMENT OF SCIENCE LICENSE TERMS AND CONDITIONS

Dec 01, 2020

This Agreement between Clemson University -- Manjula Senanayake ("You") and The American Association for the Advancement of Science ("The American Association for the Advancement of Science") consists of your license details and the terms and conditions provided by The American Association for the Advancement of Science and Copyright Clearance Center.

License Number	4960450480881
License date	Dec 01, 2020
Licensed Content Publisher	The American Association for the Advancement of Science
Licensed Content Publication	Science
Licensed Content Title	Multiblock Polymers: Panacea or Pandora's Box?
Licensed Content Author	Frank S. Bates,Marc A. Hillmyer,Timothy P. Lodge,Christopher M. Bates,Kris T. Delaney,Glenn H. Fredrickson
Licensed Content Date	Apr 27, 2012
Licensed Content Volume	336

Licensed Content Issue	6080
Volume number	336
Issue number	6080
Type of Use	Thesis / Dissertation
Requestor type	Scientist/individual at a research institution
Format	Electronic
Portion	Text Excerpt
Number of pages requested	1
Title	SOLVENT AS A TOOL TO TUNE THE ASSOCIATION OF STRUCTURED IONIC BLOCK CO-POLYMERS: NEUTRON SCATTERING AND COMPUTATIONAL STUDY
Institution name	Clemson University
Expected presentation date	Dec 2020
Portions	Fig. 1 A subset of the vast structural complexity with two (k = 2) or three (k = 3) block types produced by varying the number of blocks (n) and the functionality of the connector at each block-block juncture (difunctional,
Requestor Location	Clemson University 930 George town street

CLEMSON, SC 29631
United States
Attn: Clemson University

Total 0.00 USD

Terms and Conditions

American Association for the Advancement of Science TERMS AND CONDITIONS

Regarding your request, we are pleased to grant you non-exclusive, non-transferable permission, to republish the AAAS material identified above in your work identified above, subject to the terms and conditions herein. We must be contacted for permission for any uses other than those specifically identified in your request above.

The following credit line must be printed along with the AAAS material: "From [Full Reference Citation]. Reprinted with permission from AAAS."

All required credit lines and notices must be visible any time a user accesses any part of the AAAS material and must appear on any printed copies and authorized user might make.

This permission does not apply to figures / photos / artwork or any other content or materials included in your work that are credited to non-AAAS sources. If the requested material is sourced to or references non-AAAS sources, you must obtain authorization from that source as well before using that material. You agree to hold harmless and indemnify AAAS against any claims arising from your use of any content in your work that is credited to non-AAAS sources.

If the AAAS material covered by this permission was published in Science during the years 1974 - 1994, you must also obtain permission from the author, who may grant or withhold permission, and who may or may not charge a fee if permission is granted. See original article for author's address. This condition does not apply to news articles.

The AAAS material may not be modified or altered except that figures and tables may be modified with permission from the author. Author permission for any such changes must be secured prior to your use.

Whenever possible, we ask that electronic uses of the AAAS material permitted herein include a hyperlink to the original work on AAAS's website (hyperlink may be embedded in the reference citation).

AAAS material reproduced in your work identified herein must not account for more than 30% of the total contents of that work.

AAAS must publish the full paper prior to use of any text.

AAAS material must not imply any endorsement by the American Association for the Advancement of Science.

This permission is not valid for the use of the AAAS and/or Science logos.